Supporting material

Syntheses and Electronic Structures of μ-Nitrido Bridged Pyridine, Diimine Iridium Complexes

Friedrich Angersbach-Bludau, Christopher Schulz, Julia Schöffel, and Peter Burger [*]

[*] Institut für Anorganische und Angewandte Chemie, Fachbereich Chemie, Universität Hamburg, Martin-Luther-King-Platz 6, 20146 Hamburg, Germany Fax: +49-40-42838-6097

To whom correspondence should be addressed: Email: burger@chemie.uni-hamburg.de

Table of Contents

1) Experimental Section

a) General

All manipulations of the complexes were performed under standard Schlenk techniques or in a dinitrogen filled glovebox. Toluene, *n*-pentane, *n*-hexane, diethyl ether (Et$_2$O) and tetrahydrofuran (THF) were distilled under N$_2$ from sodium benzophenone ketyl and stored under nitrogen or were obtained from a MBraun solvent purification system. Isotopically labelled NaN$_3$ (terminal ^{15}N, 98%) was used as purchased from Cambridge Isotope Laboratories. All other reagents were purchased from commercial sources and were used as received. The dinuclear Ir precursor [Ir(C$_2$H$_4$)$_2$Cl]$_2$,[S1] the ligand N$_3$Me$_4$,[S2] the acid [H(Et$_2$O)$_2$][Al(pftb)$_4$][S3] and 4-*tert*-butyl-2,6-diacetylpyridine[S4] were prepared as described in literature. The following complexes were prepared according to literature procedures: **[Ir(Me$_4$N$_3$)N$_3$], [Ir(Me$_4$N$_3$)(THF)][OTf], [Ir(Me$_4$N$_3$)(THF)][Al(pftb)$_4$], [Ir(^{tBu}Me$_4$N$_3$)(Me)(OTf)$_2$].**[S4, S5]

[Ir(Me$_4$N$_3$)N$_3$]   **[Ir(Me$_4$N$_3$)(THF)][OTf]**   **[Ir(^{tBu}Me$_4$N$_3$)(Me)(OTf)$_2$]**   **[Al(pftb)$_4$]**
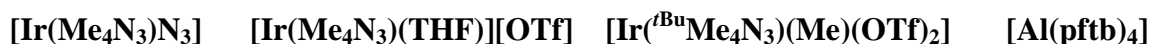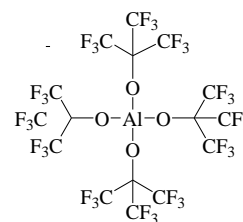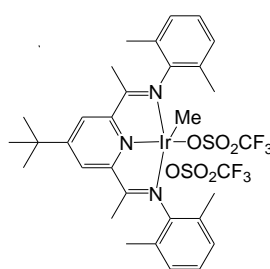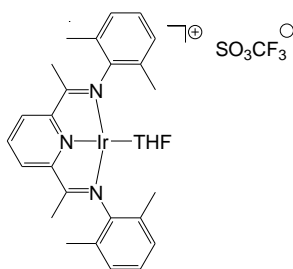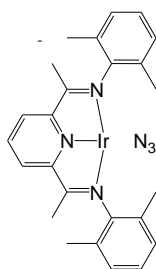
Me$_4$N$_3$ =   2,6-Bis-[1-(2,6-Dimethylphenylimino)ethyl]pyridine

^{1}H, ^{13}C, ^{11}B, ^{15}N and ^{19}F NMR spectra were recorded on Bruker Avance 400, Bruker DRX 500 and Varian Gemini 2000 BB NMR spectrometers. The ^{1}H and ^{13}C NMR spectra are referenced to the residual resonances of the solvent. The ^{19}F NMR shifts are referenced to CCl$_3$F as an external standard. ^{13}C and ^{19}F resonances are singlets if not otherwise stated. The assignments of the ^{13}C NMR spectra were carried out by combined analyses of DEPT and ^{13}C-^{1}H correlated spectra (HSQC and HMBC). The numbering scheme for the assignment of the ^{1}H and ^{13}C NMR resonances is displayed below.

R = H, *t*Bu
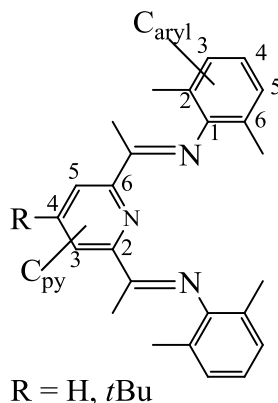
For the description of the multiplets, the following abbreviations are used: **s**: singlet, **d**: doublet, **dd**: doublet of doublet, **t**: triplet, **q**: quartet, **sept**: septet, **m**: multiplet. For paramagnetic NMR spectra, **br** stands for broad peak and **vbr** corresponds to a very broad peak.

The effective magnetic moments (μ_{eff}) in THF-d$_8$ solution were determined by the Evans' method using a coaxial double NMR tube.[S6, S7] A solution of the paramagnetic complex was placed in the outer tube, while the inner tube contained only THF-d$_8$. The magnetic moment μ_{eff} was calculated at 298 K from the following equations:

$$\chi_g = (-3\Delta f)/(4\pi fm) + \chi_0 + [\chi_0\,(d_0 - d_s)]/m$$

$$\chi_M = 477 \cdot \frac{\Delta v}{Q v_I c}$$

$$\mu_{eff} = 2.828(\chi_M T)^{1/2}$$

Δf corresponds to the chemical shift differences of the NMR solvent in the inner and outer coaxial tube. The spectrometer frequency (f or v_I) is used in Hz, m equals to the mass of the substance per cm^3 of solution, respectively c to the concentration per volume, χ_0 is the mass susceptibility of the THF-d$_8$ solvent.[S8] The last term is neglected due to its minimal contribution to the mass susceptibility of the solute. The density of the pure solvent is given by d$_O$ and d$_S$ is the density of the solution (in [g/cm^3]). The molar susceptibility (χ_m) is the product of χ_g multiplied by the molecular weight of the paramagnetic complex.

IR spectra were recorded as KBr pellets on a Bruker Vertex 70 IR spectrometer. The intensities of the vibrational bands are indicated as follows: **vs**: very strong, **s**: strong, **m**: medium, **w**: weak. UV/vis spectra were measured on a Cary 50 Scan UV/Vis spectrometer. Elemental analyses were measured by: Zentrale Elementaranalyse, Universität Hamburg. Thermogravimetry coupled mass spectrometry (TG-MS) measurements were recorded on a Netzsch STA 409C/CD instrument coupled with a Balzers MID quadrupole mass spectrometer. EPR spectra were measured on an X-band Bruker Elexsys E500 CW machine. CV measurements were performed using a BAS100BW potentiostat with a standard three-electrode configuration in a single cell. A glassy carbon disk working electrode (diameter = 3.0 mm) was utilized in combination with a Pt (wire) auxiliary electrode. The reference electrode consisted of an Ag wire pseudo-reference; cyclic voltammograms were referenced against the $[Cp_2Fe]^{+/0}$ couple added to the solution at the end of the measurement. The CVs were recorded at RT under a nitrogen atmosphere in THF using $[NBu_4][PF_6]$ as supporting electrolyte. The working electrode was polished with alumina slurry to achieve a mirror finish, then thoroughly rinsed with purified water (LaboStarTM Range of UltraPureWater System) and dried in a 40°C oven. The electrochemical solvent (THF, Chromasolv, Fluka) was distilled from sodium/benzophenone, degassed and stored under N_2 in a J. Young Teflon tapped solvent vessel. The conductivity salt $[NBu_4][PF_6]$ was recrystallized twice from methanol and thoroughly dried at 100 °C under vacuum. **XPS** spectra were recorded at the Christian-Albrechts-Universität Kiel on an Omicron Full-Lab (Omicron GmbH) XPS spectrometer using X-ray Al Kα radiation. All spectra were referenced to the C(1s) ionization potential of 284.6 eV. The program XPSPEAK for WIN95/98 version 4.1 was used for the data analysis and the Ir(4f) signals were fitted as a doublet with fixed spin orbit splitting of 2.98 eV in consideration of the different intensity ratios of the spin split f-states. The sample preparation of the crystalline samples was performed quickly under non-inert condition to avoid contact with the atmosphere. ESI-MS measurements were performed on a Finnigan ThermoQuest MAT 95 XL-spektrometer or for Cryo ESI MS measurements on an ultra high resolution electrospray quadrupole TOF mass spectrometer (Bruker Maxis) coupled with cryospray at the University of Erlangen. Samples were prepared in THF with concentrations of 40-50 µg/ml. The capillary was heated to 80°C and the low temperature measurements were recorded at -40 °C.

b) Synthesis and Spectroscopic Data

1. Synthesis of $Ir_2N_3^+OTf^-$

To a -35 °C cold suspension of 41.5 mg (638 μmol) **NaN₃** in THF (5 ml) was added a -35 °C cold solution of 500 mg (638 μmol) **[Ir(Me₄N₃)(THF)][OTf]** in THF (5 ml). This mixture was stirred at room temperature for 4 h. After filtering off the solid precipitate, the filtrate was evaporated to dryness in vacuum. The black solid residue can be used without further purification. Yield: 621 mg (472 μmol, 74%). Single crystals for X-ray diffraction were obtained by vapor diffusion of pentane into a concentrated solution of the complex in THF. **UV/vis λ_{max}(THF) [nm]** = 323, 427, 537, 830. **IR (KBr) [cm^{-1}]** = 2145s ($\nu_{as}(N_3)$), 1271 vs ($\nu_{as}(OTf)$). **^{1}H NMR (200 MHz, THF-d_8) δ [ppm]** = 8.55 (2 H, t, ^3J = 7.9 Hz, $C_{py}(4)H$), 8.06 (4 H, d, ^3J = 7.9 Hz, $C_{py}(3,5)H$), 7.01 - 6.85 (12 H, m, $C_{arom}(3,4,5)H$), 1.93 (24H, s, CH_3), 1.41 (12H, s, N=C-CH_3). **^{13}C{^{1}H} NMR (100 MHz, THF-d_8) δ [ppm]** = 175.5 (C=N), 163.7 ($C_{py}(2,6)$), 152.7 ($C_{arom}(1)$), 131.5 ($C_{arom}(2,6)$), 129.7 and 127.6 ($C_{arom}(3,4,5)$), 128.5 ($C_{py}(4)$), 124.6 ($C_{py}(3,5)$), 18.9 (CH_3), 18.2 (N=C-CH_3). **^{19}F{^{1}H} NMR (188 MHz, THF-d_8) δ [ppm]** = -78.9 (s, 3F, CF_3). Presumably due to the thermal instability of this compound correct elemental analytical data could not be obtained.

2. Synthesis of $Ir_2N_3^+Al^-$

To a solution of 28 mg (47 μmol) **[Ir(N₃Me₄)N₃]** in 1.5 ml THF 75 mg (47 μmol) of the cationic complex (**[Ir(N₃Me₄)(THF)][Al(pftb)₄]**) dissolved in 1.5 ml THF was added, upon which an immediate color change to violet was noticed. After stirring for 20 min at RT, the solvent was removed in vacuum. Yield: 98 mg (46 μmol; 98 %). **UV/vis λ_{max}(THF) [nm]** = 317, 423, 531, 824. **IR (KBr) [cm^{-1}]** = 2151(s) ($\nu_{as}(N_3)$). **^{1}H NMR (400 MHz, THF-d_8) δ [ppm]** = 8.52 (t, 2H, ^3J = 8.0 Hz, $C_{py}H(4)$); 7.97 (d, 4H, ^3J = 8.0 Hz, $C_{py}H(3,5)$); 7.00 (d, 8H, ^3J = 7.5 Hz, $C_{arom}H(3,5)$); 6.89 (t, 4H, ^3J = 7.5 Hz, $C_{arom}H(4)$); 1.92 (s, 24H, CH_3); 1.40 (s, 12H, NC-CH_3). **^{13}C{^{1}H} NMR (100 MHz, THF-d_8) δ [ppm]** = 174.7 (C=N); 163.1 ($C_{py}(2,6)$); 151.9 ($C_{arom}(1)$); 130.8 ($C_{arom}(2,6)$); 129.4 ($C_{arom}(3,5)$); 127.8 (($C_{py}(4)$); 127.3 ($C_{arom}(4)$); 124.0 ($C_{py}(3,5)$); 18.4 (CH_3); 17.8 (NC-CH_3). The signals of the quaternary carbons of the $C(CF_3)_3$ group of the counter anion could not be detected. **^{19}F{^{1}H} NMR (188**

MHz, THF-d_8) δ [ppm] = -74.3 (s, 36F, CF_3). Due to the thermal instability of this compound correct elemental analytical data could not be obtained.

3. Synthesis of ^{tBu}Ir$_2$N$_3$$^{+BPh4-}$

To a solution of 200 mg (306 μmol) of the chlorido complex **[Ir(^{tBu}N$_3$Me$_4$)Cl]** in 6 ml THF was added a solution of 105 mg (306 μmol) **Na[BPh$_4$]** and 20 mg (306 μmol) **NaN$_3$** in 5 ml THF. After one hour stirring at room temperature, the color changed from green through brown to finally deep violet. After filtering off the solid precipitate the filtrate was evaporated to dryness in vacuum. After co-evaporation several times with n-pentane, the solid was dried in vacuum for 4 hours. Yield: 390 mg (245 μmol, 80%). **IR (KBr) [cm^{-1}]** = 2143 (s) ($\nu_{as}(N_3)$). **^{1}H NMR (400 MHz, THF-d_8):** δ [ppm] = 7.97 (d, 4H, ^{3}J = 8.0 Hz, C$_{py}$$H$(3,5)); 7.00 (d, 8H, ^{3}J = 7.5 Hz, C$_{arom}$$H$(3,5)); 6.89 (t, 4H, ^{3}J = 7.5 Hz, C$_{arom}$$H$(4)); 1.92 (s, 24H, C$H_3$); 1.40 (s, 9H, C$_{py}CCH_3$); 1.32 (s, 12H, NC–C$H_3$). **^{13}C{^{1}H} NMR (100 MHz, THF-d_8):** δ [ppm] = 174.7 NC–CH$_3$); 163.1 (C_{py}(2,6)); 151.9 (C_{arom}(1)); 130.8 (C_{arom}(2,6)); 129.4 (C_{arom}(3,5)); 127.8 ((C_{py}(4)); 127.3 (C_{arom}(4)); 124.0 (C_{py}(3,5)); 18.4 (CH$_3$); 17.8 (NC–CH$_3$). **^{11}B NMR 200 MHz, THF-d_8)** δ [ppm] = -29(q, BPh$_4$). **MS (ESI/THF): [m/z]** = 1273.4 [(^{tBu}Me$_4$N$_3$)Ir(μ-1,3-N$_3$)Ir(^{tBu}Me$_4$N$_3$)]$^+$; 319 [B(Ph)$_4$]$^-$ (100%). **EA** calculated for C$_{82}$H$_{90}$BIr$_2$N$_9$: C 61.67%; H 5.68%; N 7.89%; found: C 61.23%; H 5.73%; N 7.34%.

Synthesis of ^{tBu}Ir$_2$$^{14/15}N_3$$^{+BPh4-}$

To a solution of 98 mg (150 μmol) of the chlorido complex **[Ir(^{tBu}N$_3$Me$_4$)Cl]** in 6 ml THF was added a solution of 51 mg (150 μmol) **Na[BPh$_4$]** and a suspension of 10 mg (152 μmol) **Na$^{14/15}$N$_3$** in 5 ml THF. After 1.5 h stirring at room temperature, the color changed slowly from green to deep violet. After filtering off the solid precipitate the filtrate was evaporated to dryness in vacuum. After co-evaporation several times with n-pentane, the solid was dried in vacuum for 4 hours. Yield: 180 mg (113 μmol, 75%). **IR (KBr) [cm^{-1}]** = 2127 (s) ($\nu_{as}(^{15}N_3)$). **^{1}H NMR (400 MHz, THF-d_8):** δ [ppm] = 7.97 (d, 4H, ^{3}J = 8.0 Hz, C$_{py}$$H$(3,5)); 7.00 (d, 8H, ^{3}J = 7.5 Hz, C$_{arom}$$H$(3,5)); 6.89 (t, 4H, ^{3}J = 7.5 Hz, C$_{arom}$$H$(4)); 1.92 (s, 24H, C$H_3$); 1.40 (s, 9H, C$_{py}CCH_3$); 1.32 (s, 12H, NC–C$H_3$).

4. Synthesis of Ir$_2$N^{+OTf-} (photolysis route)

A solution of 100 mg (76 μmol) **Ir$_2$N$_3$$^{+OTf-}$** in 100 ml of a mixture of THF/ether (4:1) was photolyzed for 3 h in a "donut shaped" Schlenk tube with high vacuum teflon tap at room temperature with a medium pressure mercury lamp (Philips HPK-125-UV) using a 1M NaNO$_2$ solution as UV cutoff filter (λ > 400 nm). The obtained burgundy red solution was dried in vacuum. After co-evaporating several times with n-pentane the compound was dried for 3h in vacuum. Yield: 96 mg (75 μmol, 98%). Crystals suitable for X-ray diffraction formed during photolysis. **UV/vis λ_{max}(THF) [nm]** = 368, 505, 625, 770. **^{1}H NMR (400 MHz, RT, THF-d_8) δ [ppm]** = 118 (vbs, $\omega_{1/2}$ 70 Hz (0.18 ppm), 6H, NC–CH_3)); 21.87 (bs, $\omega_{1/2}$ 15 Hz (0.038 ppm), 2H, C$_{py}H$(3,5)); 11.32 (d, 4H, ^{3}J = 14 Hz, C$_{arom}H$(3,5)); 5.94 (t, 2H, ^{3}J = 14 Hz, C$_{arom}H$(4)); 3.98 (s, 12H, CH_3), -88.55 (vbs, $\omega_{1/2}$ 60 Hz (0.15 ppm), 1H, C$_{py}H$(4)). **^{19}F{^{1}H} NMR (188 MHz, THF-d_8) δ [ppm]** = -78.9 (s, 3F, CF_3). Correct elemental analytical data could not be obtained.

5. Synthesis of Ir$_2$N^{+Al-} (photolysis route)

A solution of 160 mg (75 μmol) of **Ir$_2$N$_3$$^{+Al-}$** in 100 ml of a mixture of THF/ether/hexane (4:1:1) was transferred to a "donut shaped" Schlenk tube with teflon tap and photolyzed for 3 hours at room temperature by a medium pressure mercury lamp (Philips HPK-125-UV). A filter solution of 1M NaNO$_2$ was used as a UV cutoff filter (λ > 400 nm). The obtained burgundy red solution was dried in vacuum, then co-evaporated several times with n-pentane and finally dried for 3h in vacuum. Yield: 153 mg (73 μmol; 96%). **UV/vis λ_{max}(THF) [nm]** = 368, 505, 625, 770. **^{1}H NMR (400 MHz, RT, THF-d_8): δ [ppm]** = 121.23 (vbs, $\omega_{1/2}$ 70 Hz (0.18 ppm), 6H, NC–CH_3)), 22.81 (bs, $\omega_{1/2}$ 15 Hz (0.038 ppm), 2H, C$_{py}H$(3,5)), 11.32 (d, 4H, ^{3}J = 16 Hz, C$_{arom}H$(3,5)), 5.94 (t, 2H, ^{3}J = 16 Hz, C$_{arom}H$(4)), 3.98 (s, 12H, CH_3), -88.55 (vbs, $\omega_{1/2}$ 60 Hz (0.15 ppm), 1H, C$_{py}H$(4)). **^{19}F{^{1}H} NMR (188 MHz, RT, THF-d_8): δ [ppm]** = −76.1 (s, 36F, CF_3). **MS (ESI/THF): [m/z]** = 1136.4 [(Me$_4$N$_3$)Ir(N)Ir(Me$_4$N$_3$)]$^+$ (100%); 967.0 [Al(pftb)$_4$]$^-$ (100%). **EA** calculated for C$_{78}$H$_{78}$AlF$_{36}$Ir$_2$N$_7$O$_5$: C 40.93%; H 3.43%; N 4.28%; found: C 40.50%; H 4.00%; N 4.96%.

6. Synthesis of ^{tBu}Ir$_2$N^{+BPh4-} (photolysis route)

A solution of 96 mg (60 μmol) of the cationic azido compound ^{tBu}Ir$_2$N$_3$$^{+BPh4-}$ in 100 ml of a mixture of THF/ether/hexane (2:1:1) was photolyzed by a medium pressure mercury lamp

(Philips HPK-125-UV) for 3h using a 1M $NaNO_2$ UV cutoff filter. The obtained burgundy red solution was dried in vacuum, co-evaporated a few times with n-pentane; the product was finally dried for 5h in vacuum. Yield: 90 mg (57 μmol; 95%). X-ray crystals could be isolated from the obtained burgundy red solution. **^{1}H-NMR (400 MHz,** RT, THF-d_8): δ [ppm] =129.91 (vbs, $\omega_{1/2}$ 75 Hz (0.19 ppm), 6H, NC–CH_3)); 20.03 (bs, $\omega_{1/2}$ 15 Hz (0.038 ppm), 2H, $C_{py}H(3,5)$); 11.64 (d, 4H, ^3J = 16 Hz, $C_{arom}H(3,5)$); 5.46 (t, 2H, ^3J = 16 Hz, $C_{arom}H(4)$); 4.03 (s, 12H, CH_3); 3.54 (s, 9H (overlapping with THF at RT, 9H at lower temperature), $C_{py}CCH_3$). Susceptibility measurements by the Evans method at 298 K: ν = 400 MHz, Δf = 2.25 Hz, $c(^{tBu}Ir_2N^{+BPh4-})$ = 4.5 mM, Q = 2 (superconducting magnet factor), T = 293 K, , μ_{eff} = 3.23 μ_B. **^{11}B NMR (200 MHz, THF-d_8): δ [ppm]** = -8(q, BPh_4). **MS (ESI/THF): [m/z]** = 1249.5 $[(^{tBu}Me_4N_3)Ir(N)$ $Ir(^{tBu}Me_4N_3)]^+$ (100%) simulated: 1249.5 $[(^{tBu}Me_4N_3)Ir(N)Ir(^{tBu}Me_4N_3)]^+$ (75%). **EA** calculated for $C_{82}H_{90}BIr_2N_7$: C 62.78%; H 5.78%; N 6.25%; found: C 62.60%; H 5.85%; N 7.01%.

Synthesis of Ir_2N^{+OTf-} (solid thermolysis route)

Solid **$Ir_2N_3^{+OTf-}$** (184 mg, 140 μmol) was placed in a teflon tapped Schlenk tube and was heated to 100 °C for one day under permanent vacuum, upon which the color changed to burgundy red. Further purification is not required. Yield: 180 mg (139 μmol, 99%).

Synthesis of Ir_2N^{+Al-} (solid thermolysis route)

100 mg (47 μmol) **$Ir_2N_3^{+Al-}$** were kept in a teflon tapped Schlenk tube under vacuum at 100 °C for one day. After this period the color changed to burgundy red and the N_2 extrusion was complete. Yield: 99 mg (47 μmol, quantitative).

Synthesis of $^{tBu}Ir_2N^{+BPh4-}$ (solid thermolysis route)

120 mg (75 μmol) $^{tBu}Ir_2N_3^{+BPh4-}$ were thermolyzed under vacuum in a teflon tapped Schlenk tube at 110 °C for one day. After this period the color changed to burgundy red and the N_2 extrusion was complete. Yield: 115 mg (73 μmol, 98%).

Synthesis of $^{tBu}Ir_2{}^{14/15}N^{+}BPh_4{}^{-}$ (solid thermolysis route)

20 mg (12 μmol) $^{tBu}Ir_2{}^{14/15}N_3{}^{+}BPh_4{}^{-}$ were placed a teflon tapped Schlenk tube under vacuum at 110 °C for one day. After this period the color changed to burgundy red and the N_2 extrusion was complete. Yield: 19 mg (122μmol, quantitative).

7. Synthesis of Ir_2N

To a solution of 20 mg (10 μmol) of **Ir_2N^{+Al-}** in 5 ml THF at -35 °C was added a solution of 20 μl (20 μmol) **NaHBEt₃** in 5 ml THF. After 10 min stirring at room temperature the color changed from burgundy red to deep violet. The solvents were removed in vacuum and the residue was dried for six hours in vacuum. Residual solvents were co-evaporated with two portions of 10 ml pentane each. The product was extracted from the residue into pentane. After drying in vacuum for 4 hours 11 mg (9.7 μmol, 97%) of the product was obtained as a violet powder. **UV/vis λ$_{max}$(THF) [nm]** = 546. **^{1}H NMR (200MHz, RT, THF-d_8) δ [ppm]** = 153 (bs, 6H, NC–CH_3)); 15.4 (bs, 2H, C$_{py}H$(3,5)); 13.00 (d, 4H, J = 8 Hz, C$_{arom}H$(3,5)); 4.91 (s, 12H, CH_3); 4.36 (t, 2H, J = 8 Hz, C$_{arom}H$(4)); -91 (bs, 1H, C$_{py}H$(4)). **^{1}H NMR (400 MHz, C_6D_6): δ [ppm]** = 151.0 (bs, 6H, NC–CH_3)); 15.4 (bs, 2H, C$_{py}H$(3,5)); 13.0 (d, 4H, ^3J = 8 Hz, C$_{arom}H$(3,5)); 4.9 (s, 12H, CH_3); 4.4 (t, 2H, ^3J = 8 Hz, C$_{arom}H$(4)); -91 (vbs, 1H, C$_{py}H$(4)). **MS (ESI/THF): [m/z]** = found: 1136.4 [(Me₄N₃)Ir(μ-N)Ir(Me₄N₃)]$^+$ (98%); simulated: 1136.4 [(Me₄N₃)Ir(μ-N)Ir(Me₄N₃)]$^+$ (98%). **EA** calculated for $C_{50}H_{54}Ir_2N_7$: C 52.80%; H 4.79%; N 8.62%; found: C 52.70%; H 4.39%; N 9.00%

8. Synthesis of $^{tBu}Ir_2N$

To a cooled solution (-35 °C) of 30 mg (19 μmol) $^{tBu}Ir_2N^{+}BPh_4{}^{-}$ in 5 ml THF was added 40 μl (40 μmol) of a 1M THF solution of **NaHBEt₃** diluted in 5 ml THF. After one hour stirring at room temperature the color changed from burgundy red to deep violet. After filtering off a solid precipitate, the filtrate was evaporated to dryness in vacuum, then 3x co-evaporated with n-pentane. After drying in vacuum for 4 hours a violet powder was obtained. Yield 21 mg (17 μmol, 95 %). **^{1}H NMR (400 MHz, RT, C_6D_6): δ [ppm]** = 150.89 (vbs, ω$_{1/2}$ 400 Hz (1.0 ppm), 6H, NC–CH_3)); 15.35 (bs, 2H, ω$_{1/2}$ 11 Hz (0.028 ppm), C$_{py}H$(3,5)); 13.00 (d, 4H, ^3J = 8 Hz, C$_{arom}H$(3,5)); 4.91 (s, 12H, CH_3); 4.36 (t, 2H, ^3J = 8 Hz, C$_{arom}H$(4)); 3.34 (s, 9H, C$_{py}$CCH_3). Susceptibility by Evans method: ν = 300 MHz, Δf = 12 Hz, c($^{tBu}Ir_2N$) = 8.6 mM, Q = 2 (superconducting magnet factor), T = 293 K, , μ$_{eff}$ = 3.03 μ$_B$. **MS (ESI/THF): [m/z]** =

1250.5 $[(Me_4N_3)Ir(\mu-N)Ir(Me_4N_3)]^+$ (100%). **EA** calculated for $C_{58}H_{70}Ir_2N_7$: C 55.74%, H 5.65%, N 7.85%, found: C 55.87%, H 5.71%, N 8.14%

Comproportionation of $^{tBu}Ir_2N^{+BPh4-}$ and $^{tBu}IrN_2^{-Na+}$ to $^{tBu}Ir_2N$

To a solution of 20 mg (16 μmol) $^{tBu}Ir_2N^{-Na+}$ in 0.4 ml THF-d_8 was a solution of 22 mg (16.5 μmol) $^{tBu}Ir_2N^{+BPh4-}$ in 0.4 ml THF-d_8 added (in portions of 0.1 ml). Complete conversion was determined by **^{1}H NMR** (1:1 ratio, see Figure S20).

Alternative with Cobaltocene [Cp$_2$Co] or TDAE ((NMe$_2$)$_2$C=C(NMe$_2$)$_2$):

To a solution of 14 mg (8.8 μmol) $^{tBu}Ir_2N^{+BPh-}$ in 0.4 ml THF-d_8 was added a solution of 2 μL (5 μmol) TDAE in 0.4 ml THF-d_8. Complete conversion was determined by **^{1}H NMR**.

To a solution of 10 mg (6.4 μmol) $^{tBu}Ir_2N^{+BPh-}$ in 0.4 ml THF-d_8 was added a solution of 2.5 mg (13 μmol) **[Cp$_2$Co]** in 0.4 ml THF-d_8. Complete conversion was determined by **^{1}H NMR**. No consecutive reaction to $^{tBu}Ir_2N^-$ was observed.

9. Synthesis of Ir$_2$N^{-Na+}

To a solution of 22 mg (19 μmol) **Ir$_2$N** in 5 ml THF was added a solution of 7 mg (38 μmol) **NaN(SiMe$_3$)$_2$** in 5 ml THF. The mixture was stirred for 20 min at room temperature and the solvent was removed in vacuum. After recrystallization from THF/pentane and drying in vacuum a violet powder was obtained. Yield: 23 mg (18.6 μmol, 98%). **UV/vis λ_{max}(THF) [nm]** = 380, 450 (shoulder), 550 (intensive), 880 (broad). **^{1}H-NMR (300 MHz, THF-d_8): δ [ppm]** = 8.16 (d, 2H, ^3J = 7.5 Hz C$_{py}H$(3,5)); 6.50 (t, 1H, ^3J = 7.5 Hz C$_{py}H$(4)); 6.58 (s, 6H, C$_{arom}H$(3,4,5)). 1.86 (s, 6H, NC–CH_3); 1.40 (s, 12H, CH_3). **^{13}C{^{1}H}-NMR (100 MHz, C$_6D_6$) δ [ppm]** = 150.1 (NC–CH$_3$); 147.0 (C_{py}(2,6)); 145.6 (C_{arom}(1)); 138.9 (C_{arom}(2,6)); 128.9 (C_{arom}(3,5)); 112.0 ((C_{py}(4)); 128.9 (C_{arom}(4)); 118.7 (C_{py}(3,5)); 18.4 (CH_3); 15.9 (NC–CH_3). **MS (ESI/THF): [m/z]** = 1164.6 $[(Me_4N_3)Ir(\mu-N)Ir(Me_4N_3)]^-$ (100%). **EA** calculated for $C_{50}H_{54}Ir_2N_7Na$: C 51.75%; H 4.69%; N 8.45%, found.: C 51.69%; H 4.52%; N 8.48%

10. Synthesis of $^{tBu}Ir_2N^{-Na+}$

To a solution of 21 mg (19 μmol) $^{tBu}Ir_2N$ in 5 ml THF was added a solution of 7 mg

(38μmol) **NaN(SiMe₃)₂** in 5 ml THF. The mixture was stirred for 20 min at room temperature, then the solvent was removed in vacuum. After recrystallization from THF/pentane a violet powder was obtained, which was dried in vacuum. Yield: 22 mg (17 μmol; 94 %). **¹H-NMR (300 MHz, THF-d₈): δ [ppm]** = 2.14 (s, 6H, NC–C*H₃*); 8.30 (s, 2H, C$_{py}$*H*(3,5)); 6.62 (s, 6H, C$_{arom}$*H*(3,4,5)); 1.48 (s, 12H, C*H₃*); 1.53 (s, 9H, C(C*H₃*)₃). **EA** calculated for C₅₈H₇₀Ir₂N₇Na: C 54.74%; H 5.54%; N 7.70% , found: C 54.03%; H 5.43%; N 8.07%.

c) X-ray Crystallographic Studies

General

Crystals of $Ir_2N_3^{+OTf-}$, Ir_2N^{+OTf-}, $^{tBu}Ir_2N^{+BPh4-}$ and Ir_2N^{-Na+} suitable for X-ray structural determinations were mounted in polybutene oil on a glass fibre and transferred on the goniometer head to the precooled instrument. Crystallographic measurements were carried out on:

Bruker AXS smart APEX 3-circle single-crystal diffractometer equipped with

- APEX I CCD detector

- molybdenum source Incoatec Microfocus Source IμS™ (30 watts, air cooling)

- cryostream nitrogen flow cooling, 100-300 K (Oxford Cryosystems)

SuperNova 4-circle single-crystal diffractometer from Oxford Diffraction

- molybdenum and copper source (dual unit), microfocus tubes

- cryostream-700 plus-nitrogen flow cooling, 100 - 500 K (Oxford Cryosystems)

The structures were solved by direct methods and refined against F^2 by full matrix least squares (SHELX97)[S9] using all unique data. All non-hydrogen atoms were refined with isotropic thermal parameters unless otherwise reported; the carbon bound hydrogen atoms were placed in geometrically calculated positions and refined using a riding model. Molecular graphics were prepared using ORTEP3.[S10] Details of the data collection and refinement are given below.

The asymmetric unit of the crystal structure of complex $Ir_2N_3^{+OTf-}$ contains one co-crystallized toluene molecule.

In the asymmetric unit of the crystal structure of complex Ir_2N^{+OTf-} the nitrido nitrogen atom N4 is located on special positions (2-fold rotational axis, 2). The OTf has s.o.f. converged at 0.5 (value was checked). Furthermore, the asymmetric unit of the crystal structure of complex Ir_2N^{+OTf-} contains 1/4 co-crystallized THF and 1/8 co-crystallized ether molecule on a special position. Both have a s.o.f. of 0.5 and were refined with anisotropic thermal parameters.

The asymmetric unit of the crystal structure of complex $^{tBu}Ir_2N^{+BPh4-}$ contains one co-crystallized THF on two sites and a half co-crystallized hexane molecule. Both are disordered and have a s.o.f. of 0.5, which were refined with isotropic thermal parameters. The bond lengths and angles of THF and hexane were restrained to a suitable geometry.

Table S1: Selected distances and angles for compounds $\mathbf{Ir_2N_3^{+OTf-}}$, $\mathbf{Ir_2N^{+OTf-}}$ and $\mathbf{Ir_2N^{-Na+}}$.

↓ parameter \ compound →	$\mathbf{Ir_2N_3^{+OTf-}}$		$\mathbf{Ir_2N^{+OTf-}}$ [a]		$\mathbf{Ir_2N^{-Na+}}$	
	Ir1	**Ir2**	**Ir1**	**Ir1**[i]	**Ir1**	**Ir2**
distances Ir-$N_{azido,nitrido}$ [Å]	1.992(7)	1.971(8)	1.8067(3)		1.8450(23)	1.8380(23)
angle (Ir-$N_{nitrido}$-Ir) [°]	-		167.3(2)		156.3(1)	
distance C_{py}-C_{imi} [Å]						
C9-C11 C41-C40	1.469(12)	1.479(11)	1.4370(33)		1.4171(41)	1.4154(43)
C15-C16 C34-C36	1.428(12)	1.463(11)	1.4357(37)		1.4095(40)	1.3993(41)
distance C_{imi}-N_{imi} [Å] [b]						
N1-C9 N9/7-C41	1.322(11)	1.299(10)	1.3357(37)		1.3432(37)	1.3421(37)
N3-C16 N7/5-C34	1.306(11)	1.322(9)	1.3285(34)		1.3623(35)	1.3696(37)

[a]The $N_{nitrido}$ nitrogen atom is located on a special position (2-fold rotational axis).

[b]for labeling see Figures S2, S3 and S5.

Table S2: Summary of crystal data and structure refinement[†] for **Ir$_2$N$_3$$^{+OTf-}$**, **Ir$_2$N^{+OTf-}**, **^{tBu}Ir$_2$N^{+BPh4-}** and **Ir$_2$N^{-Na+}**.

	Ir$_2$N$_3$$^{+OTf-}$	**Ir$_2$N^{+OTf-}**	**^{tBu}Ir$_2$N^{+BPh4-}**	**Ir$_2$N^{-Na+}**
Chemical formula	C$_{58}$H$_{62}$Ir$_2$N$_9$O$_3$S	C$_{54}$H$_{60.5}$F$_3$Ir$_2$N$_7$O$_{3.75}$S	C$_{180}$H$_{202}$B$_2$Ir$_4$N$_{14}$O	C$_{54}$H$_{62}$Ir$_2$N$_7$ONa
Formula Mass	1406.63	1341.05	3368.11	1232.50
Crystal system	monoclinic	monoclinic	monoclinic	Monoclinic
Space group	$P2_1$/c (Nr. 14)	$C2$/c (No.15)	$P2_1$ (No.4)	$P2_1$/n (No.14)
a [Å]	18.049(3)	23.7205(6)	11.8882(3)	10.693(1)
b [Å]	15.450(3)	15.3311(4)	23.2366(5)	26.427(2)
c [Å]	20.890(4)	16.5083(4)	15.1330(3)	16.8108(1)
β [°]	97.103(3)	122.479(1)	95.974(10)	94.351(7)
Unit cell volume [Å^3]	5780.6(19)	5064.4(2)	4157.7(2)	4736.8(2)
Temperature [K]	153(2)	100(2)	100(2)	100(2)
Z	4	2	2	2
Detector type[†]	CCD	CCD	CCD	CCD
Radiation type	MoKα	MoKα	MoKα	MoKα
Reflections measured	61202	63622	105248	62794
Independent reflections	11346	9158	29402	11211
Ind. reflections ($I > 2\sigma(I)$)	6968	7646	24963	9875
Data/ restraints / parameter	11346/2/696	9158/0/375	29402/8/909	11211/0/598
θ_{max} [°] / completeness	2.14-26/0.999	2.04-32.5/0.999	2.04-32.5/0.998	2.88-28/0.98
R_{int}	0.1442	0.0327	0.0510	0.0360
Final R_1 values ($I > 2\sigma(I)$)	0.0521	0.0243	0.0423	0.0220
Final $wR(F^2)$ values ($I > 2\sigma(I)$)	0.0850	0.0569	0.0873	0.0455
Final R_1 values (all data)	0.1024	0.0342	0.0570	0.0296
Final $wR(F^2)$ values (all data)	0.0959	0.0638	0.0980	0.0489
Goodness of fit on F^2	0.877	1.116	1.062	1.059
Max / min $\Delta\rho$ [e Å^{-3}]	-1.641/1.340	-0.771/2.511	-1.746/2.235	-0.714/1.426
Flack parameter	-	-	0.003	-

[†]: see general section above for details
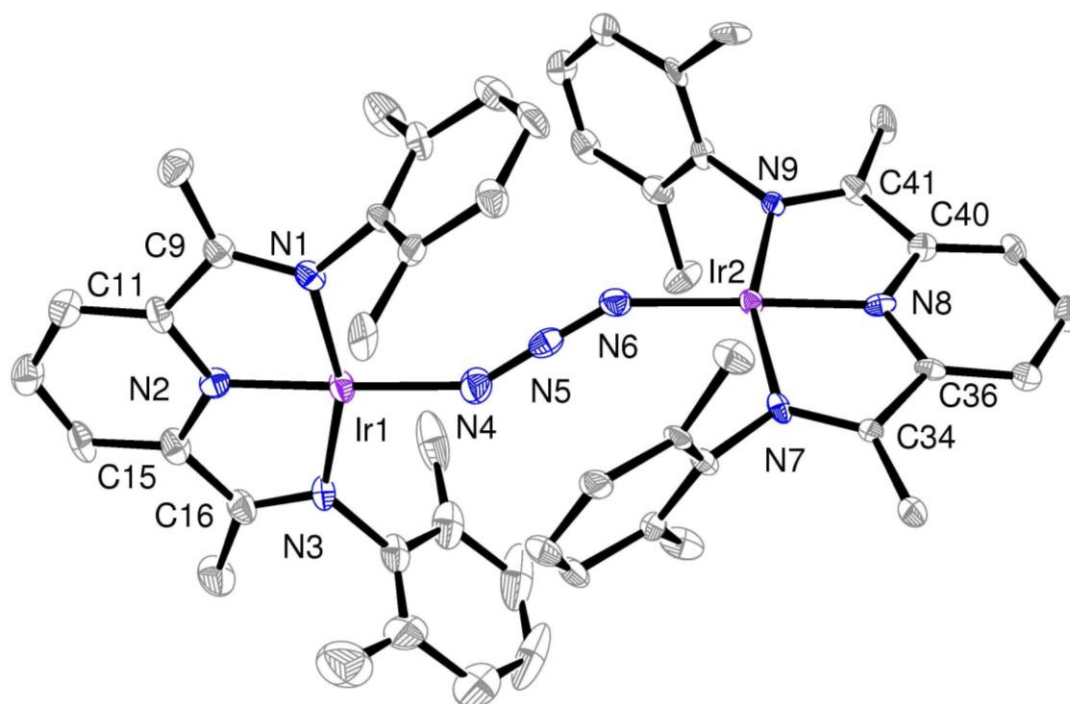
Figure S2: Ortep representation of **Ir₂N₃$^{+OTf-}$** with anisotropic displacement parameters shown at the 50% probability level. Hydrogen atoms and the co-crystallized solvent molecule (toluene) are omitted for clarity. Selected bond lengths [Å] and angles [°] with esd's in parentheses: Ir1-N1 1.972(7), Ir1-N2 1.858(7), Ir1-N3 1.992(7), Ir1-N4 1.956(9), N4–N5 1.204(10), N6–N5 1.175(10), Ir2-N6 1.971(8), Ir2–N7 1.991(7), Ir2-N8 1.867(7), Ir2-N9 2.003(7), N1–C9 1.322(11), C9-C11 1.469(12), N2–C15 1.3879(10), C15-C16 1.428(12), N3–C16 1.306(11), N7–C34 1.322(9), C34-C36 1.463(11), N8-C36 1.343(9), N9-C41 1.299(10), C41-C40 1.479(11), N1–Ir1–N2 79.7(3), N7–Ir2–N8 79.6(3), N3–Ir1–N2 79.3(3), N9–Ir2–N8 79.6(3), N3–Ir1–N4 101.8(3), N7–Ir2–N6 99.9(3), N1–Ir1–N4 99.2(3), N9–Ir2–N6 100.8(3), Ir1–N4–N5 149.0(7), N8–Ir2–N6 178.4(3), N4–N5–N6 178.7(10); Angle between the planes Ir1N1N2N3–Ir2N8N7N9 75.7(2).
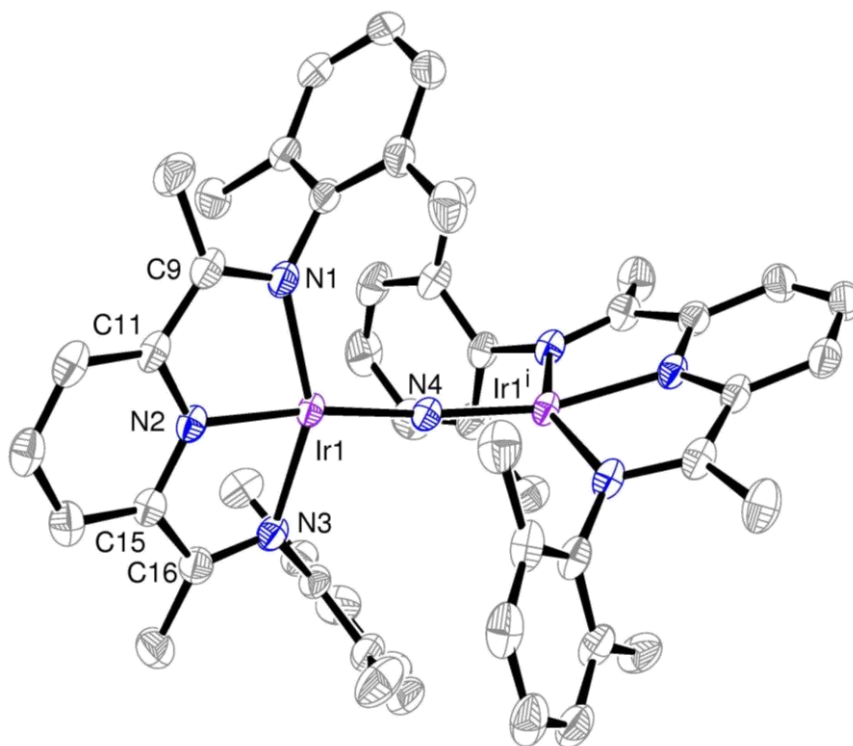
Figure S3: Ortep representation of **Ir₂N⁺OTf⁻** with anisotropic displacement parameters shown at the 50% probability level. Hydrogen atoms are omitted for clarity. Selected bond lengths [Å] and angles [°] with esd's in parentheses: Ir1-N1 2.0710(21); Ir1-N2 1.9725(21); Ir1-N3 2.0215(21); Ir1-N4 1.8067(3); Ir1-Ir2 3.59; C9-N1 1.3375(33); C9-C11 1.4370(33); N2-C11 1.3669(31); N2-C15 1.3724(34); C16-C15 1.4357(37); C16-N3 1.3285(34); Ir1-N4-Ir[i] 167.3(2); N2-Ir1-N4 165.8(1); N1-Ir1-N3 151.9(1); N3-Ir1-N4 100.2(1); N1-Ir1-N4 107.7(1); N1-Ir1-N2 77.0(1); N3-Ir1-N2 77.1(1).
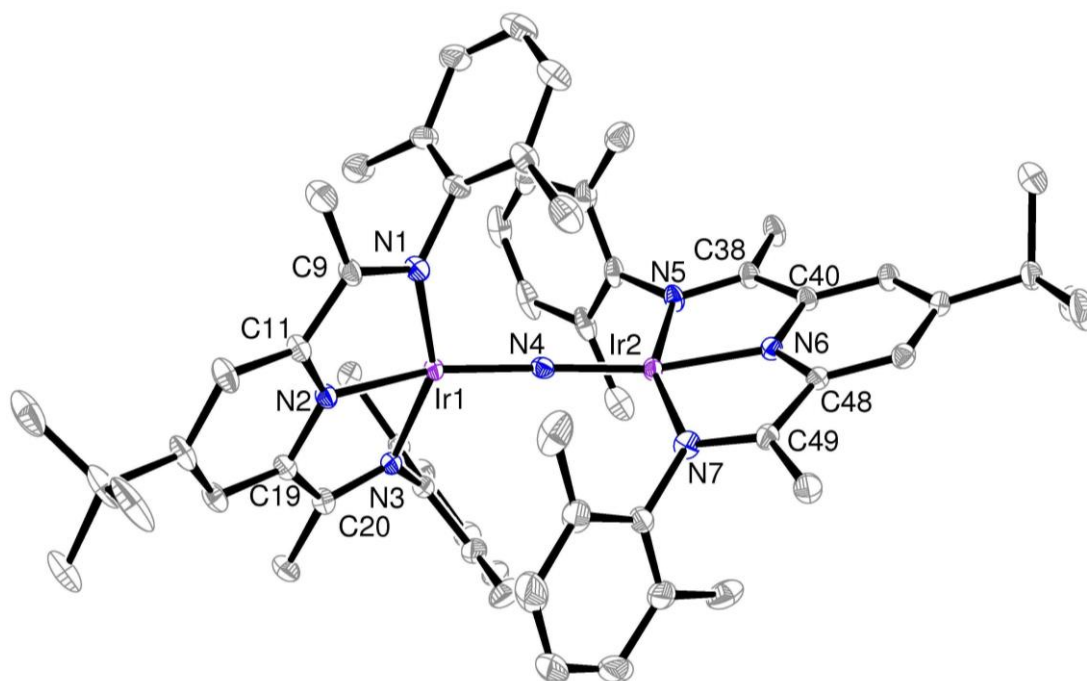
Figure S4: Ortep representation of $^{Bu}Ir_2N^{+BPh4-}$ with anisotropic displacement parameters shown at the 50% probability level. Hydrogen atoms and the co-crystallized solvent molecules (THF/hexane) are omitted for clarity. Selected bond lengths [Å] and angles [°] with esd's in parentheses: Ir1-N1 2.0460(41); Ir1-N2 1.9682(40); Ir1-N3 2.0481(43); Ir1-N4 1.7969(44); Ir2-N5 2.0290(40); Ir2-N6 1.9568(39); Ir2-N7 2.0532(38); Ir2-N4 1.7949(45); Ir1-Ir2 3.562; C9-N1 1.3137(63); C9-C11 1.4367(70); N2-C11 1.3680(67); N2-C19 1.3686(61); C19-C20 1.4611(73); C20-N3 1.3321(65); C49-N7 1.3264(66); C49-C48 1.4459(69); N6-C40 1.3733(61); N6-C48 1.3715(66); C38-C40 1.4411(68); C38-N5 1.3403(62); Ir1-N4-Ir2 165.3(3); N2-Ir1-N4 159.5(2); N1-Ir1-N3 152.1(2); N3-Ir1-N4 104.7(2); N1-Ir1-N4 103.2(2); N1-Ir1-N2 77.3(2); N3-Ir1-N2 77.2(2); N5-Ir2-N6 78.0(2); N7-Ir2-N6 77.3(2); N5-Ir2-N4 99.4(2); N7-Ir2-N4 105.6(2); N6-Ir2-N4 168.9(2); N5-Ir2-N7 154.8(2).
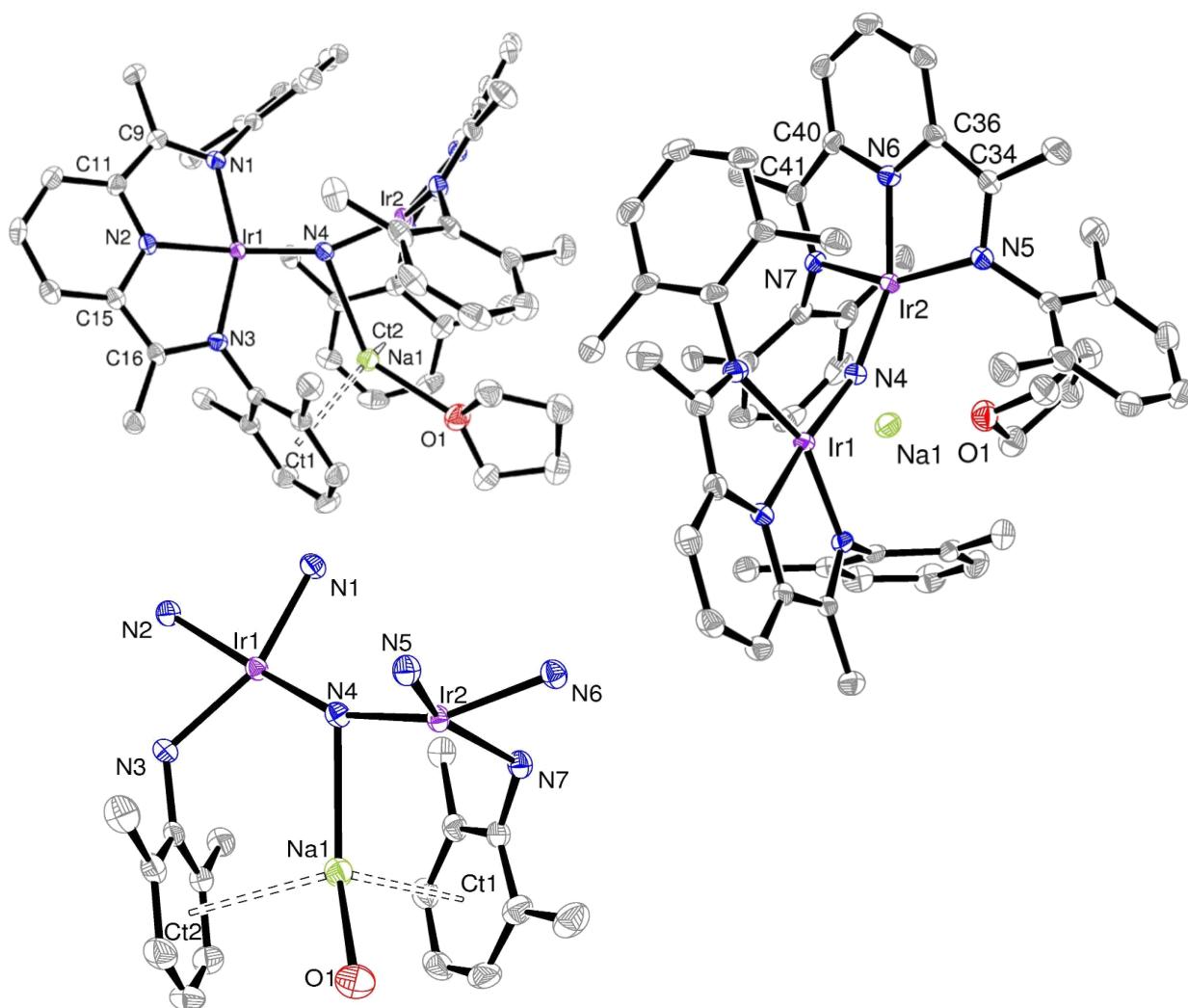
Figure S5: Ortep representations (different orientations. top) of **Ir₂N⁻ᴺᵃ⁺ 5** with anisotropic displacement parameters shown at 50% probability level (right; sodium contacts omitted for clarity). The bottom view shows sodium bound positions. Hydrogen atoms are omitted for clarity. Selected bond lengths [Å] and angles [°] with esd's in parentheses: Ir1-N1 2.0382(24); Ir1-N2 1.9366(23); Ir1-N3 2.0111(23); Ir1-N4 1.8450(23); Ir2-N4 1.8380(23); Ir2-N5 2.0250(24); Ir2-N6 1.9340(24); Ir2-N7 2.0250(24); Ir1-Ir2 3.601; Na-N4 2.6102(27); C9-N1 1.3432(37); C9-C11 1.4171(41); N2-C11 1.3928(37); N2-C15 1.4009(36); C16-C15 1.4095(40); C16-N3 1.3623(35); C34-N5 1.3696(37); C34-C36 1.3993(41); N6-C36 1.3955(38); N6-C40 1.3972(37); C40-C41 1.4154(43); C41-N7 1.3421(37); Ir1-N4-Ir2 156.3(1); N2-Ir1-N4 169.9(1); N6-Ir2-N4 152.9(1); N1-Ir1-N3 155.1(1); N5-Ir2-N7 153.6(1); N3-Ir1-N4 103.0(1); N7-Ir2-N4 100.3(1); N1-Ir1-N4 102.0(1); N5-Ir2-N4 106.1(1); N1-Ir1-N2 77.6(1); N5-Ir2-N6 78.5(1); N2-Ir1-N4 170.0(1); N6-Ir2-N4 152.9(1).

d) Spectroscopic Characterization

UV-vis spectroscopy
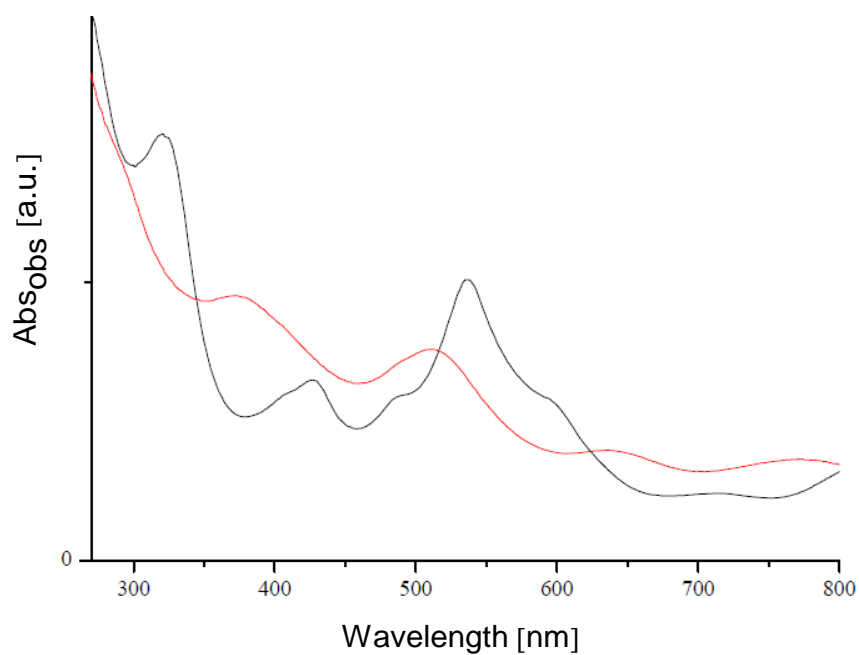
Figure S6: UV/vis spectrum (THF) of $\textbf{Ir}_2\textbf{N}_3{}^{+\textbf{Al-}}$ (black line) and $\textbf{Ir}_2\textbf{N}^{+\textbf{Al-}}$ (red line).
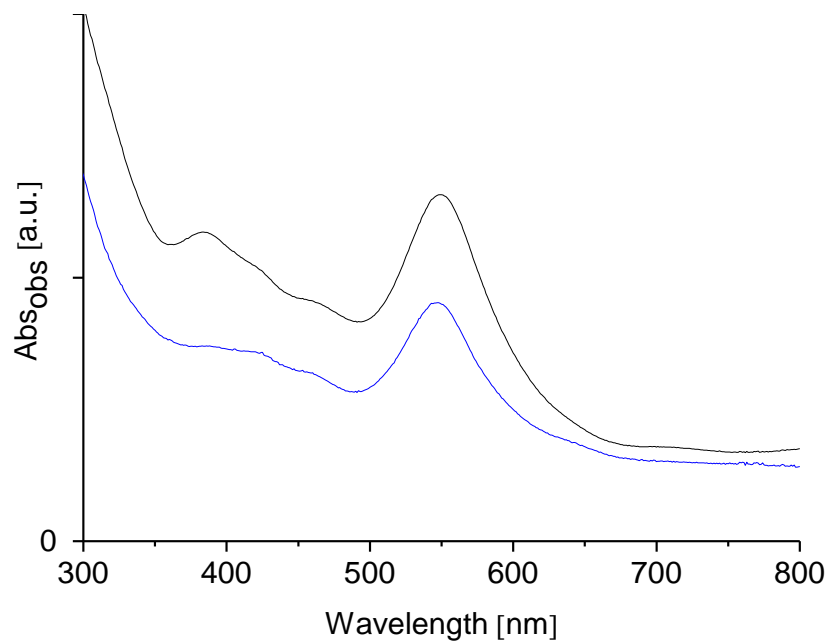
Figure S7: UV/vis spectrum (pentane) of $^{\textbf{tBu}}\textbf{Ir}_2\textbf{N}$ (blue line) and $^{t\textbf{Bu}}\textbf{Ir}_2\textbf{N}^{-\textbf{Na+}}$ (black line)**.**

NMR-Spectra
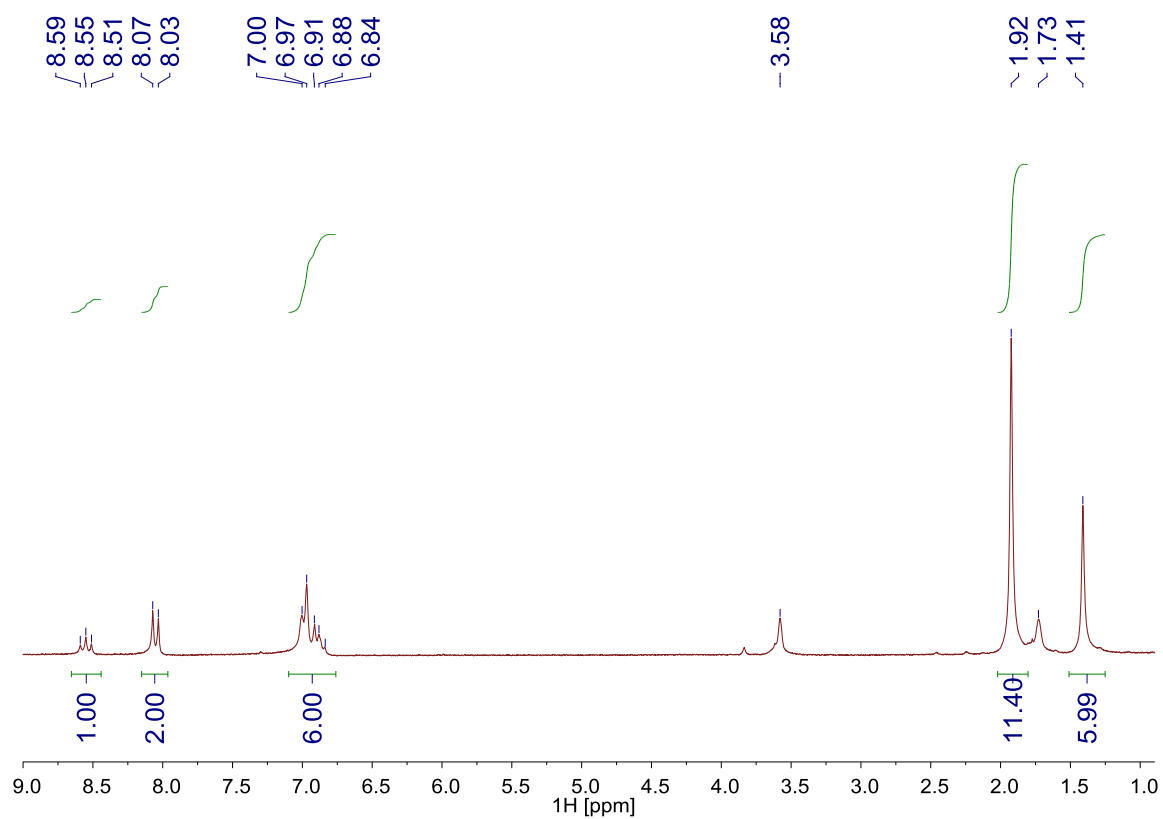
Figure S8: ^{1}H NMR spectrum (400 MHz, THF-d$_8$) of **Ir$_2$N$_3$$^{+OTf-}$**.

Figure S9: ^{1}H NMR spectrum (400 MHz, RT, THF-d$_8$) of **Ir$_2$N^{+OTf-}**.

Figure S10: ^{1}H NMR spectrum (400 MHz; THF-d$_8$) of **Ir$_2$N$_3$$^{+Al-}$**.
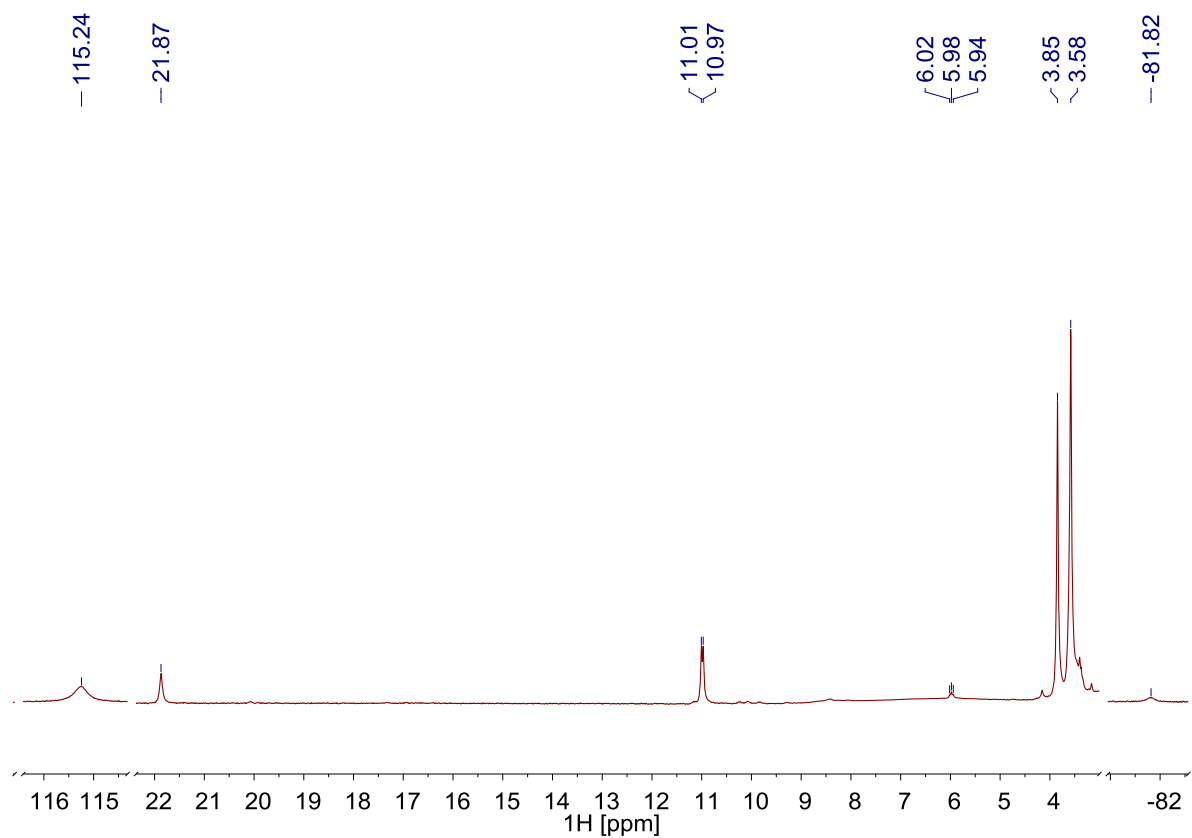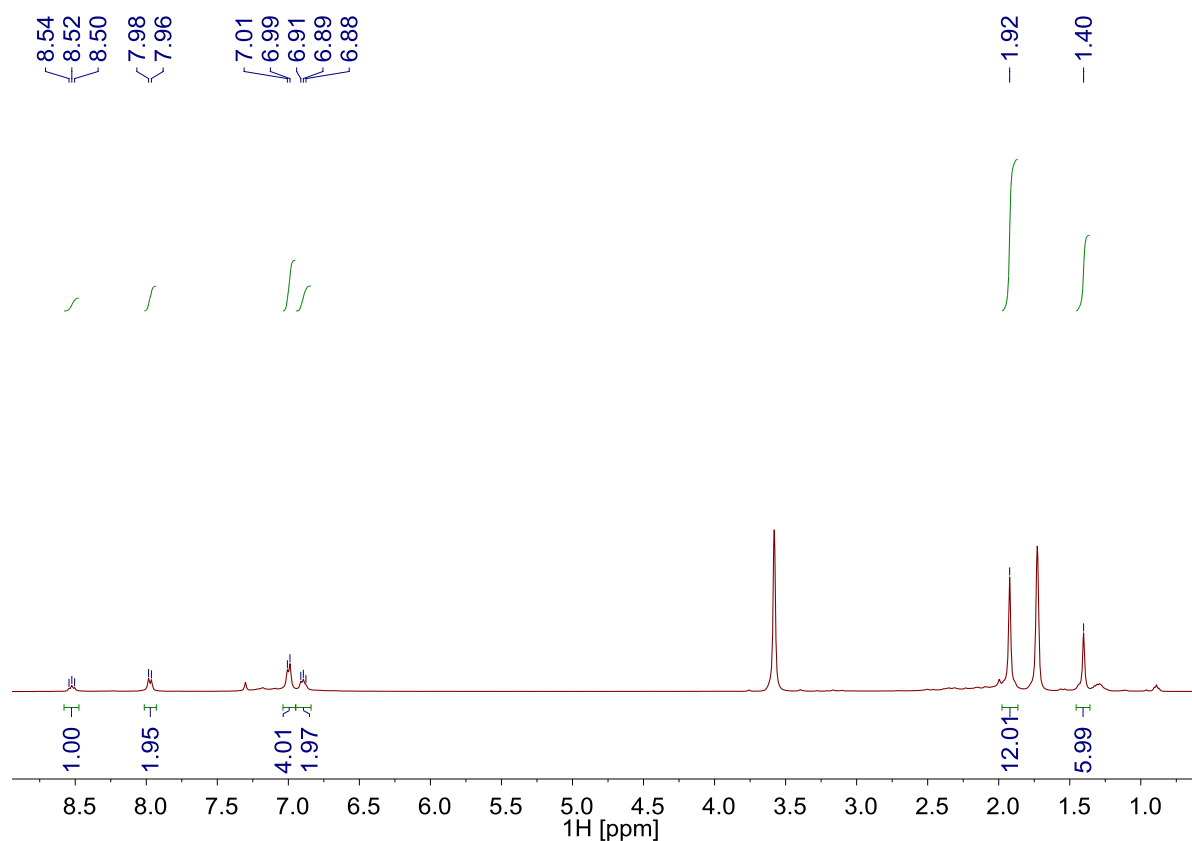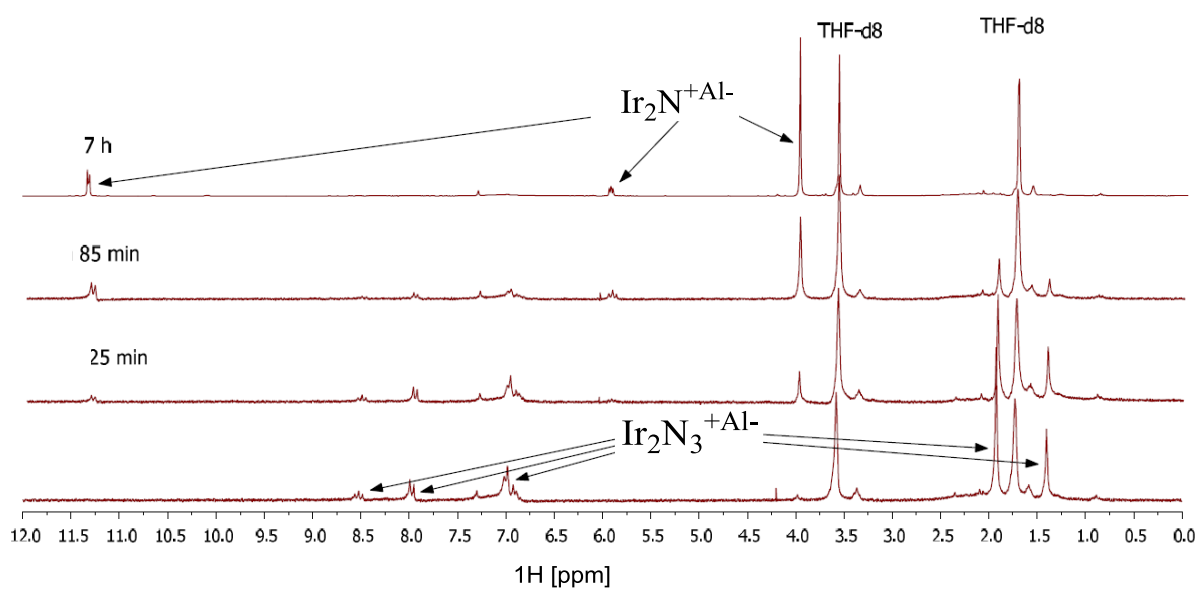
Figure S11: ^{1}H NMR spectrum (400 MHz, RT THF-d$_8$) after 25 min, 85 min, 7 h photolysis with blue light: **Ir$_2$N$_3$$^{+Al-}$** → **Ir$_2$N^{+Al-}**.

Figure S12: ^{1}H-NMR (400 MHz; THF-d$_8$) of **Ir$_2$N^{+Al-}** at RT.

Figure S13: vT ^{1}H-NMR spectrum (400 MHz; THF-d$_8$) of **Ir$_2$N^{+Al-}** in the temperature range between 183 K and 313 K.

Table S3: vT ^{1}H-NMR shifts (δ [ppm]) of **Ir$_2$N$^{+Al\text{-}}$** between 183 K and 313 K.

T [K]	H1 (12H)	H2 (4H)	H3 (8 H)	H4 (4 H)	H5 (24 H)	H6 (2 H)
183	92.72	20.74	10.31	6.35	2.97	-66.72
193	98.41	20.94	10.49	6.25	3.17	-70.51
203	103.26	21.25	10.67	6.18	3.32	-74.00
213	107.83	21.60	10.81	6.13	3.46	-77.31
223	111.31	21.89	10.92	6.08	3.58	-79.97
233	114.73	22.19	11.04	6.04	3.66	-82.59
243	117.45	22.44	11.14	6.01	3.75	-84.67
253	119.51	22.62	11.21	5.99	3.82	-86.27
263	120.97	22.74	11.26	5.96	3.88	-87.41
273	121.87	22.80	11.29	5.95	3.92	-88.13
283	122.31	22.82	11.31	5.94	3.96	-88.50
293	122.36	22.80	11.32	5.93	3.98	-88.55
303	122.06	22.74	11.31	5.93	4.00	-88.34
313	121.51	22.65	11.28	5.92	4.01	-87.95

Fig. S14. Non-linear Curie-Weiss dependence of the ^{1}H-NMR resonances for the protons in complex **Ir$_2$N^{+Al-}**.

Fig. S15. Fits to the Van-Vleck equation (S=1 ⇆ S=0) of the ^{1}H-NMR shifts in **Ir$_2$N^{+Al}**.

The plots of the temperature dependent ^{1}H NMR resonances of complex **Ir$_2$N^{+Al}** presented in Fig. S16 were fitted to a S=0 ⇆ S1 spin equilibrium using the equation developed by Horrocks[S11] et al., which is shown below. The fitting curves are presented as red lines in Fig. S15.

$$H_{obs} = H_{dia} + \frac{H_O \cdot A \cdot g \cdot \beta \cdot (6 \cdot e^{-E/kT})}{(\gamma_H/2\pi) \cdot 3 \cdot k \cdot T \cdot (1 + 3 \cdot e^{-E/kT})}$$

H_{obs} and H_{dia} correspond to the observed and diamagnetic chemical shift (S=0), γ_e and γ_H are the gyromagnetic ratios of the electron and proton, β is the Bohr magneton, k is the Boltzmann constant, g is the g-factor of the unpaired electron, A is the hyperfine splitting constant of the observed proton, E is the singlet→triplet energy gap; a value of R ln3 corresponding to the electronic contribution for the entropy change is incorporated.

It has to be stressed that this treatment is only appropriate if the observed paramagnetic shifts can be solely attributed to a *contact-shift*, i.e., *through bond* term. This assumption was justified by the ^{1}H NMR resonances of a derivative of complex **Ir$_2$N^{+Al}**, which carried a mesityl

rather than a 2,6-Me$_2$-phenyl (ortho xylyl) substituent of the ketimine group. As anticipated for a contact-shift mechanism, the sign of the hyperfine splitting for the protons in the para position of the phenyl ring changed due to the incorporation of one further bond in the methyl substituted (mesityl) derivative.

With γ_e = -8.9412 10^{10} 1/Ts, γ_H = 4.78943 10^7 1/Ts, g = 2.00232, β = 9.27402 10^{-24} J/T, k = 1.38066 10^{-23} J/K, δ = (H-H(0))/H(0), A (T), H (J/mol) and T in K

$$\delta_{observed} = \delta_{dia} - 10^6 * 823.194 * A/(T*(1+exp((\Delta H - T*9.134)/(8.31451*T))))$$

is obtained, which was used for the non-linear curve fit using the commercial Origin program (ver. 9.0) package for the vT dependent ^{1}H NMR shifts shown in Fig. S16. The free fitting variables are δ_{dia}, A and ΔH.

The obtained fitting parameters are compiled in Table S3. The values derived for ΔH from the fits of the six independent ^{1}H NMR resonances H1 – H6 lie in a reasonably narrow range of 3975 – 4311 J/mol with an average value $\Delta H_{average}$ = 4075 kJ/mol (341 cm^{-1}). The fits for the diamagnetic chemical shifts δ_{dia} seem reasonable for protons H3-H6, for the methyl protons H1 the fitted parameters of δ_{dia} = -15 ppm deviates strongly from the anticipated value of δ_{dia} in the range (1-2 ppm.) This holds also to some extent for the meta-pyridine protons H2, for which δ_{dia} converged at 13 ppm and proton H6, which displays a large standard deviation for δ_{dia}. Some problems with the fits for these protons can be envisaged through inspection of the deviations of the fitting curves and the measured data in Fig. S15. This can be in parts attributed to the very broad signals for protons H1, H2 and H6, which leads to significant errors for the determination of their chemical shifts; it should be noted that the line broadening of these signals is also strongly temperature dependent. When the parameters for H1, H2 and H6 were constrained to their anticipated diamagnetic values in the non-linear curve fit, ΔH remained essentially unchanged at ~4000 J/mol, while notable changes were observed for the hyperfine splitting constants in these cases.

Table S3. Fit to the Van-Vleck equation for a S=0 ⇆ S1 equilibrium.

Proton	δ_{dia} (ppm)	A (MHz)	ΔH (J/mol)
H1	-15 ($\pm$5)	-130 $\pm$ 4)	3975 ($\pm$33)
H2	13 ($\pm$1)	-9 $\pm$ 1	4037($\pm$128)
H3	6.8($\pm$0.2)	-4 $\pm$ 0	4017($\pm$42)
H4	7.6($\pm$0.1)	2 $\pm$ 0	4086($\pm$45)
H5	0.5($\pm$0.1)	4 $\pm$ 0	4311($\pm$27)
H6	8.3($\pm$4.9)	95 $\pm$ 0	4033 ($\pm$48)

Figure S16: ^{1}H NMR spectrum (400 MHz; THF-d$_8$) of ^{tBu}**Ir$_2$N$_3$**$^{+BPh4-}$.

Figure S17: ^{1}H NMR spectrum (400 MHz, RT, THF-d$_8$) of ^{tBu}**Ir$_2$N**$^{+BPh4-}$.

Figure S18: ^{1}H NMR spectrum (400 MHz, RT, C_6D_6) of ^{tBu}Ir$_2$N.

Figure S19: vT ^{1}H-NMR spectrum (400 MHz; THF-d$_8$) of ^{tBu}Ir$_2$N in the temperature range of 183 – 323 K.

Figure S20: Curie-Weiss plots ($\Delta\delta$ [ppm] vs 1/T [1/K]) for $^{tBu}Ir_2N$ in THF-d_8. Linear dependence of the ^1H NMR shifts on reciprocal temperature for resonances at δ = 151.22 ppm, 15.62 ppm, 13.09 ppm and 4.39 ppm at RT. The signals at δ = 4.52 ppm and 3.52 ppm are overlapped by the resonances of the THF solvent.

Figure S21: ^1H NMR spectrum (400 MHz, RT, THF-d_8) of the comproportionation reaction $^{tBu}Ir_2N^{+BPh4-}$ + $^{tBu}Ir_2N^{-Na+}$ → $^{tBu}Ir_2N$.

Figure S22: ^{1}H NMR spectrum (400 MHz; THF-d$_8$) of **Ir$_2$N^{-}Na^{+}**.

Figure S23: ^{1}H NMR spectrum (400 MHz; THF-d$_8$) of **^{tBu}Ir$_2$N^{-}Na^{+}**.

Thermoanalysis: DTA/DTG/MS

Figure S24: DTA- and DTG-MS (heating rate 10K/min) for **Ir$_2$N$_3$$^{+Al-}$** (2% weight loss measured; calculated 2.1% for loss of N$_2$; see MS trace: m/z = 28 and m/2z = 14)
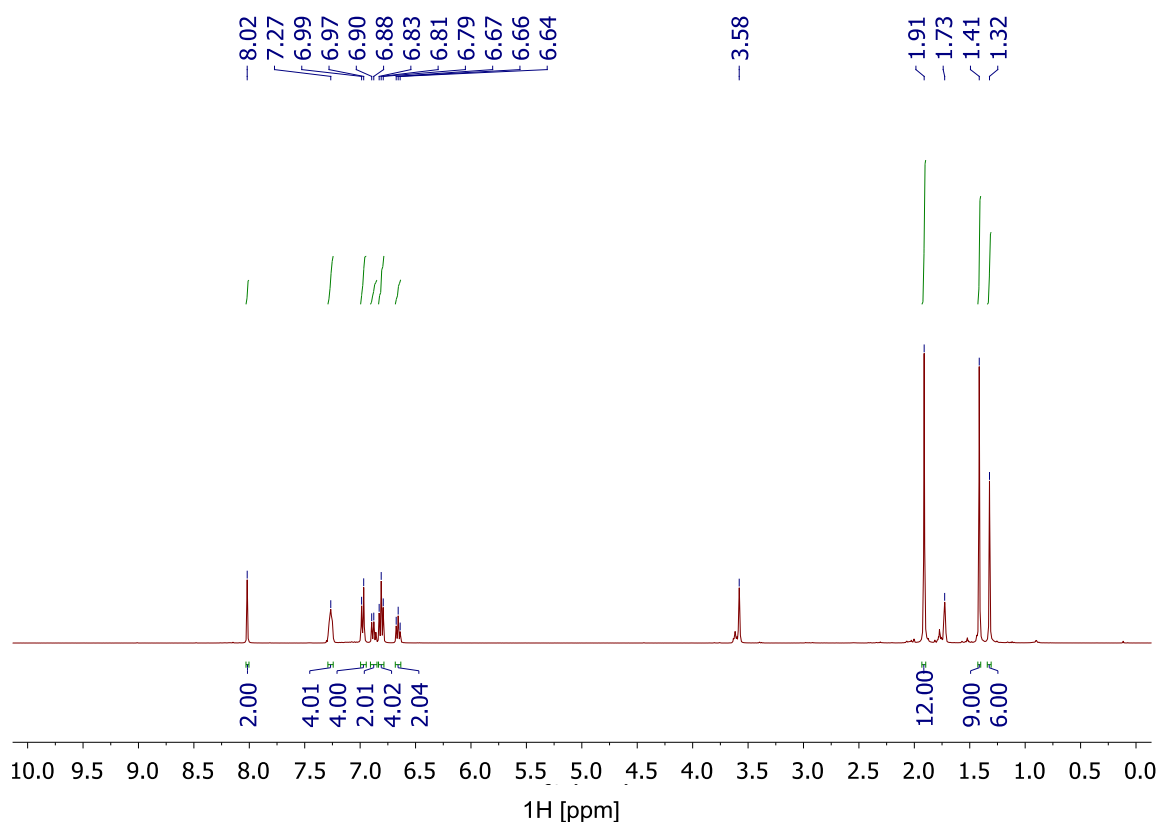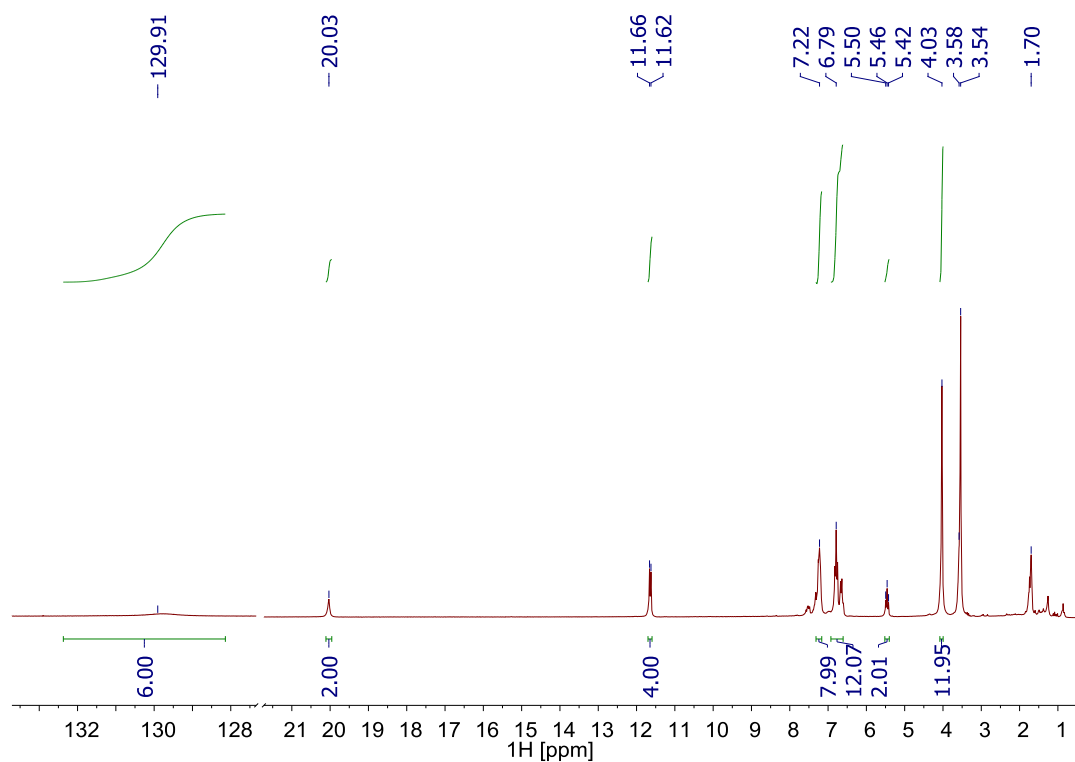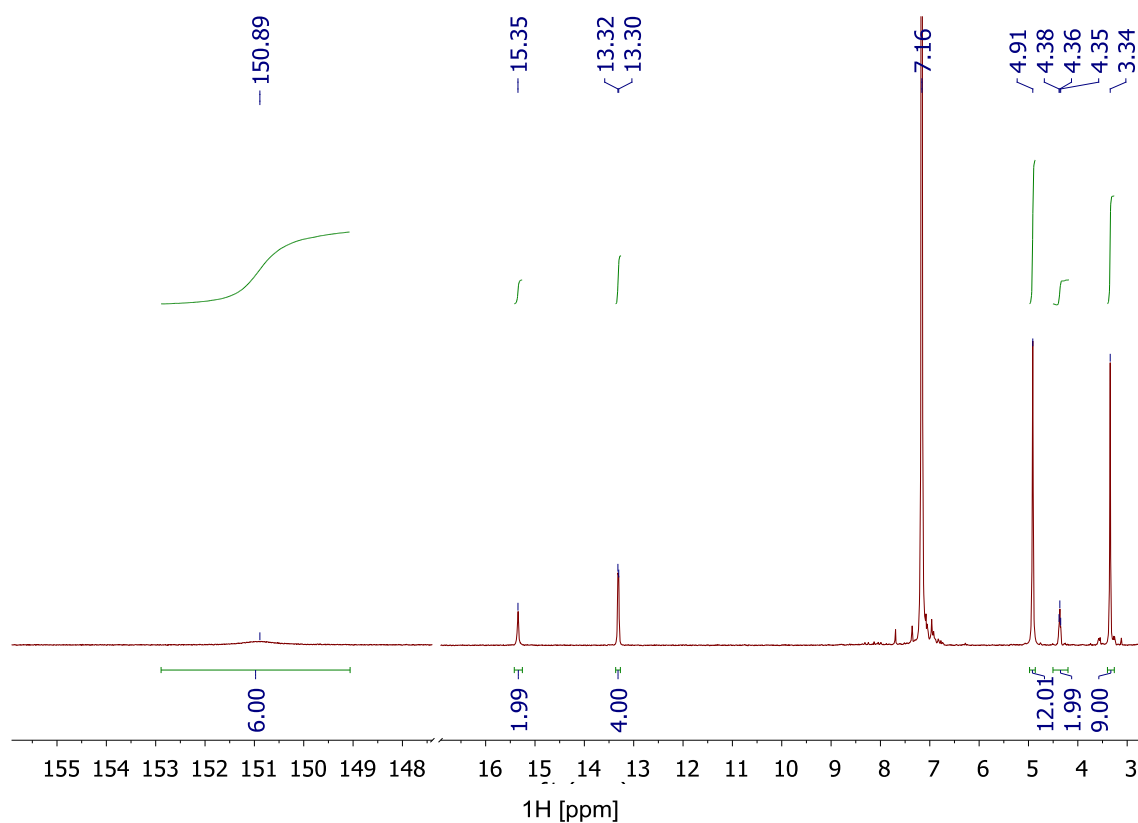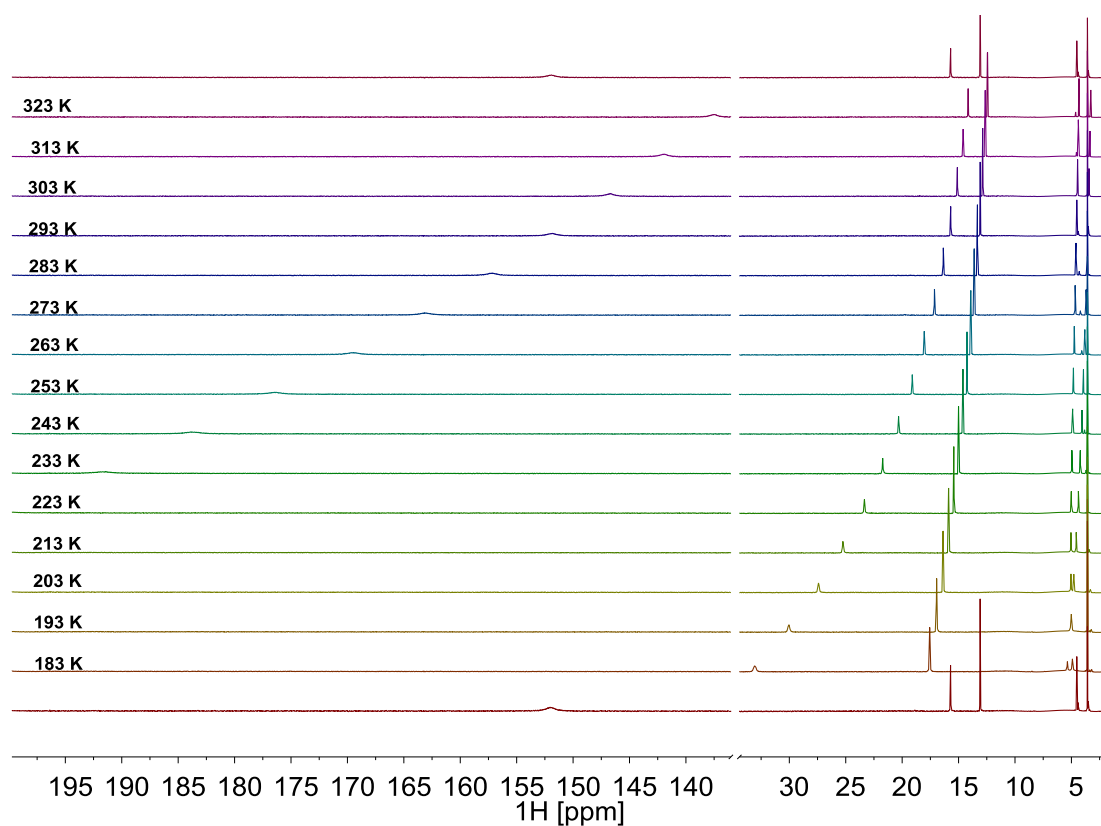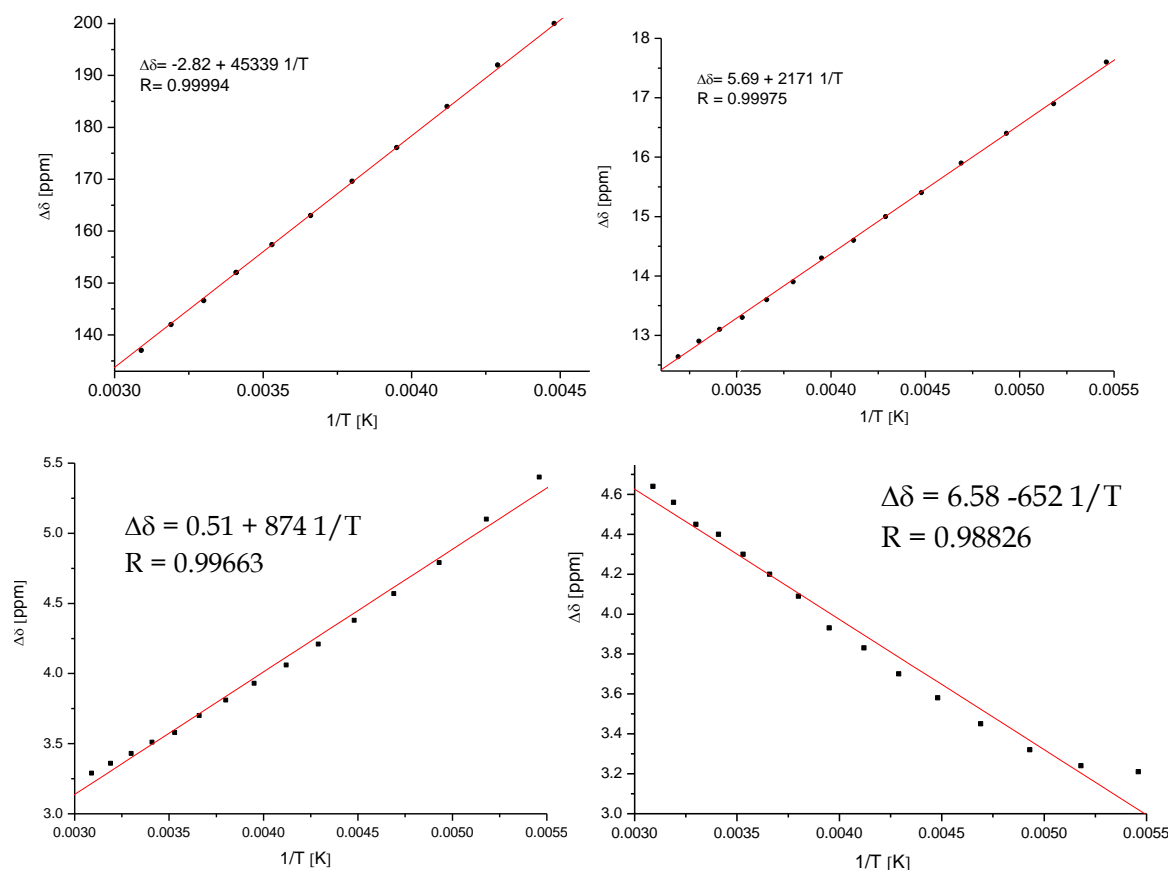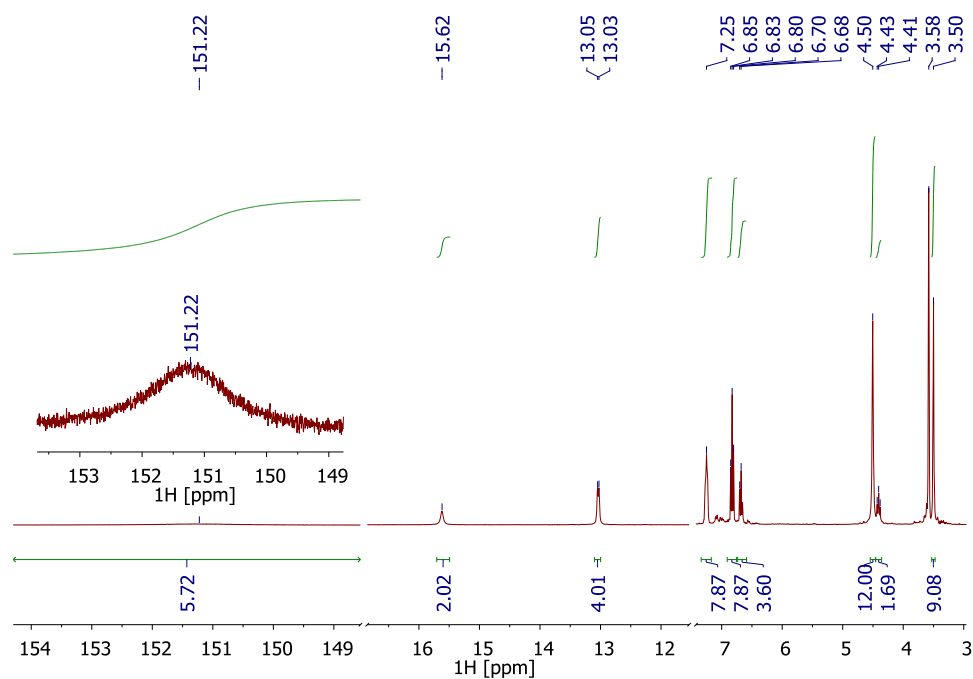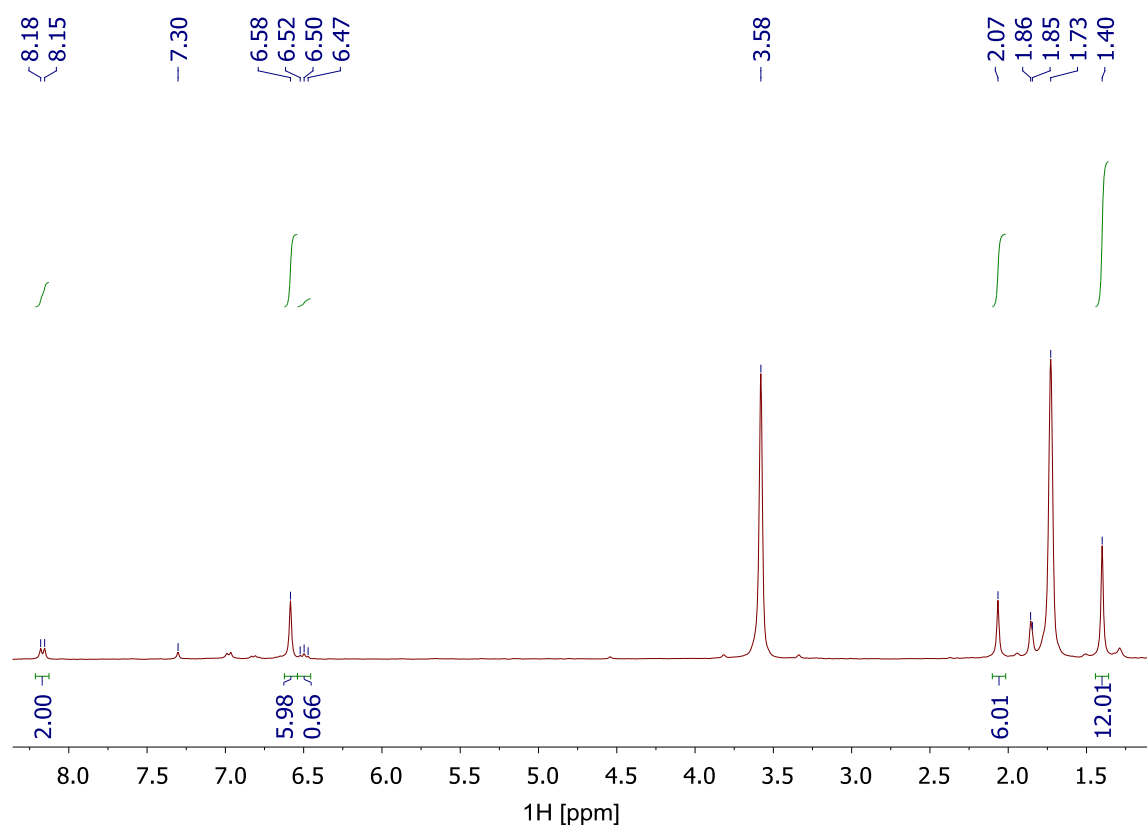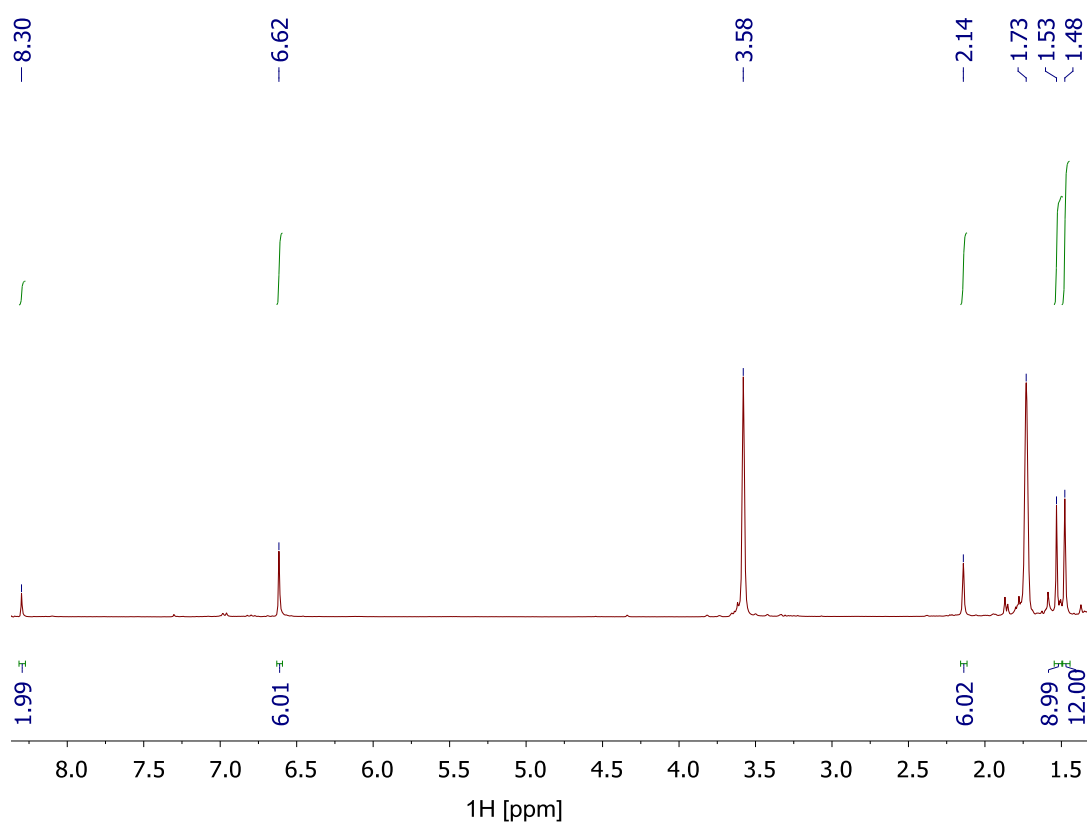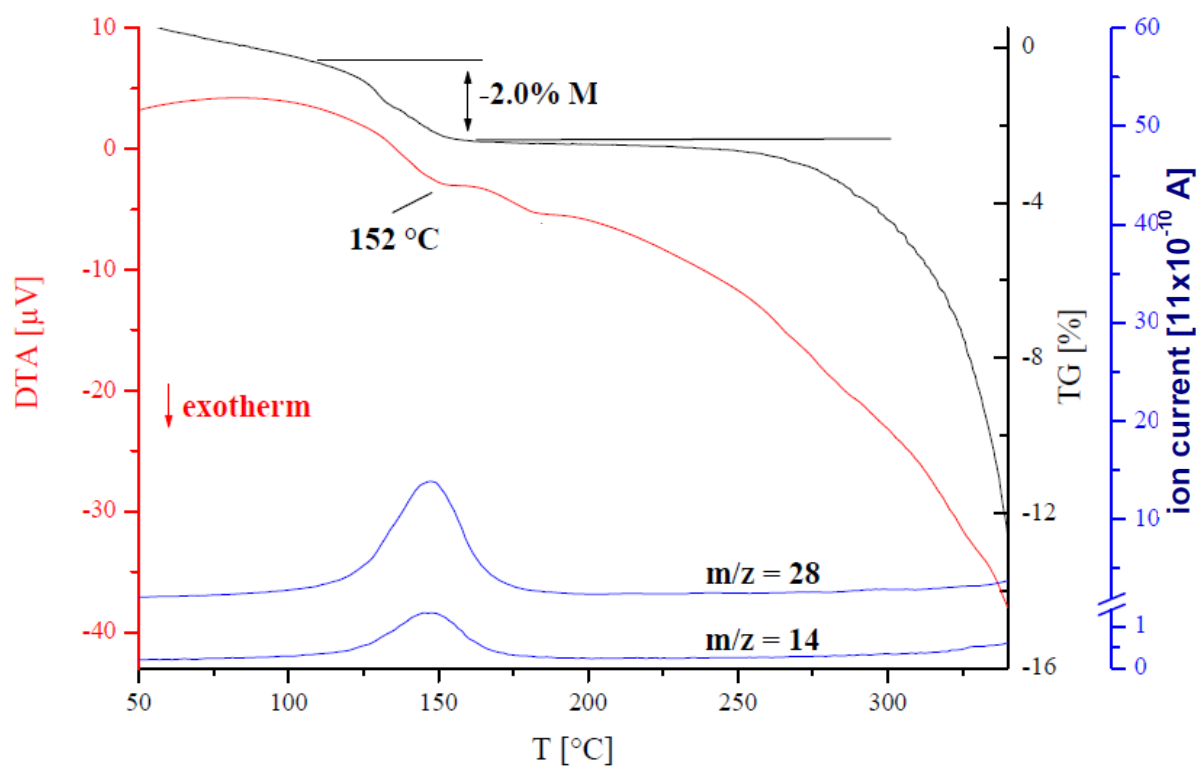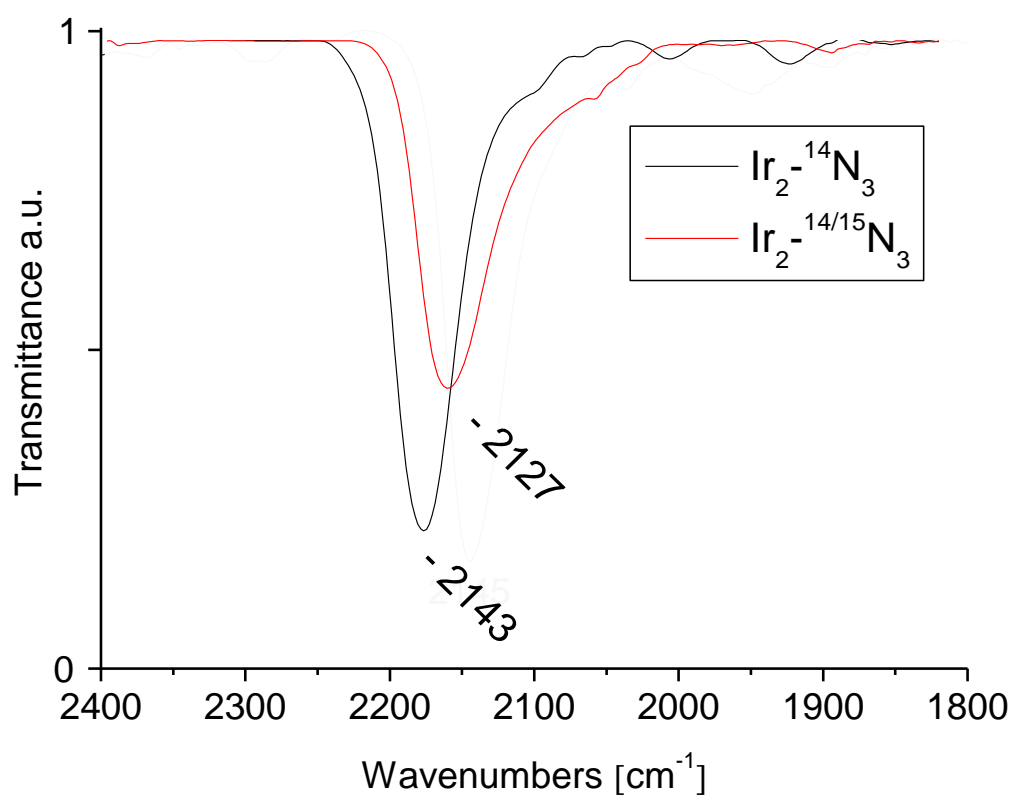
IR-Spectra

Figure S25: IR spectrum (KBr) of **tBuIr₂N₃+BPh4-** (black) and its ^{15}N isotopologue: **Ir-¹⁴N-¹⁴N-¹⁵N-Ir+BPh4-** (red).

Cyclic voltammogram
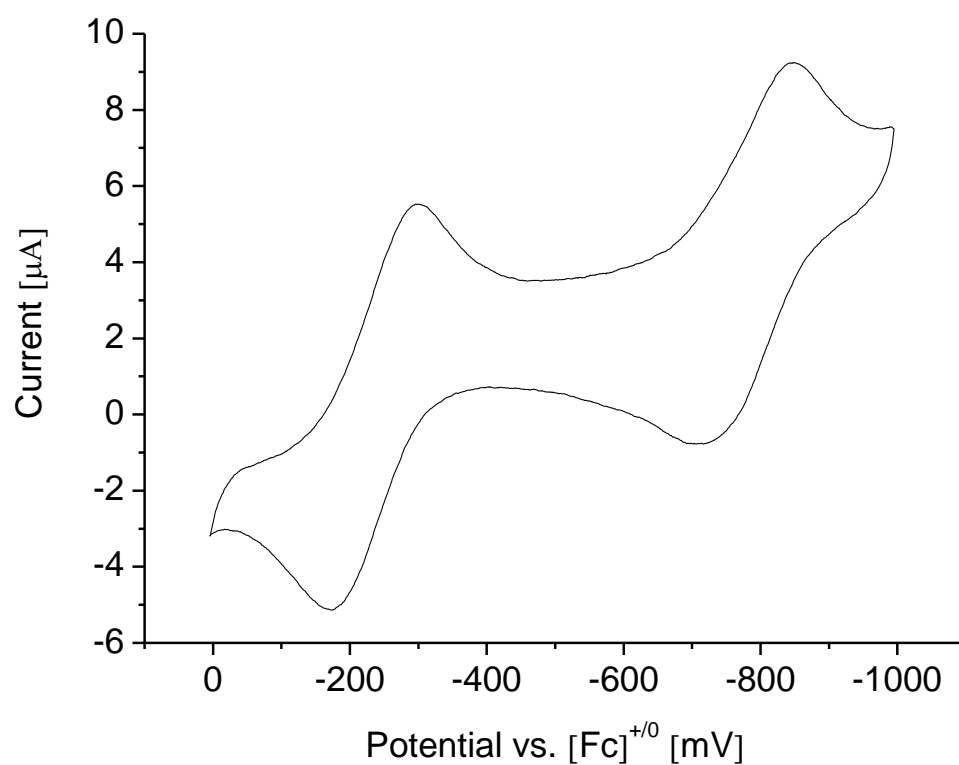
Figure S26: Cyclic voltammogram for complex ^{tBu}Ir₂N^{+BPh4-} [0.3 mM] in THF vs [Cp₂Fe]$^{+/0}$ at a scan rate of 100 mVs^{-1}, GC (glassy carbon) disk electrode (diameter = 3.0 mm) in 1 M NBu₄PF₆ THF solution.

EPR-Spectra
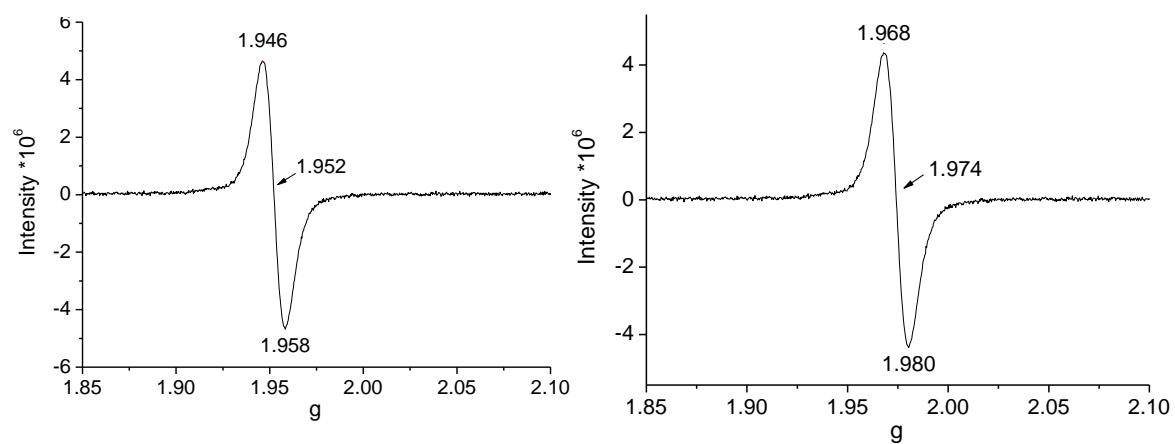
Figure S27: EPR spectra (THF) of $^{tBu}\text{Ir}_2\text{N}^{+BPh4-}$ (2 K left) and $^{tBu}\text{Ir}_2\text{N}$ (100 K right).

XPS-Spectra
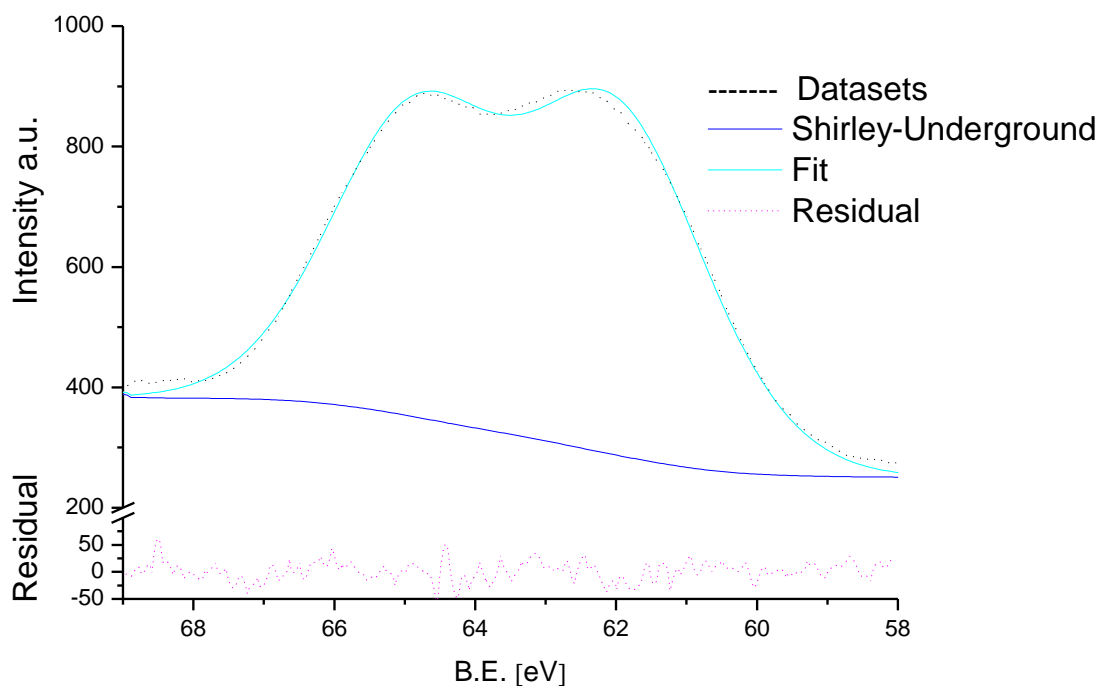
Figure S28: Ir(4f) XPS spectrum of $\mathbf{Ir_2N_3^{+Al\,-}}$, peak position 64.4 eV; Gaussian Lorentzian 45%; maxima $4f_{7/2}$: 62.2 eV $4f_{5/2}$: 65.0 eV. Problems with reference caused by fluorine.
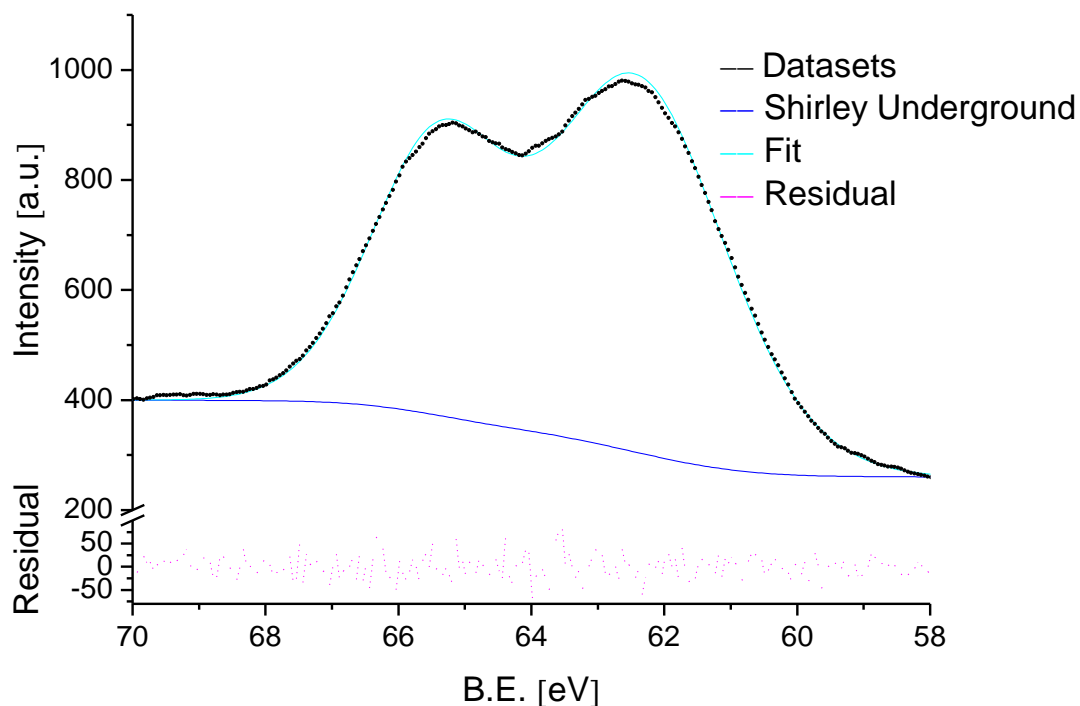
Figure S29: Ir(4f) XPS spectrum of $\mathbf{^{tBu}Ir_2N^{+BPh4-}}$, peak position 64.8 eV; FWHM 2.377 eV; Gaussian Lorentzian 45%; maxima $4f_{7/2}$: 62.5 eV $4f_{5/2}$: 65.3 eV.
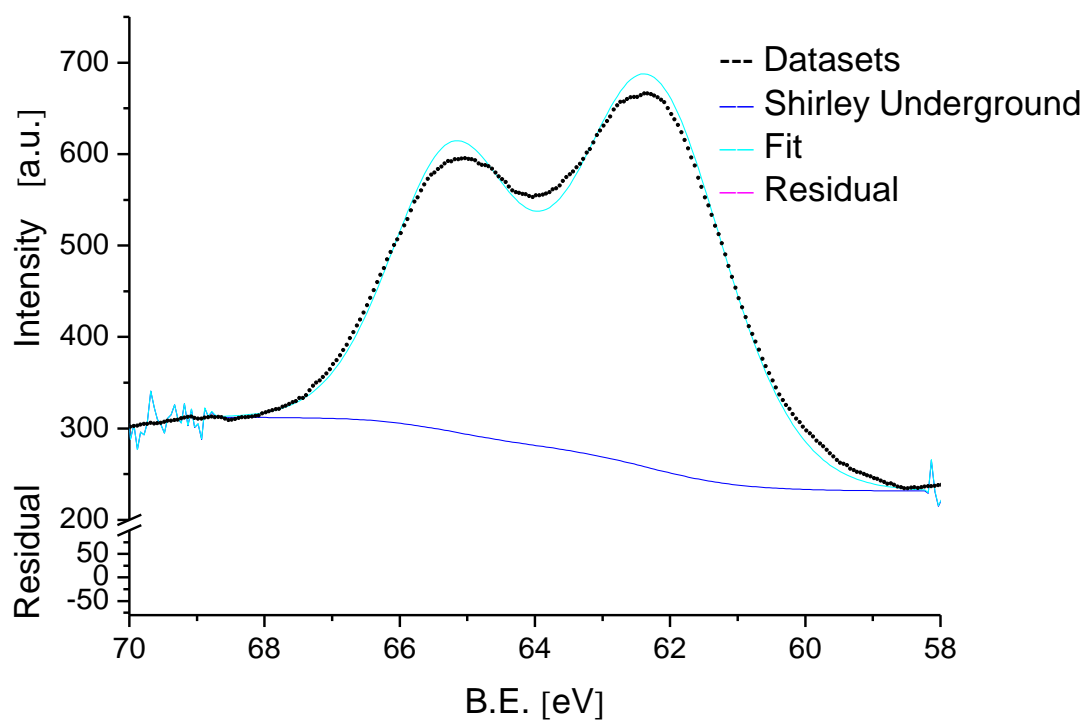
Figure S30: Ir(4f) XPS-spectrum of **Ir₂N⁻Na⁺**, peak position 64.5 eV; FWHM 2.256 eV; Gaussian Lorentzian 45%; maxima $4f_{7/2}$: 61.9 eV $4f_{5/2}$: 64.8 eV.
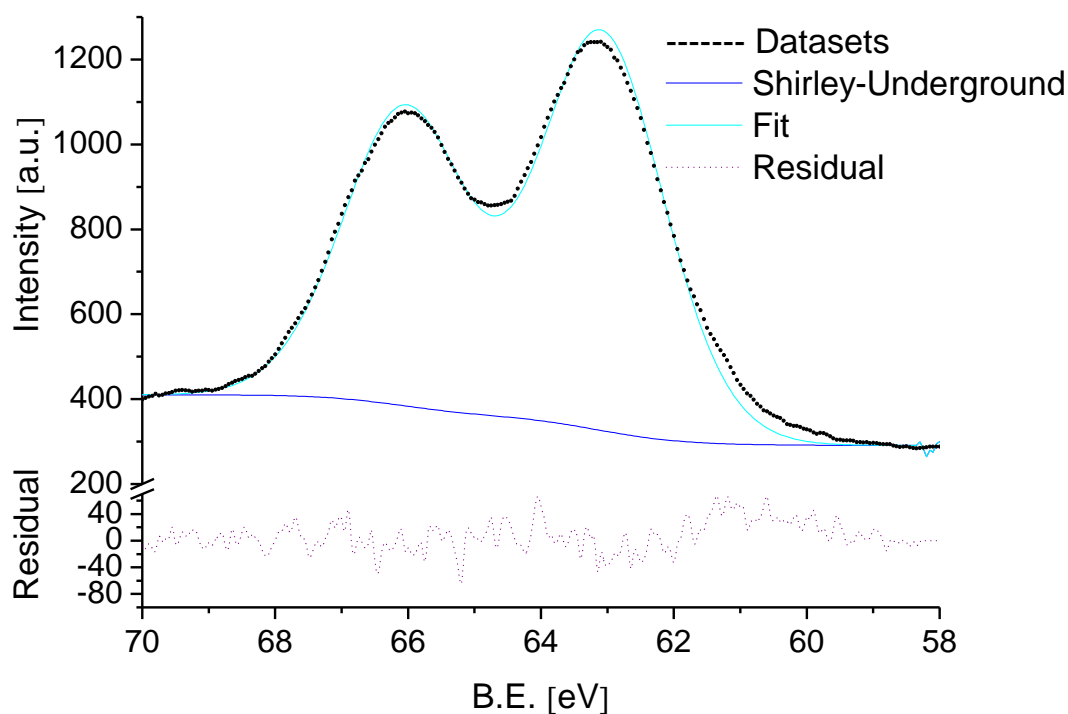
Figure S31: Ir(4f) XPS-spectrum of **[Ir(ᵗᴮᵘN₃Me₄)(Me)(OTf)₂)]**, peak position 64.2 eV; FWHM 2.087 eV; Gaussian Lorentzian 45%; maxima $4f_{7/2}$: 63.0 eV $4f_{5/2}$: 66.0 eV.

ESI-MS
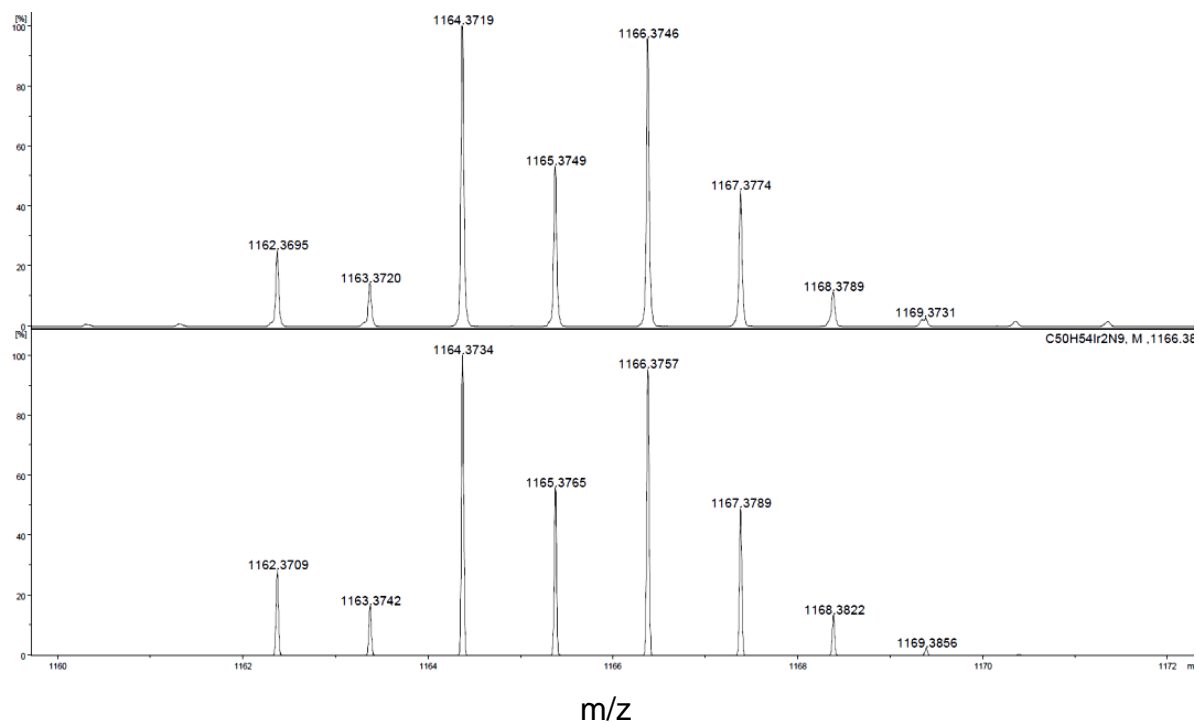
Figure S32: ESI-MS (THF, 80°C, positive mode) of **Ir$_2$N$_3$$^{+Al-}$**.
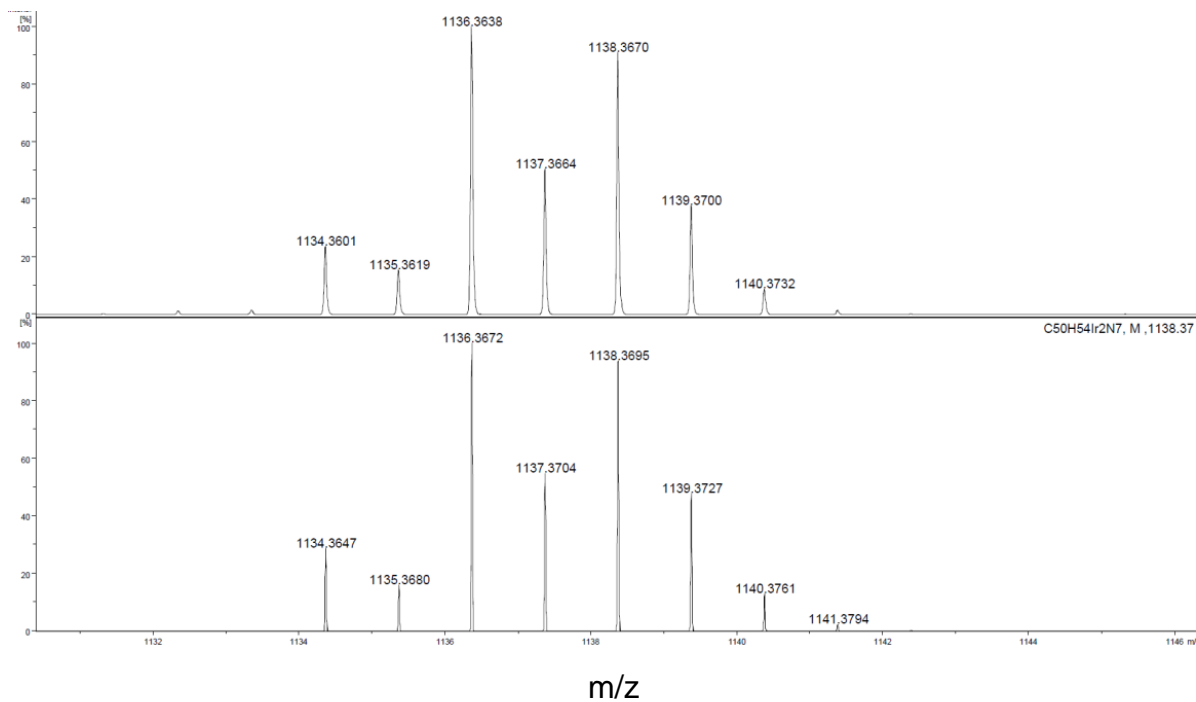
Figure 33: ESI-MS (THF, 80°C, positive mode) of **Ir$_2$N^{+Al-}**.
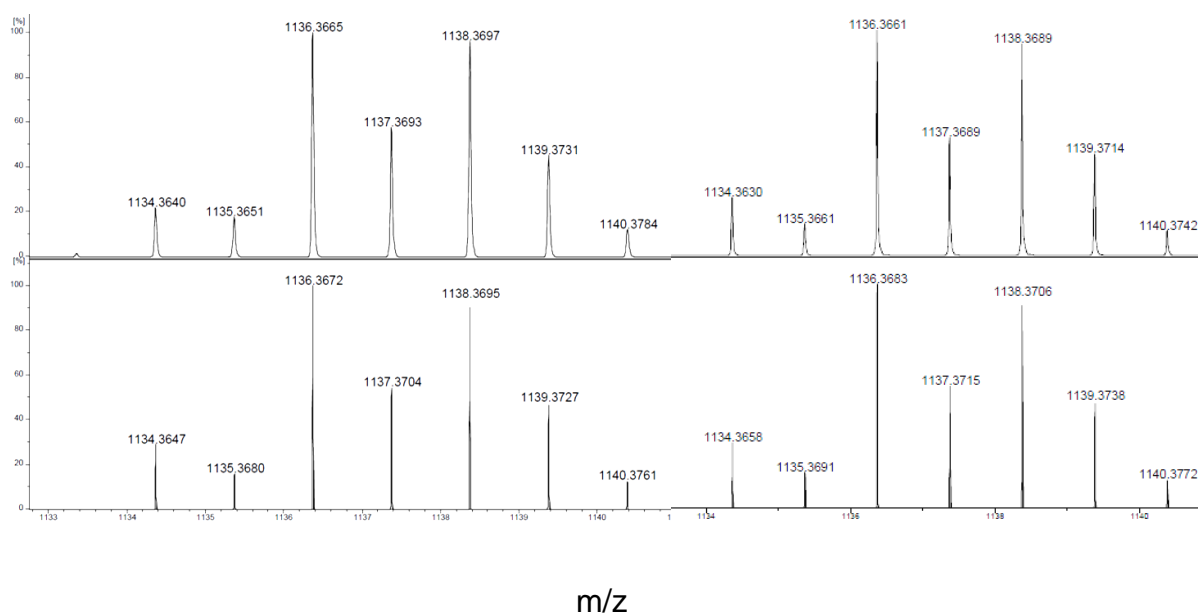
Figure S34: ESI-MS (THF, 80°C, left positive and right negative mode) of **Ir$_2$N**.
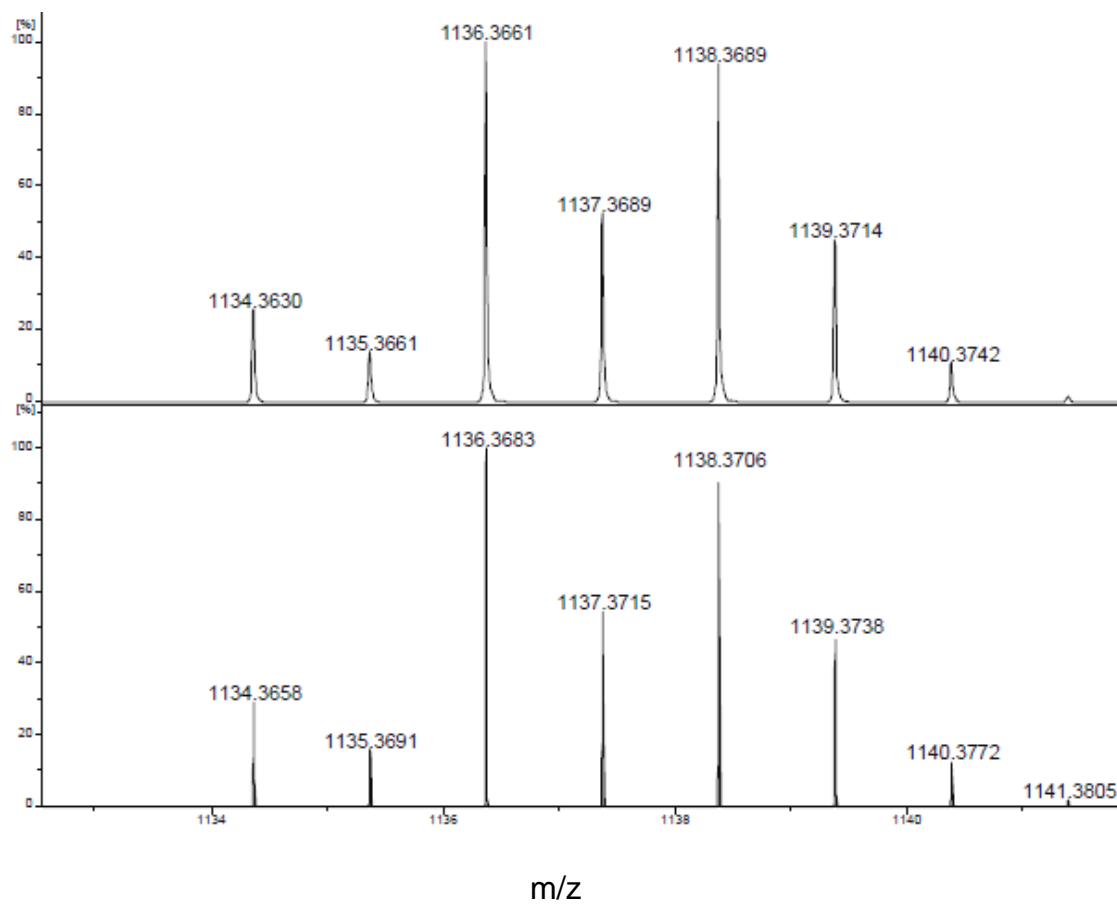
Figure S35: ESI-MS (THF, 80°C, negative mode) of **Ir$_2$N-$^{Na+}$.**

2) Computational Studies

The DFT calculations were carried out with the parallelized version 6.5 of Turbomole.[S12] The Becke-Perdew (BP-86) functional[S13,S14] was used for the geometry optimizations employing the resolution of identity (RI) methodology[S12] available in Turbomole (ridft, rdgrad). For calculations of open-shell systems the unrestricted formalism was employed. For the C, Cl, H and N atoms Ahlrichs def-SV(P) basis sets (double zeta with polarization functions for C, Cl and N) were employed. For iridium a larger Ahlrichs def2-TZVP triple-ζ basis set with polarization together with a Stuttgart-Dresden (ECP-60-MWB) pseudopotential[S15] was used throughout in the calculations. Natural population analysis charges (NPA)[S16] charges were calculated with the Turbomole program package.

The geometries were optimized with either C_{2v}- or D_{2d}-symmetry constraints. They were verified as ground states by probing for different spin states and characterized as stationary points by the calculation of analytical second derivatives through the absence of imaginary frequencies. This is also valid for the neutral Ir_2N model system, which is deemed to undergo a Jahn-Teller distortion due to its electron configuration (Fig. 3, 2 e^3). The X-ray crystal structure of the azido-bridged complex $Ir_2N_3^+$ displays a bent Ir-N$_3$-Ir unit, while the linear orientation of this entity is clearly the (DFT) energy minimum of the model complex. DFT geometry optimizations of the full complex also converge at the linear structure and, only after Grimme's (D3) dispersion corrections are applied, the bent structure is correctly reproduced. The total energies and the final optimized geometries are tabulated in Tables S7-S13, respectively.

For the localized orbital bond analysis (LOBA)[S17] Pipek-Mezey localized bond orbitals (LMOs) were generated and subjected to a subsequent Mulliken population analyses for the metal based orbitals with > 10% contribution. This procedure was performed with the Turbomole program. Natural orbitals for the open shell systems were also created with the Turbomole program.

The starting orbitals for the broken symmetry wavefunction (S=0) of the cationic model complex for Ir_2N^+ were obtained from the wavefunction of the S=1 system using the "Canossa" program, which was generously provided to the authors by Christoph van Wüllen (TU Kaiserslautern). For the cationic model system Ir_2N^+ we have performed calculations for the S=1 state and the S=0 broken symmetry solution of the open shell singlet for different DFT functionals in the gas phase as well as in the liquid phase (THF $\varepsilon = 7.4$) using the COSMO dielectric continuum model (Table S5).

Mayer bond orders were calculated with the Multiwfn ver. 3.3 program package[S18] using Molden input files generated by Turbomole in combination with the Molden2AIM ver. 2.2.3[S19] program (Table S6).

The orbital plots were obtained from Turbomole generated cube files with the Chemcraft program package.[S20]

Table S5. Singlet Triplet Energy Gap for different functionals of IrN_2^+ model system.

DFT Functional	Triplet, S =1		Broken Symmetry (BS) Open Shell Singlet (@triplet geometry)		E(S=1)-E(BS)	$J_{S=1/BS}$[a]
	Total Energy[H]	$<S^2>$	Total Energy [H]	$<S^2>$	[kJ/mol]	[cm^{-1}]
BP86	-1133.56315	2.01	-1133.56306	1.01	-0.2	-17
PBE	-1132.19665	2.01	-1132.19655	1.01	-0.3	-25
TPSS	-1133.36281	2.01	-1133.36273	1.02	-0.2	-19
PBE0	-1132.05196	2.06	-1132.05256	1.10	+1.6	+142
TPSSH	-1133.18711	2.03	-1133.18724	1.04	+0.3	+25
B3LYP	-1132.52718	2.04	-1132.52752	1.06	+0.9	+77
BP86 COSMO, ε=7.4[b]	-1133.62254	2.01	-1133.62243	1.01	-0.3	-25

[a] J = E(BS(S=1))-E(BS open shell singlet)/($<S^2$(triplet)>- $<S^2$(BS open shell singlet)>).[S21]

[b] COSMO dielectric continuum model

Table S6. Electronic and structural properties of the chlorido, azido and nitrido complexes IrCl, IrN, Ir$_2$N$_3^+$, Ir$_2$N$^+$, Ir$_2$N, Ir$_2$N$^-$ with selected calculated values for the corresponding model compounds.

Parameter	IrCl	IrN	Ir$_2$N$_3^+$	Ir$_2$N$^+$	Ir$_2$N	Ir$_2$N$^-$
ground state	S=0	S=0	S=0	S=0[a]	S=½	S=0
EPR g-value	-	-	-	1.95	1.92	-
XPS [eV][b] Ir(4f$_{7/2}$) Ir(4f$_{5/2}$)	62.0 65.0	63.1 66.0	62.2 65.0	62.5 65.3	61.9 64.8	61.9 64.8
LOBA ox. state el. config.	Ir(I) d^8	Ir(III) d^6	Ir(I) d^8	Ir(I) d^8	Ir(I) d^8	Ir(I) d^8
MPAs (%) d$_{z2}$ d$_{yz}$ d$_{xy}$[d] d$_{xz}$ ligand	99 80 98 67 -	99 90 62 57 70	99 85 90 72 -	99/99 87/87 78/78 64/64 38/38	99/99 84/84 84/84 62/62 74/74	99/99 81/81 84/84 63/63 73/73
PDI ligand charge	0	-2	0	-1	-1.5	-2
Ir-N$_{azido,,nitrido.}$ exp. distance [Å],[c] calc. distance [Å],[c] Mayer bond order	n/a	1.646 1.692 2.54	1.965 1.933 0.90	1.807 1.791 1.52	n/a 1.80 1.49	1.845 1.813 1.47
NPA charges spin. dens.						
Ir	0.55	0.77	0.62	0.69 0.16	0.67 0.08	0.64
N$_{nitrido, azido}$	-	-0.32	-0.32	-0.39 0.17	-0.46 0.08	-0.52
N$_{pyridine}$	-0.44	-0.64	-0.44	-0.54 0.14	-0.58 0.08	-0.63
N$_{imine}$	-0.63	-0.69	-0.63	-0.65 0.08	-0.67 0.05	-0.69
C$_{py}$-C$_{imi}$ exp. distance [Å],[c] calc. distance [Å],[c] Mayer bond order	1.451 1.441 1.18	1.424 1.422 1.24	1.460 1.441 1.17	1.440 1.444 1.16	n/a 1.432 1.22	1.410 1.421 1.28
C$_{imi}$-N$_{imi}$ exp. distance [Å],[c] calc. distance [Å],[c] Mayer bond order	1.331 1.335 1.56	1.329 1.344 1.44	1.314 1.330 1.58	1.33 1.334 1.54	n/a 1.348 1.45	1.35 1.363 1.37

[a]open shell singlet with S=0 ⇄ S=1 spin state crossover; [b]values for Ir(III) reference compound **[Ir^{III}(tBuN$_3$Me$_4$)(Me)(OTf)$_2$)]** 4f$_{7/2}$: 63.0, 4f$_{5/2}$: 66.0 [eV]. [c]averaged values for symmetry related bonds; [d]averaged values for α and β orbitals.

aryl =

[Ir^{III}(tBuN$_3$Me$_4$)(Me)(OTf)$_2$)]
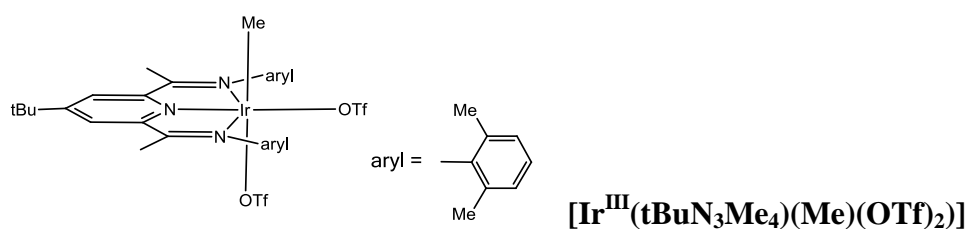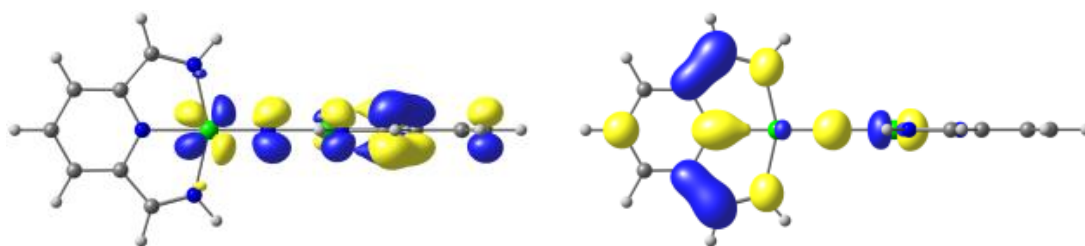
Fig. S36. Natural orbitals (SNMOs) of the model complex for Ir_2N^+.
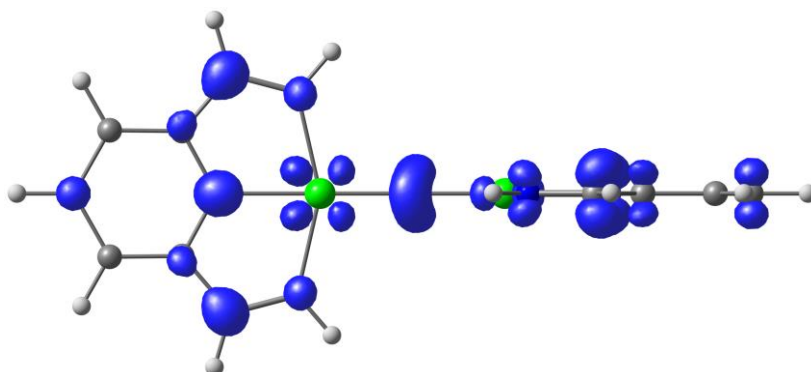
Fig. S37. Spin density of the cationic model complex **Ir_2N^+ (S=1);** isosurface value 0.007.
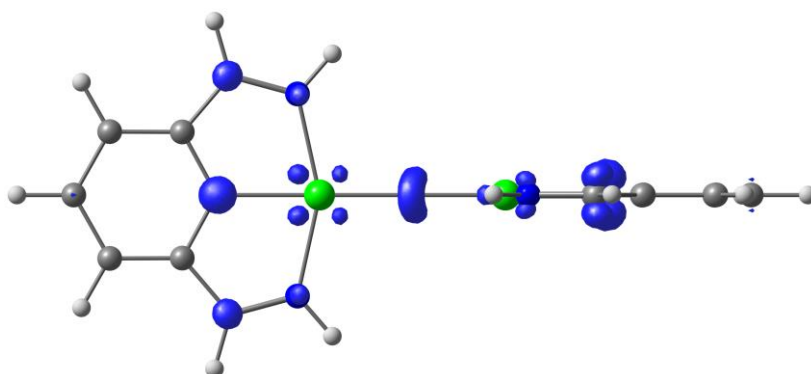
Fig. S38. Spin density of the neutral model complex **Ir_2N** (S=1/2); isosurface value 0.007.
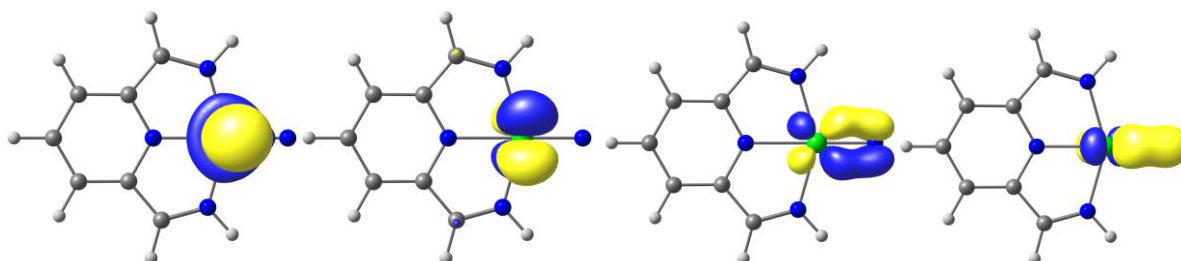
Fig. S39. Metal centered Pipek-Mezey localized molecular orbitals used in the LOBA of the **IrN** model complex, (Mulliken pop. $d_{z2}(99\%)$, $d_{yz}(90\%)$, $d_{xy}(62\%)$, $d_{xz}(57\%)$ left to right).
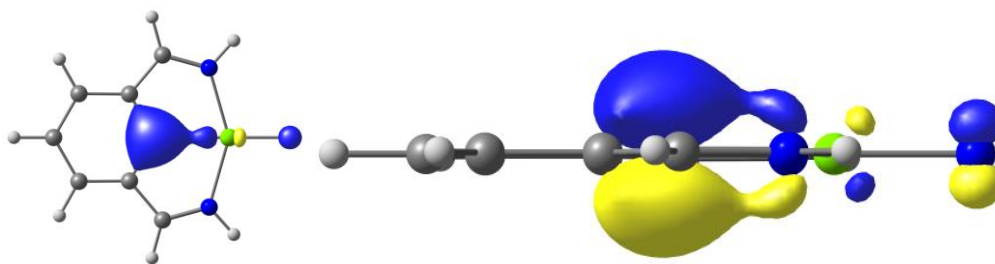
Fig. S40. Pipek-Mezey localized orbital (LMO) related to the non-innocent PDI ligand in the nitrido complex **IrN** (top and side view).

The extra electrons in the neutral and anionic complexes **Ir₂N** and **Ir₂N⁻** are essentially located on the PDI ligands. This is partially supported by the LOBA for the μ-bridged nitrido model systems. The LOBA for the α-electrons of Ir_2N^+ (S=1) model revealed one ligand based LMO for each PDI ligand. For the β-electrons the corresponding LMOs were missing, suggesting singly reduced PDI^{-1} ligands. In the LOBA for the anionic model system of Ir_2N^-, which carries two further electrons, both, the α- and β-based LMOs of this type were observed, consistent with a doubly reduced PDI^{2-} ligand. This analysis is stretched to its limits, since 4 (2α and 2β) of these unique LMOs were derived for the neutral model system of Ir_2N although only 3 were expected.

restricted Kohn-Sham DFT, BP86 functional; MPA values with contributions of > 10% are given.
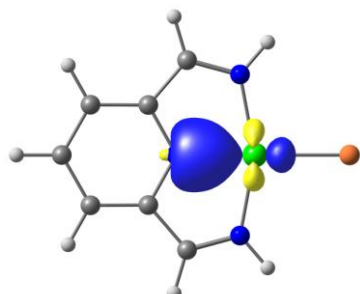
LMO 25: 0.44 e⁻ Ir / 1.58 e⁻ N$_{pyridine}$
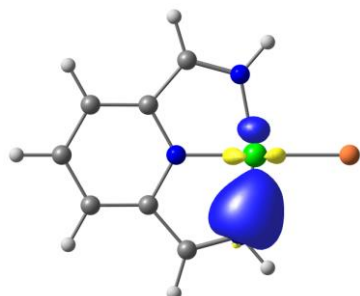
LMO 26: 0.36 e⁻ Ir / 1.70 e⁻ N$_{imine}$
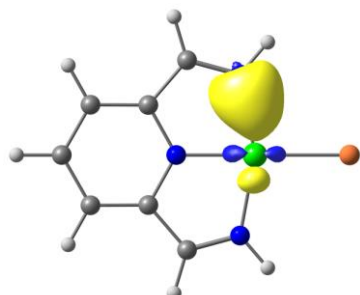
LMO 27: 0.36 e⁻ Ir / 1.70 e⁻ N$_{imine}$
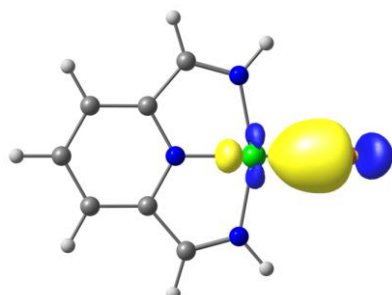
LMO 41: 0.38 e⁻ Ir / 1.62 e⁻ Cl
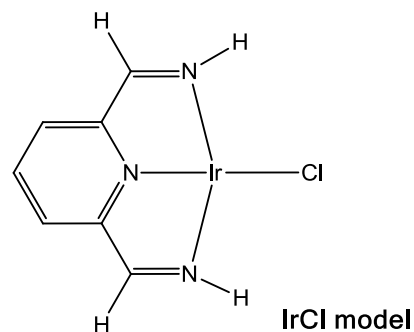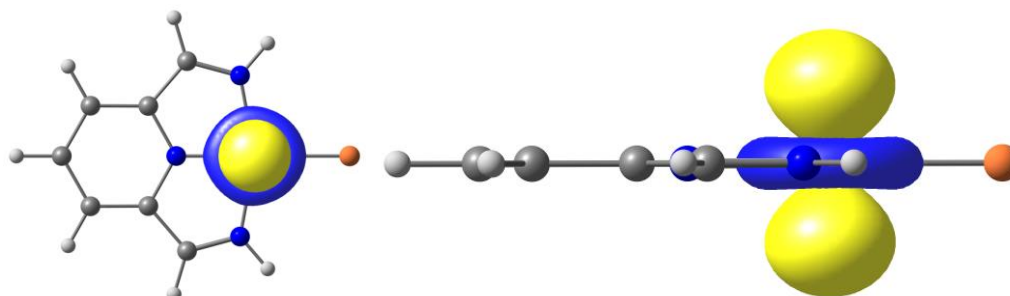
LMO 47: 2 e⁻ Ir(d$_{z2}$)
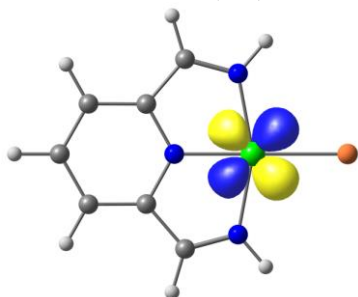
LMO 48: 1.96 e⁻ Ir(d$_{xy}$)
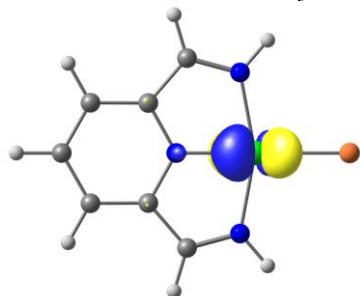
LMO 51: 1.34 e⁻ Ir(d$_{xz}$) / 0.11 e⁻ N$_{pyridine}$ / 0.10 e⁻ each pyridine carbon atoms in 2,6 positions
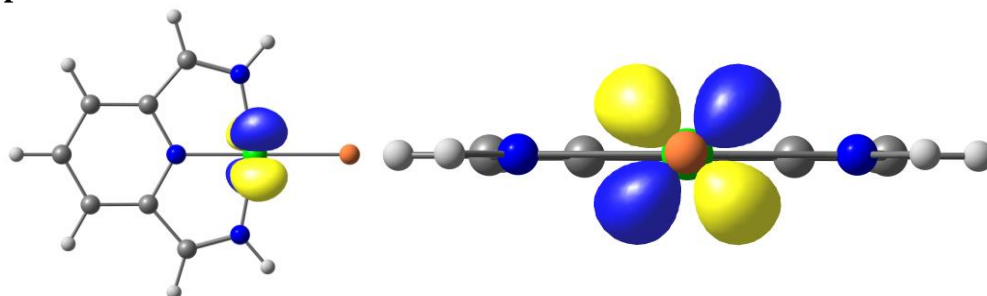
LMO 52: 1.60 e⁻ Ir(d$_{yz}$)

Mulliken Population Analysis &/ LMOs (Pipek-Mezey) for the neutral model system of IrN

restricted Kohn-Sham DFT, BP86 functional; MPA values with contributions of > 10% are given.
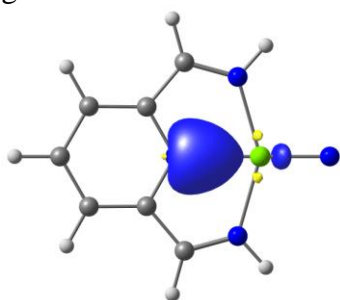
LMO 21: 0.26 e⁻ Ir / 1.72 e⁻ N$_{pyridine}$
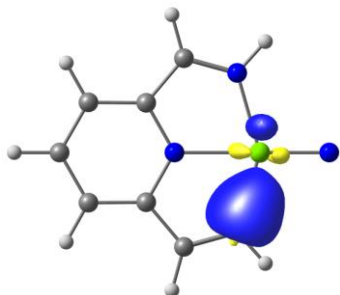
LMO 25: 0.41 e⁻Ir / 1.62 e⁻ N$_{imine}$
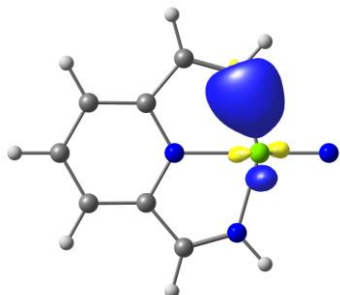
LMO 26: 0.41 e⁻ Ir / 1.62 e⁻ N$_{imine}$
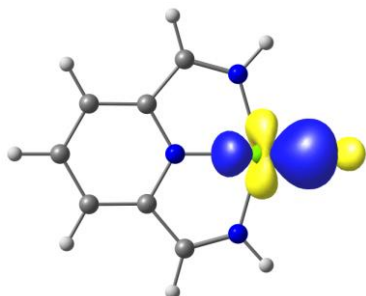
LMO 33: 0.79 e⁻ Ir / 1.21 e⁻ N$_{nitrido}$
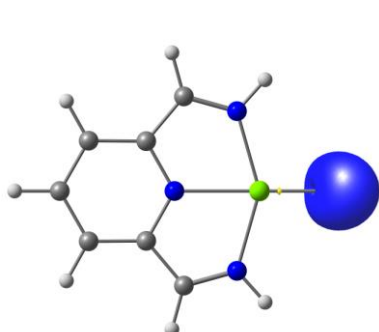
LMO 16: 0.12 e⁻ Ir / 1.88 e⁻ N$_{nitrido}$ (lone pair)

IrN model
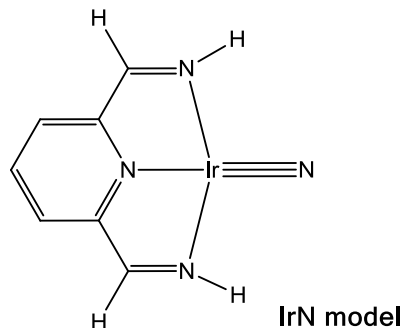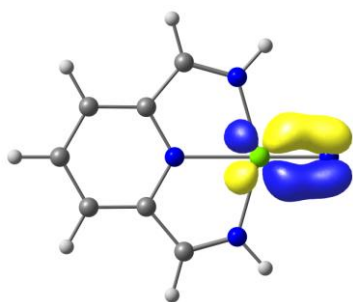
LMO 39: 1.23 e⁻ Ir (d$_{xy}$) / 0.77 e⁻ N$_{nitrido}$
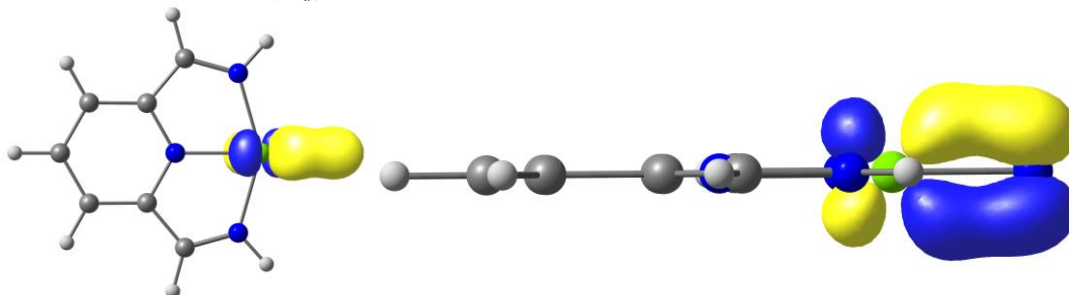
LMO 40:   1,14 e⁻ Ir (d$_{xz}$) / 0.86 e⁻ N$_{nitrido}$
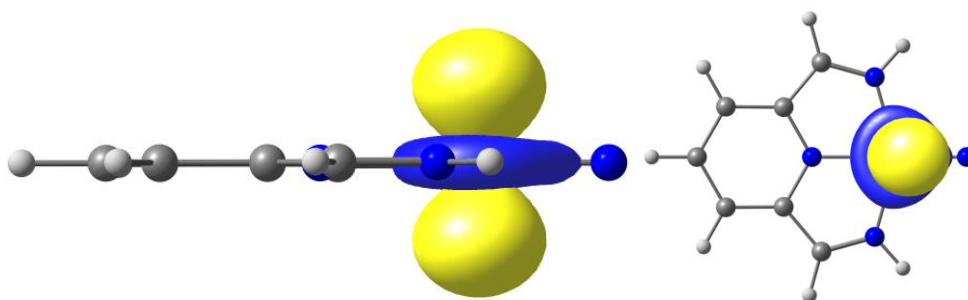
LMO 22: 1.98 e⁻ Ir (d$_{z^2}$)
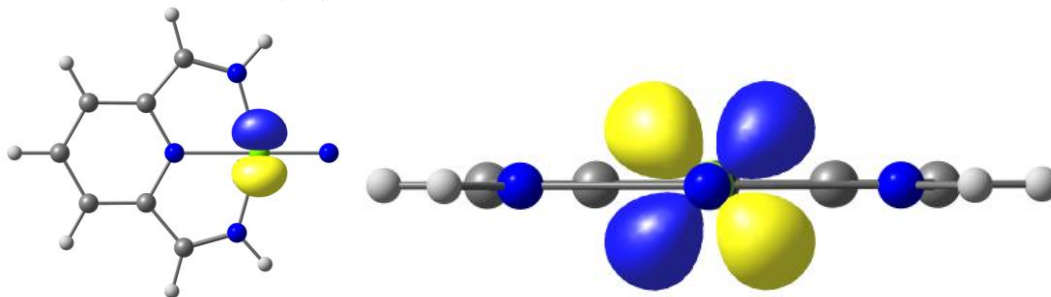
LMO 47: 1.79 e⁻ Ir(d$_{yz}$)
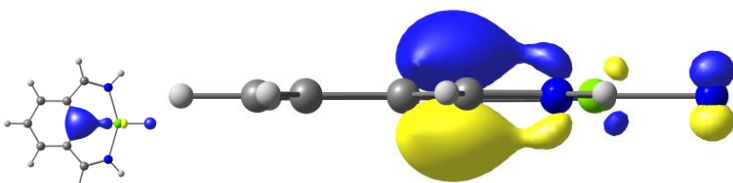
LMO 45: PDI ligand (non-innocent) 0.24 e⁻ Ir / 1.39 e⁻ N$_{pyridine}$ / 0.14 e⁻ / N$_{nitrido}$

.

restricted Kohn-Sham DFT, BP86 functional; MPA values with contributions of > 10% are given. The LMOs and MPA values for the symmetry related parts are identical.

LMO 90: 1.79 e⁻ Ir

$Ir_2N_3^+$ model
D_{2d}-symmetrical
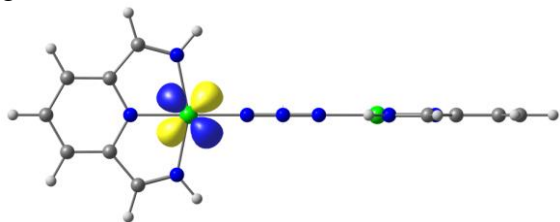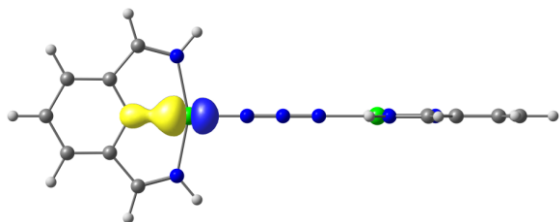
LMO 92: 1.43 e⁻ Ir / 0.36 e⁻ $N_{pyridine}$
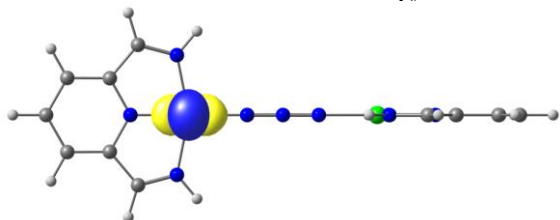
LMO 94: 1.99 e⁻ Ir
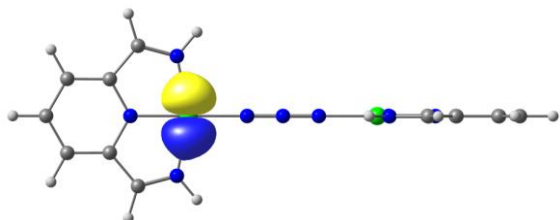
LMO 96: 1.69 e⁻ Ir
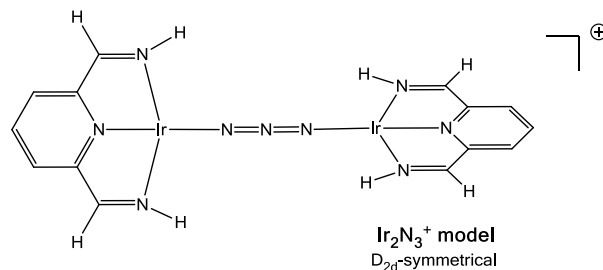
Mulliken Population Analysis &/ LMOs (Pipek-Mezey) for the cationic model system of Ir_2N^+
unrestricted Kohn-Sham DFT (S=1), BP86 functional; MPA values with contributions of > 10% are given.
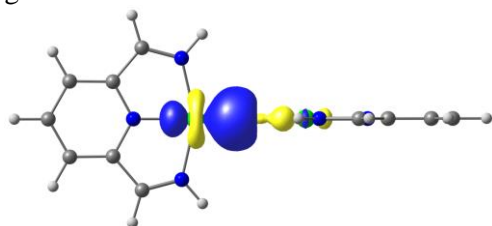

LMO 38: 0.32 e⁻ Ir1 / 0.70 e⁻ $N_{nitrido}$ (α-spin)
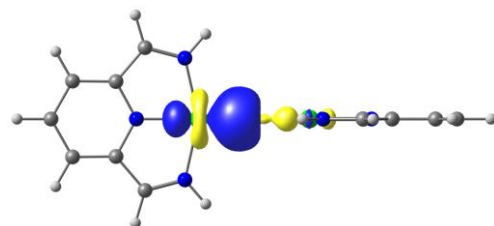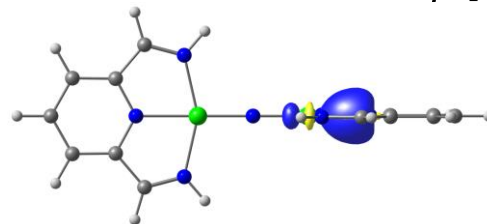

LMO 129: 0.32 e⁻ Ir1 / 0.70 e⁻ $N_{nitrido}$ (β-spin)
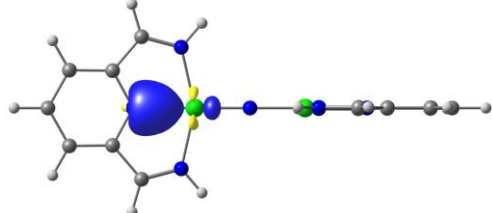
LMO 41: 0.16 e⁻ Ir1 / 0.84 e⁻ $N_{pyridine}$ (α-spin)
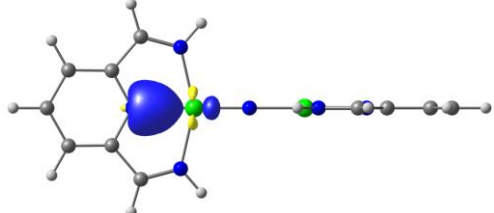
LMO 132: 0.16 e⁻ Ir1 / 0.84 e⁻ $N_{pyridine}$ (β-spin)
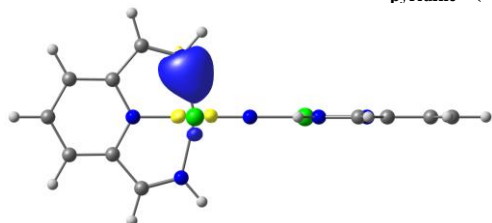
LMO 42: 0.19 e⁻ Ir1 / 0.84 e⁻ N_{imine} (α-spin)
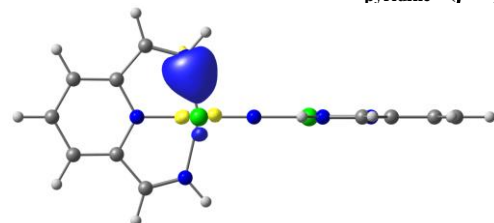
LMO 136: 0.20 e⁻ Ir1 / 0.83 e⁻ N_{imine} (β-spin)
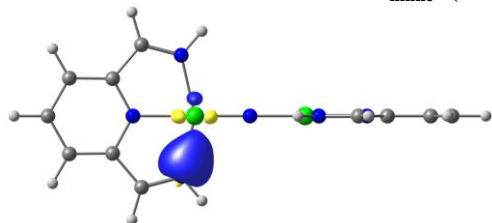
LMO 44: 0.19 e⁻ Ir1 / 0.84 e⁻ N_{imine} (α-spin)
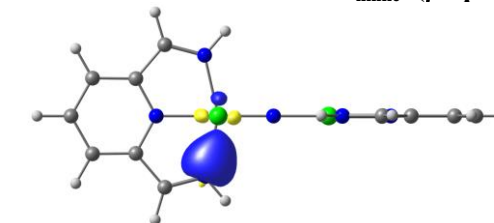
LMO 133: 0.19 e⁻ Ir1 / 0.83 e⁻ N_{imine} (β-spin)
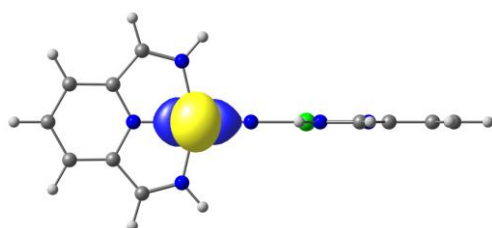
LMO 73: 1.0 e⁻ $Ir1(d_{z2})$ (α-spin)
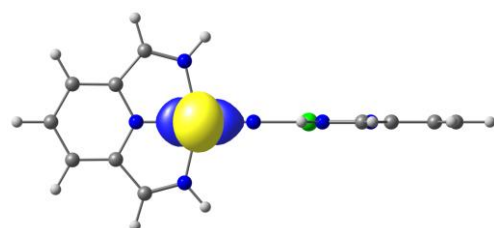
LMO 164: 1.0 e⁻ $Ir1(d_{z2})$ (β-spin)
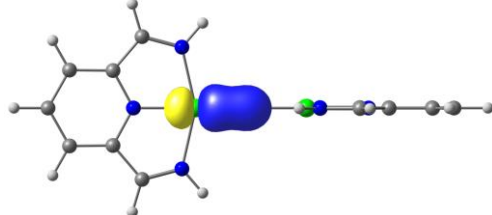
LMO 78: 0.58 e⁻ $Ir1(d_{xz})$/0.41 e⁻ $N_{nitrido}$ (α-spin) LMO 178: 0.71 e⁻ $Ir1(d_{xz})$/0.25 e⁻ $N_{nitrido}$ (β-spin)
The values for the α- and β-LMOs were averaged ((0.58+0.71)/2=0.64)
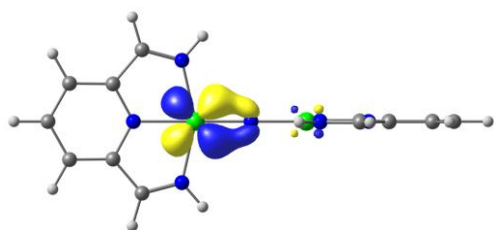
LMO 82: 0.84 e⁻ Ir1(d_xy) (α-spin)   **LMO 171: 0.71 e⁻ Ir1(d_xy) / 0.25 e⁻ N_nitrido (β-spin)**
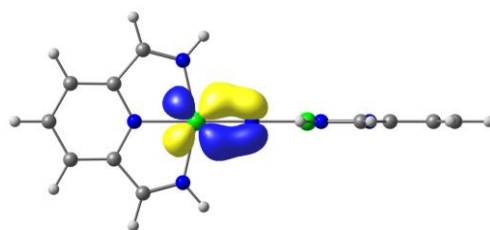
The values for the α- and β-LMOs were averaged ((0.84+0.71)/2=0.78)
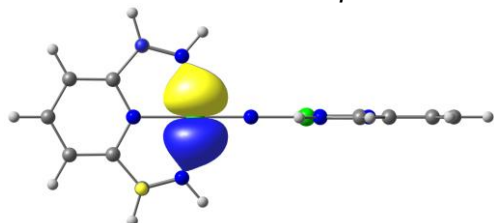
LMO 91: 0.86 e⁻ Ir1(d_yz) (α-spin)   **LMO 179: 0.88 e⁻ Ir1(d_yz) (β-spin)**
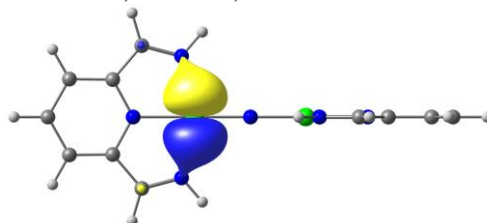
The values for the α- and β-LMOs were averaged ((0.86+0.88)/2=0.87)
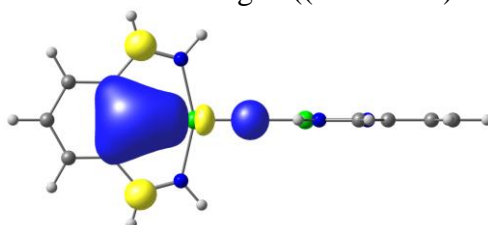
LMO 81: PDI ligand-1 (non-innocent) 0.75 e⁻ N_pyridine (α-spin)   no LMO for β-spin (!)

unrestricted Kohn-Sham DFT, BP86 functional; MPA values with contributions of > 10% are given.
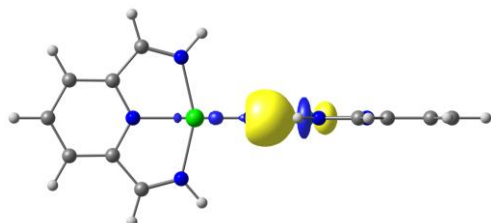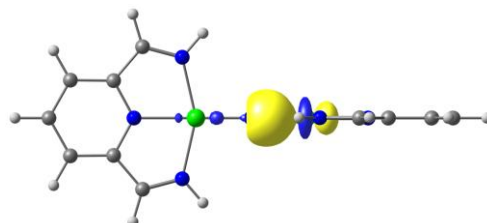
LMO 39: 0.32 e⁻ Ir2 / 0.70 e⁻ N_nitrido (α-spin)   LMO 130: 0.33 e⁻ Ir2/0.69 e⁻ N_nitrido (β-spin)
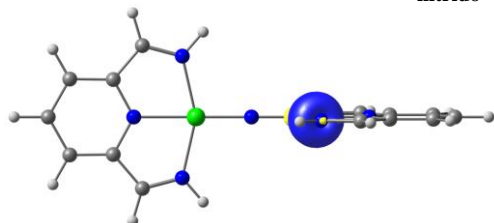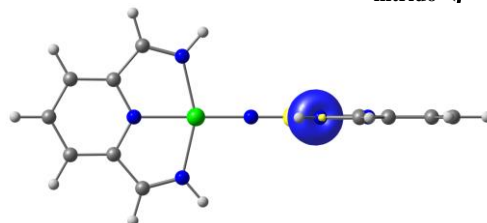
LMO 43: 0.19 e⁻ Ir2 / 0.84 e⁻ N_imine (α-spin)   LMO 134: 0.19 e⁻ Ir2 / 0.83 e⁻ N_imine (β-spin)
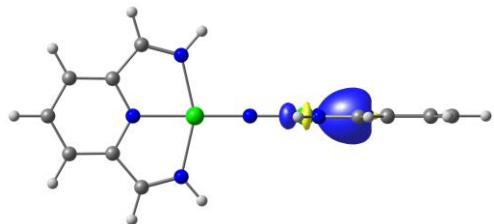
LMO 40: 0.16 e⁻ Ir2/0.84 e⁻ N_pyridine (α-spin)   LMO 131: 0.16 e⁻ Ir2/0.84 e⁻ N_pyridine (β-spin)
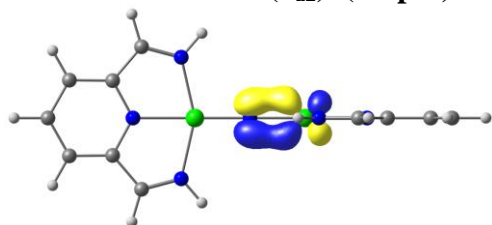
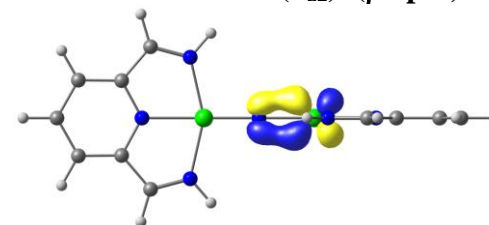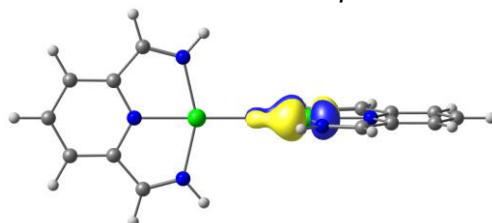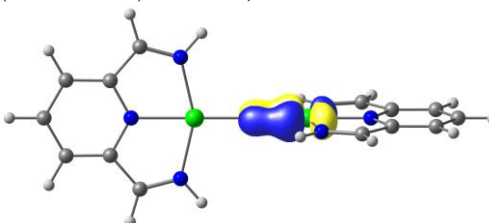**LMO 45: 0.19 e⁻ Ir2/0.84 e⁻ N_imine (α-spin)**   **LMO 135: 0.20 e⁻ Ir2/0.83 e⁻ N_imine (β-spin)**
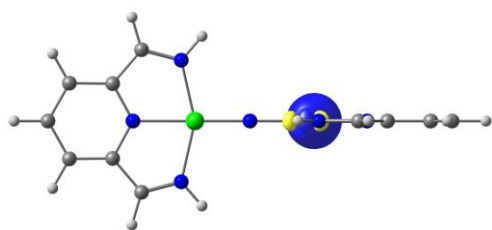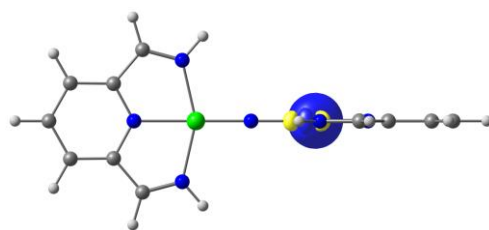
LMO 45: 0.19 e⁻ Ir2/0.84 e⁻ N_{imine} (α-spin)   **LMO 135: 0.20 e⁻ Ir2/0.83 e⁻ N_{imine} (β-spin)**
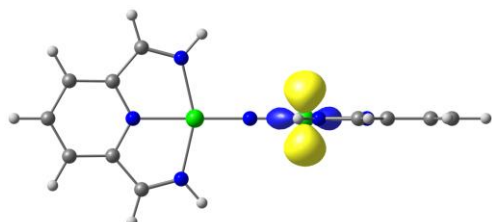
LMO 72: 1.0 e⁻ Ir2(d_{z2}) (α-spin)   **LMO 163: 1.0 e⁻ Ir2(d_{z2}) (β-spin)**
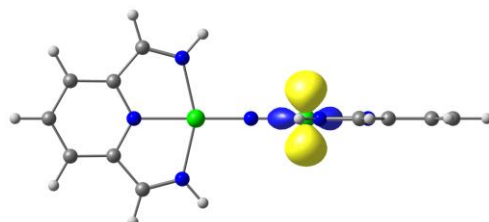
LMO 79: 0.58 e⁻ Ir2(d_{xz})/0.42 e⁻ $N_{nitrido}$ (α-spin)   LMO 177: 0.71 e⁻ Ir2(d_{xz})/0.24 e⁻ $N_{nitrido}$ (β-spin)
The values for the α- and β-LMOs were averaged $((0.58+0.71)/2=0.64)$

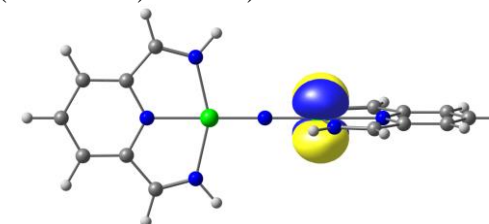**LMO 83: 0.84 e⁻ Ir2(d_{xy}) (α-spin)   LMO 172: 0.71 e⁻ Ir2(d_{xy}) / 0.25 e⁻ $N_{nitrido}$ (β-spin)**
The values for the α- and β-LMOs were averaged $((0.84+0.71)/2=0.78)$
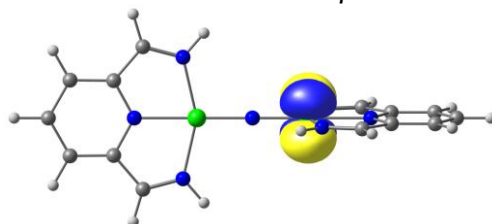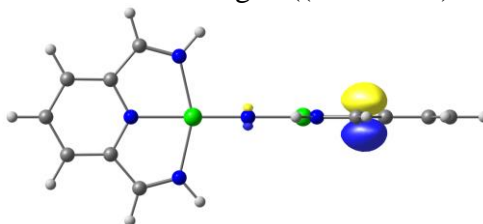
LMO 90: 0.86 e⁻ Ir2(d_{yz}) (α-spin)   LMO 180: 0.88 e⁻ Ir2(d_{yz}) (β-spin)
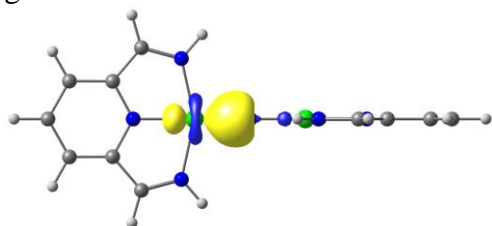The values for the α- and β-LMOs were averaged $((0.86+0.88)/2=0.87)$

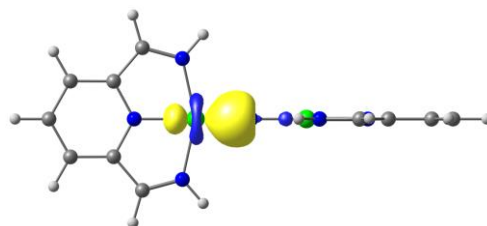**LMO 80: PDI ligand-2 (non-innocent) 0.75 e⁻ $N_{pyridine}$ (α-spin)   no LMO for β-spin (!)**

Mulliken Population Analysis &/ LMOs (Pipek-Mezey) for the neutral model system of Ir_2N
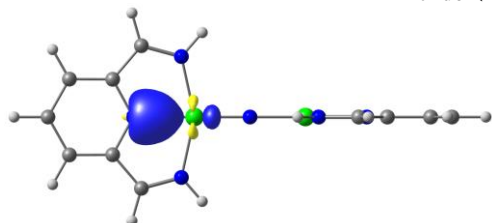
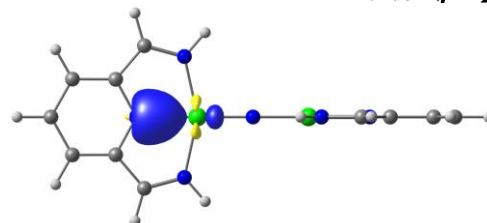unrestricted Kohn-Sham DFT, BP86 functional; MPA values with contributions of > 10% are given.
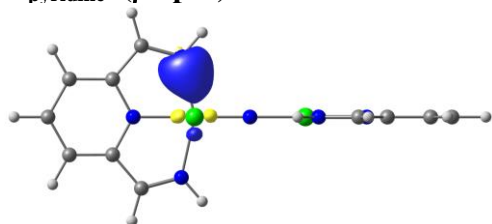

LMO 39: 0.32 e⁻ Ir1/0.70 e⁻ $N_{nitrido}$ (α-spin)   LMO 129: 0.32 e⁻ Ir1/0.70 e⁻ $N_{nitrido}$ (β-spin)
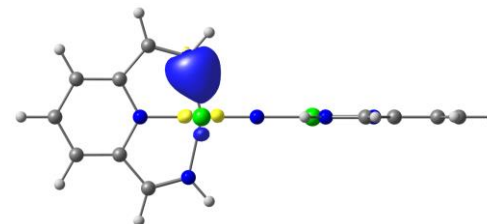

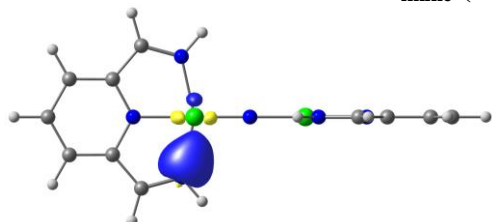**LMO 40: 0.17 e⁻ Ir1 / 0.84 e⁻ $N_{pyridine}$ (α-spin)   LMO 132: 0.17 e⁻ Ir1 / 0.84 e⁻ $N_{pyridine}$ (β-spin)**
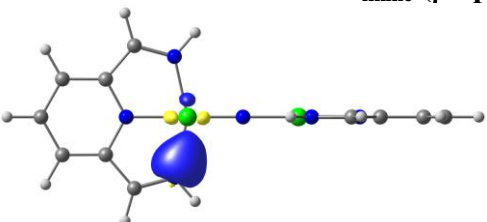

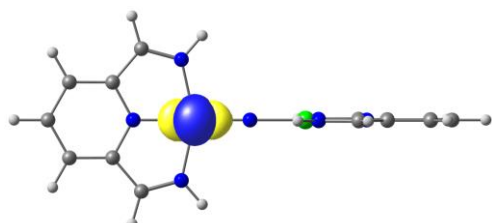**LMO 44: 0.19 e⁻ Ir1/0.84 e⁻ N_{imine} (α-spin)   LMO 133: 0.19 e⁻ Ir1/0.84 e⁻ N_{imine} (β-spin)**

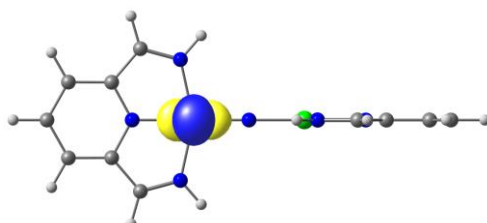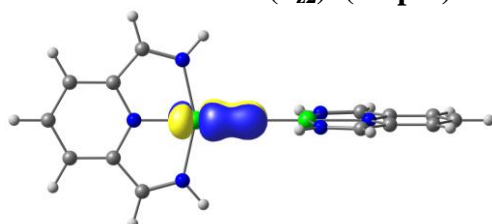**LMO 45: 0.19 e⁻ Ir1/0.84 e⁻ N_{imine} (α-spin)   LMO 133: 0.19 e⁻ Ir1/0.84 e⁻ N_{imine} (β-spin)**
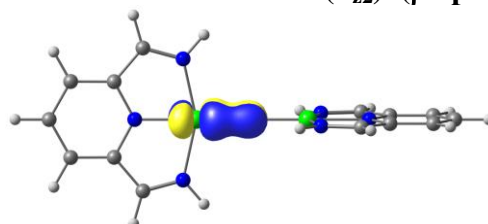

LMO 72: 1.0 e⁻ Ir1(d_{z2}) (α-spin)   LMO 164: 1.0 e⁻ Ir1(d_{z2}) (β-spin)
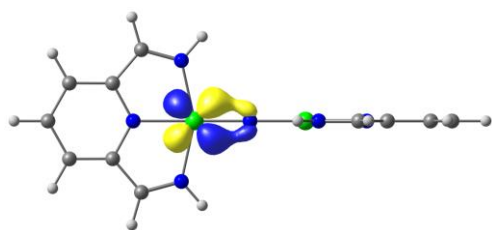

LMO 80: 0.60 e⁻ Ir1(d_{xz})/0.39 e⁻ $N_{nitrido}$ (α-spin)   LMO 169: 0.64 e⁻ Ir1(d_{xz})/0.36 e⁻ $N_{nitrido}$ (β-spin)
The values for the α- and β-LMOs were averaged ((0.58+0.71)/2=0.64)

LMO 87: 0.84 e⁻ Ir1(d$_{xy}$)/0.19 e⁻ N$_{nitrido}$ (α-spin)   LMO 175: 0.84 e⁻ Ir1(d$_{xy}$)/0.11 e⁻ N$_{nitrido}$ (β-spin)

LMO 90: 0.84 e⁻ Ir1(d$_{yz}$) (α-spin)   LMO 182: 0.85 e⁻ Ir1(d$_{yz}$) (β-spin)

The values for the α- and β-LMOs were averaged ((0.84+0.85)/2=0.85)
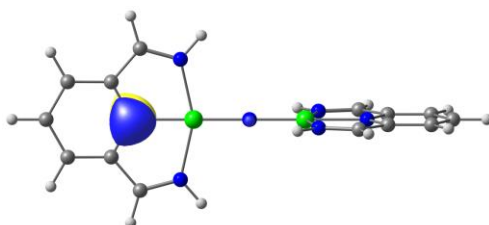
LMO 79: PDI ligand-1 (non-innocent) 0.74 e⁻ N$_{pyridine}$ (α-spin)
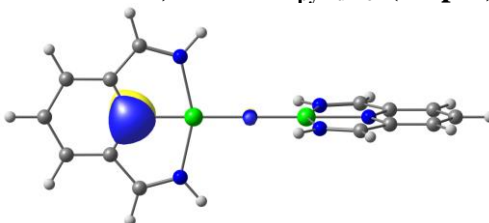
LMO177: PDI ligand-1 (non-innocent) 0.73 e⁻ N$_{pyridine}$ (β-spin)
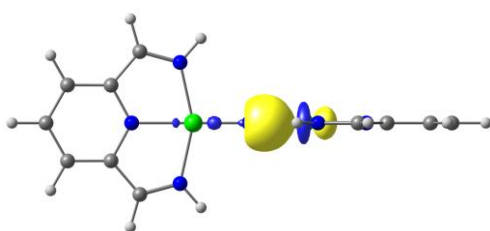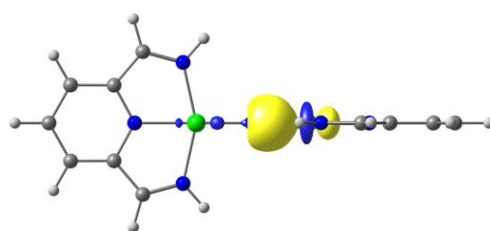
LMO 39: 0.32 e⁻ Ir2/0.70 e⁻ N$_{nitrido}$ (α-spin) LMO 130: 0.33 e⁻ Ir2/0.70 e⁻ N$_{nitrido}$ (β-spin)
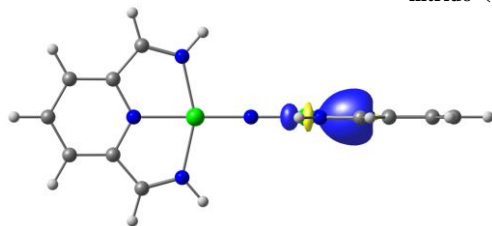
LMO 41: 0.17 e⁻ Ir2/0.84 e⁻ N$_{pyridine}$ (α-spin) LMO 131: 0.17 e⁻ Ir2/0.84 e⁻ N$_{pyridine}$ (β-spin)
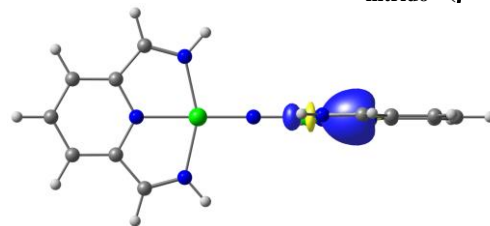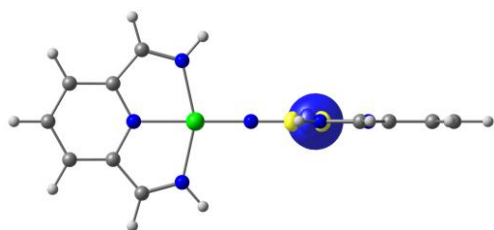
LMO 42: 0.19 e⁻ Ir2/0.84 e⁻ N$_{imine}$ (α-spin)   **LMO 136: 0.19 e⁻ Ir2/0.84 e⁻ N$_{imine}$ (β-spin)**
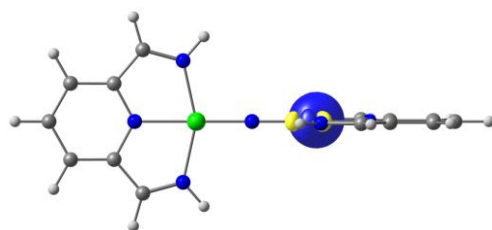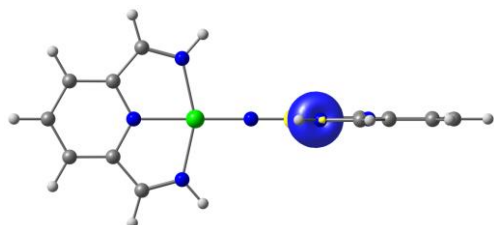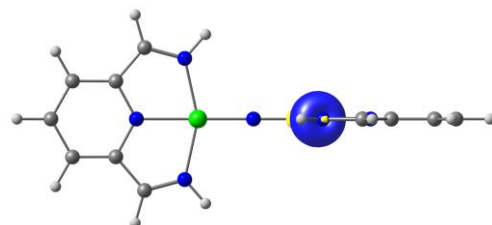
LMO 43: 0.19 e⁻ Ir2/0.84 e⁻ N$_{imine}$ (α-spin)   **LMO 135: 0.19 e⁻ Ir2 / 0.84 e⁻ N$_{imine}$ (β-spin)**
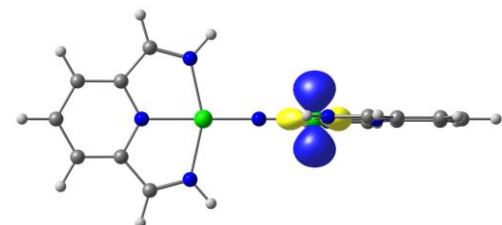
LMO 73: 1.0 e⁻ Ir2(d$_{z2}$) (α-spin)   **LMO 163: 1.0 e⁻ Ir2(d$_{z2}$) (β-spin)**
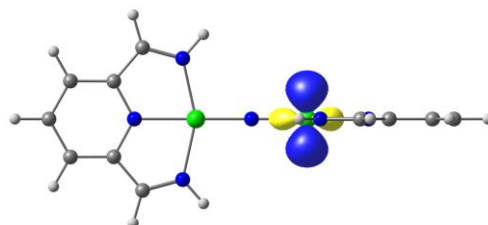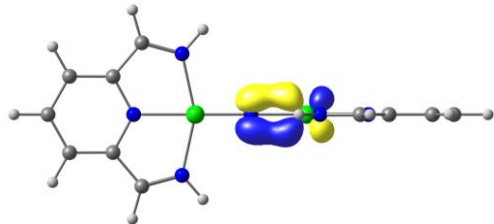
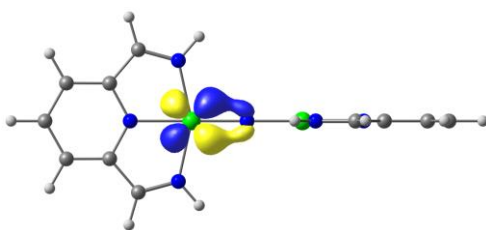**LMO 81: 0.61 e⁻ Ir2(d$_{xz}$)/0.39 e⁻ N$_{nitrido}$ (α-spin)   LMO 170: 0.64 e⁻ Ir2(d$_{xz}$)/0.36 e⁻ N$_{nitrido}$ (β-spin)**
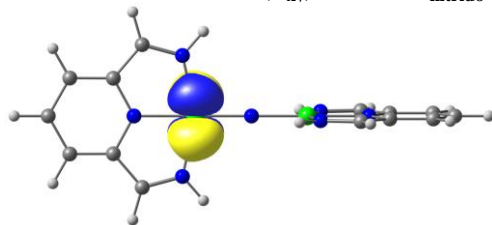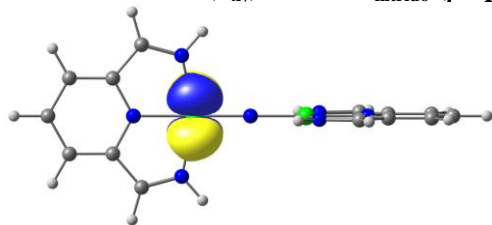The values for the α- and β-LMOs were averaged ((0.61+0.64)/2≈0.63).
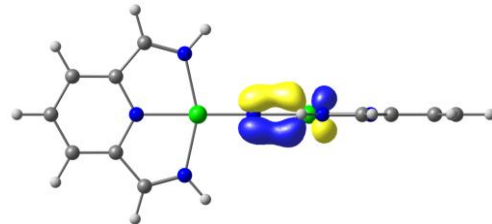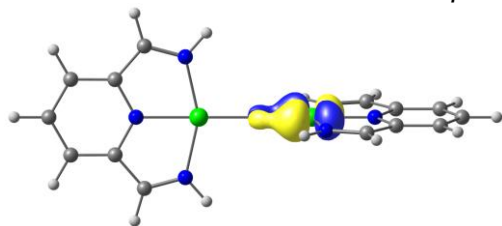
LMO 86: 0.84 e⁻ Ir2(d$_{xy}$)/0.11 e⁻ N$_{nitrido}$ (α-spin)   LMO 176: 0.84 e⁻ Ir2(d$_{xy}$)/0.11 e⁻ N$_{nitrido}$(β-spin)
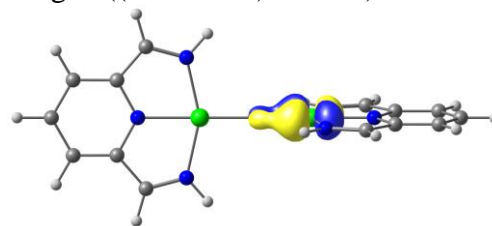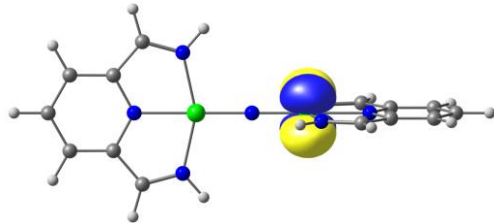
**LMO 91: 0.84 e⁻ Ir2(d$_{yz}$) (α-spin)**   **LMO 181: 0.85 e⁻ Ir2(d$_{yz}$) (β-spin)**
The values for the α- and β-LMOs were averaged ((0.84+0.85)/2≈0.85).
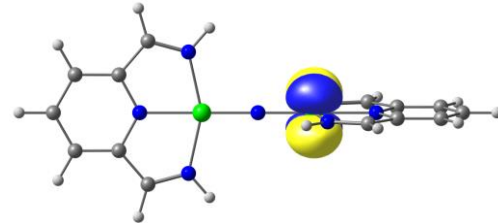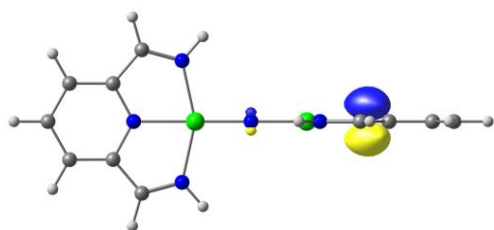
**LMO 78: PDI ligand-2 (non-innocent) 0.74 e$^-$ N$_{pyridine}$ (α-spin)**
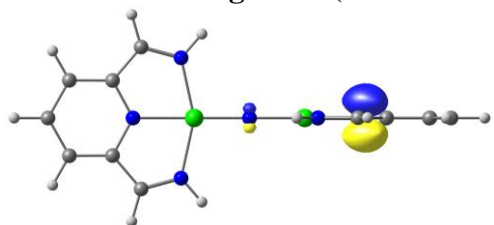
LMO 178: PDI ligand-2 (non-innocent) 0.73 e$^-$ N$_{pyridine}$ β-spin

restricted Kohn-Sham DFT, BP86 functional; MPA values with contributions of > 10% are given.

LMO 38: 0.64 e$^-$ Ir1 /   1.40 e$^-$ N$_{nitrido}$ **LMO 39: 0.64 e$^-$ Ir2 / 1.40 e$^-$ N$_{nitrido}$**
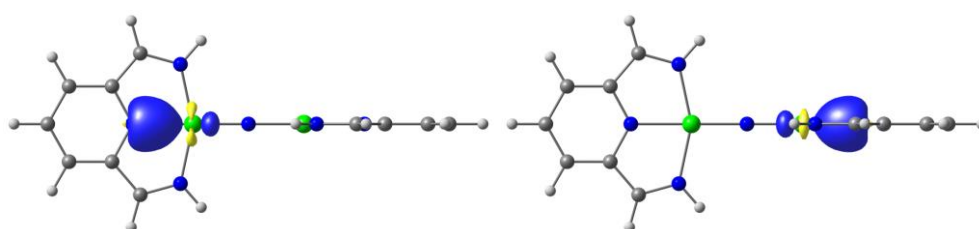
LMO 41: 0.35 e$^-$ Ir1 / 1.66 e$^-$ N$_{pyridine1}$ **LMO 40: 0.35 e$^-$ Ir1 / 1.66 e$^-$ N$_{pyridine2}$**
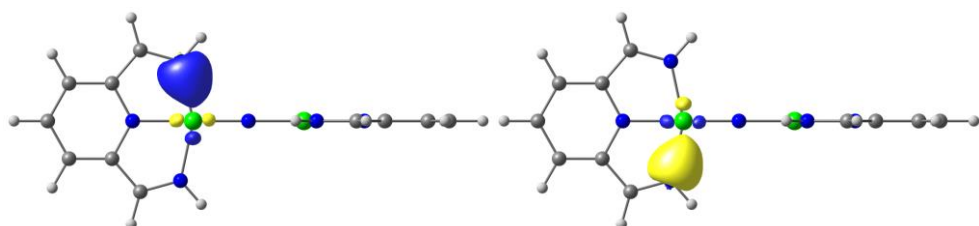
LMO 42: 0.39 Ir1 / 1.67 e$^-$ N$_{imine}$ **LMO 44: 0.39 e$^-$ Ir1 / 1.67 e$^-$ N$_{imine}$**
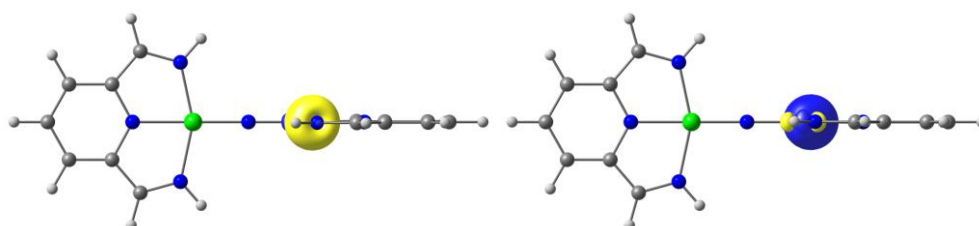
LMO 43: 0.39 e$^-$ Ir2 / 1.67 e$^-$ N$_{imine}$ **LMO 45: 0.39 e$^-$ Ir2 / 1.67 e$^-$ N$_{imine}$**
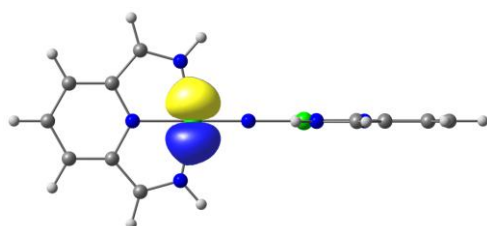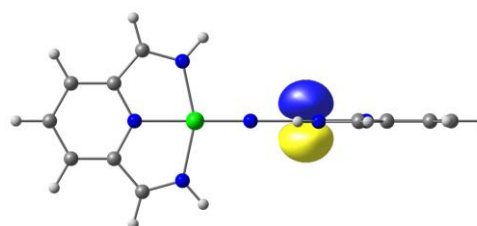
LMO 90: 1.63 e$^-$ Ir1(d_{yz})   **LMO 91: 1.63 e$^-$ Ir2(d_{yz})**
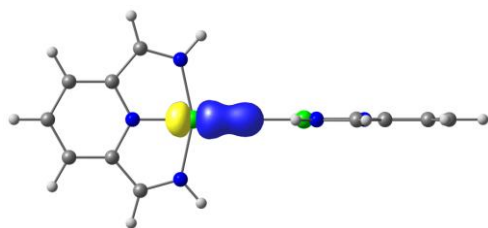
LMO 82: 1.26 e$^-$ Ir1(d$_{xz}$) / 0.72 e$^-$N$_{nitrido}$
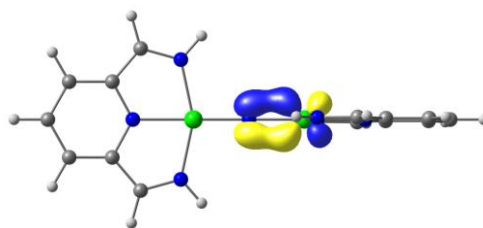
LMO 83: 1.26 e$^-$ Ir2(d$_{xz}$) / 0.72 e$^-$N$_{nitrido}$
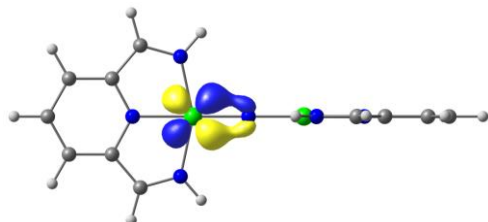
LMO 84: 1.67 e$^-$ Ir1(d$_{xy}$) / 0.22 e$^-$ N$_{nitrido}$
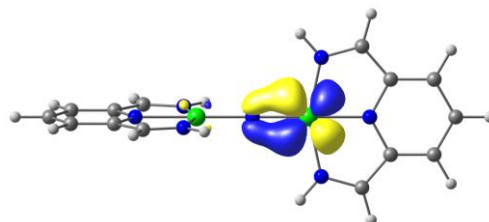
LMO 85: 1.67 e$^-$ Ir2(d$_{xy}$) / 0.22 e$^-$ N$_{nitrido}$
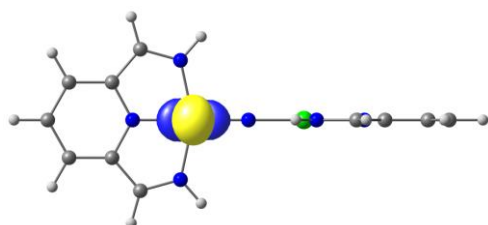
LMO 88: 2 e$^-$ Ir1(d$_{z2}$)
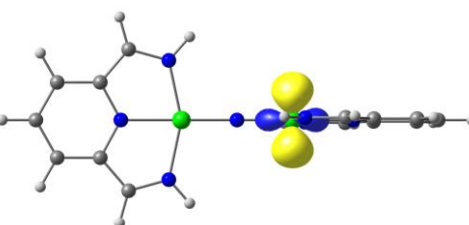
LMO 89: 2 e$^-$ Ir2(d$_{z2}$)
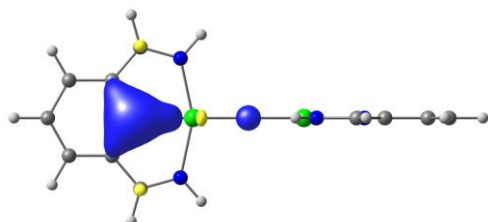
LMO 86: PDI^{2-} / 0.19 e$^-$ Ir1(d$_{xz}$) / 1.46 e$^-$ N$_{pyridine1}$ / 0.12 N$_{nitrido}$
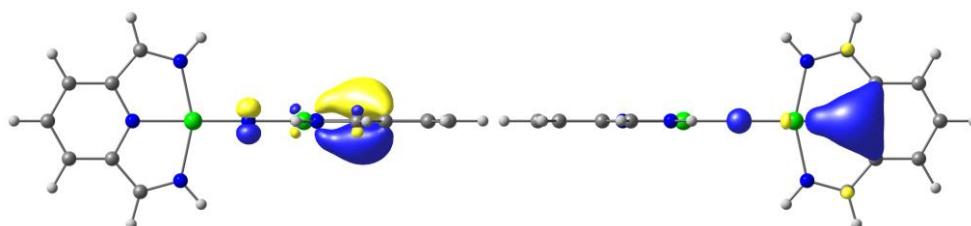
LMO 87: PDI^{2-} / 0.19 e$^-$ Ir2(d$_{xz}$) / 1.46 e$^-$ N$_{pyridine2}$ / 0.12 N$_{nitrido}$

Table S7. DFT (BP86 functional) optimized geometry of the model compound for IrCl (C$_{2v}$ symmetry, xmol xyz format in Å).

```
19
Energy = -999.6518098115 Hartree
H      2.1824678     0.0000000    -2.4503072
C      1.2232530     0.0000000    -1.9091762
C     -1.2173279     0.0000000    -0.5019571
C      1.2173279     0.0000000    -0.5019571
C      0.0000000     0.0000000    -2.6068198
C     -1.2232530     0.0000000    -1.9091762
N      0.0000000     0.0000000     0.1760927
H      0.0000000     0.0000000    -3.7081322
H     -2.1824678     0.0000000    -2.4503072
Ir     0.0000000     0.0000000     2.0893762
C      2.3088562     0.0000000     0.4384305
H      3.3654803     0.0000000     0.1238675
N      1.9604987     0.0000000     1.7275393
H      2.7455187     0.0000000     2.4001515
C     -2.3088562     0.0000000     0.4384305
H     -3.3654803     0.0000000     0.1238675
N     -1.9604987     0.0000000     1.7275393
H     -2.7455187     0.0000000     2.4001515
Cl     0.0000000     0.0000000     4.3923865
```


IrCl model
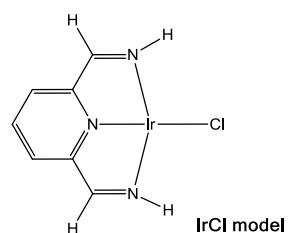
Table S8. DFT (BP86 functional) optimized geometry of the model compound for IrN (C$_{2v}$ symmetry, xmol xyz format in Å).

19
Energy = -594.1720053005 Hartree

IrN model

H	2.1825652	0.0000000	-2.4292666
C	1.2221739	0.0000000	-1.8890582
C	-1.2113551	0.0000000	-0.4834271
C	1.2113551	0.0000000	-0.4834271
C	0.0000000	0.0000000	-2.5907419
C	-1.2221739	0.0000000	-1.8890582
N	0.0000000	0.0000000	0.2031062
H	0.0000000	0.0000000	-3.6921244
H	-2.1825652	0.0000000	-2.4292666
Ir	0.0000000	0.0000000	2.2769536
C	2.2979920	0.0000000	0.4338143
H	3.3593041	0.0000000	0.1417744
N	1.9401050	0.0000000	1.7287923
H	2.7036392	0.0000000	2.4145560
C	-2.2979920	0.0000000	0.4338143
H	-3.3593041	0.0000000	0.1417744
N	-1.9401050	0.0000000	1.7287923
H	-2.7036392	0.0000000	2.4145560
N	0.0000000	0.0000000	3.9684363
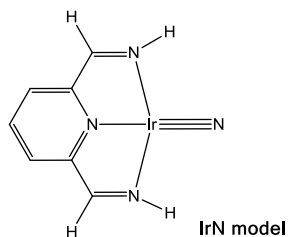
Table S9. DFT (BP86 functional) optimized geometry of the cationic model compound for $Ir_2N_3{}^+$ (D_{2d} symmetry, xmol xyz format in Å).

```
39
Energy = -1242.974709781 Hartree
H     1.5423390    -1.5423390     7.6676157
C     0.8631855    -0.8631855     7.1297886
C    -0.8565838     0.8565838     5.7238185
C     0.8565838    -0.8565838     5.7238185
C     0.0000000     0.0000000     7.8300504
C    -0.8631855     0.8631855     7.1297886
N     0.0000000     0.0000000     5.0431138
H     0.0000000     0.0000000     8.9309031
H    -1.5423390     1.5423390     7.6676157
Ir    0.0000000     0.0000000     3.1161042
C     1.6344114    -1.6344114     4.7923083
H     2.3801673    -2.3801673     5.1127892
N     1.3945192    -1.3945192     3.5067046
H     1.9525871    -1.9525871     2.8428633
C    -1.6344114     1.6344114     4.7923083
H    -2.3801673     2.3801673     5.1127892
N    -1.3945192     1.3945192     3.5067046 e
H    -1.9525871     1.9525871     2.8428633
N     0.0000000     0.0000000     0.0000000
Ir    0.0000000     0.0000000    -3.1161042
N     0.0000000     0.0000000    -5.0431138
C     0.0000000     0.0000000    -7.8300504
C    -0.8565838    -0.8565838    -5.7238185
C     0.8565838     0.8565838    -5.7238185
C     0.8631855     0.8631855    -7.1297886
C    -0.8631855    -0.8631855    -7.1297886
H     1.5423390     1.5423390    -7.6676157
H    -1.5423390    -1.5423390    -7.6676157
H     0.0000000     0.0000000    -8.9309031
C    -1.6344114    -1.6344114    -4.7923083
H    -2.3801673    -2.3801673    -5.1127892
C     1.6344114     1.6344114    -4.7923083
H     2.3801673     2.3801673    -5.1127892
N    -1.3945192    -1.3945192    -3.5067046
H    -1.9525871    -1.9525871    -2.8428633
N     1.3945192     1.3945192    -3.5067046
H     1.9525871     1.9525871    -2.8428633
N     0.0000000     0.0000000     1.1848195
N     0.0000000     0.0000000    -1.1848195
```


$Ir_2N_3{}^+$ model
D_{2d}-symmetrical
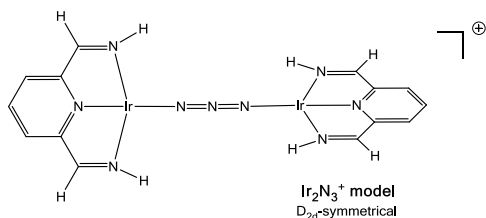
Table S10. DFT (BP86 functional) optimized geometry of the cationic model compound for Ir_2N^+ (S=1, $<S^2>$ = 2.01, D_{2d} symmetry, xmol xyz format in Å). The total energy of the broken symmetry solution amounts to -1133.5630693H, $<S^2>$ equals 1.013 (cf. Table S5).

```
37
Energy = -1133.563152940 Hartree
H    -1.5439737   -1.5439737   -6.4135007
C    -0.8672947   -0.8672947   -5.8695749
C     0.8567321    0.8567321   -4.4637809
C    -0.8567321   -0.8567321   -4.4637809
C     0.0000000   -0.0000000   -6.5650483
C     0.8672947    0.8672947   -5.8695749
N    -0.0000000    0.0000000   -3.8030816
H    -0.0000000    0.0000000   -7.6662275
H     1.5439737    1.5439737   -6.4135007
Ir    0.0000000   -0.0000000   -1.7909625
C    -1.6325942   -1.6325942   -3.5245119
H    -2.3795959   -2.3795959   -3.8379357
N    -1.3923514   -1.3923514   -2.2348713
H    -1.9434831   -1.9434831   -1.5617143
C     1.6325942    1.6325942   -3.5245119
H     2.3795959    2.3795959   -3.8379357
N     1.3923514    1.3923514   -2.2348713
H     1.9434831    1.9434831   -1.5617143
N     0.0000000    0.0000000    0.0000000
Ir    0.0000000    0.0000000    1.7909625
N    -0.0000000   -0.0000000    3.8030816
C     0.0000000    0.0000000    6.5650483
C     0.8567321   -0.8567321    4.4637809
C    -0.8567321    0.8567321    4.4637809
C    -0.8672947    0.8672947    5.8695749
C     0.8672947   -0.8672947    5.8695749
H    -1.5439737    1.5439737    6.4135007
H     1.5439737   -1.5439737    6.4135007
H    -0.0000000   -0.0000000    7.6662275
C     1.6325942   -1.6325942    3.5245119
H     2.3795959   -2.3795959    3.8379357
C    -1.6325942    1.6325942    3.5245119
H    -2.3795959    2.3795959    3.8379357
N     1.3923514   -1.3923514    2.2348713
H     1.9434831   -1.9434831    1.5617143
N    -1.3923514    1.3923514    2.2348713
H    -1.9434831    1.9434831    1.5617143
```

Table S11. DFT (BP86 functional) optimized geometry of the neutral model compound for Ir$_2$N (S=1/2, <S^2> = 0.752 D$_{2d}$ symmetry, xmol xyz format in Å).

```
37
Energy = -1133.751294045
H    -1.5447058   -1.5447058   -6.4129784
C    -0.8683143   -0.8683143   -5.8668386
C     0.8640699    0.8640699   -4.4607253
C    -0.8640699   -0.8640699   -4.4607253
C    -0.0000000    0.0000000   -6.5622485
C     0.8683143    0.8683143   -5.8668386
N     0.0000000   -0.0000000   -3.7943620
H     0.0000000    0.0000000   -7.6640907
H     1.5447058    1.5447058   -6.4129784
Ir   -0.0000000    0.0000000   -1.8014186
C    -1.6329155   -1.6329155   -3.5295855
H    -2.3813219   -2.3813219   -3.8353036
N    -1.3848245   -1.3848245   -2.2284393
H    -1.9337201   -1.9337201   -1.5525177
C     1.6329155    1.6329155   -3.5295855
H     2.3813219    2.3813219   -3.8353036
N     1.3848245    1.3848245   -2.2284393
H     1.9337201    1.9337201   -1.5525177
N     0.0000000    0.0000000    0.0000000
Ir   -0.0000000   -0.0000000    1.8014186
N     0.0000000    0.0000000    3.7943620
C    -0.0000000   -0.0000000    6.5622485
C     0.8640699   -0.8640699    4.4607253
C    -0.8640699    0.8640699    4.4607253
C    -0.8683143    0.8683143    5.8668386
C     0.8683143   -0.8683143    5.8668386
H    -1.5447058    1.5447058    6.4129784
H     1.5447058   -1.5447058    6.4129784
H     0.0000000    0.0000000    7.6640907
C     1.6329155   -1.6329155    3.5295855
H     2.3813219   -2.3813219    3.8353036
C    -1.6329155    1.6329155    3.5295855
H    -2.3813219    2.3813219    3.8353036
N     1.3848245   -1.3848245    2.2284393
H     1.9337201   -1.9337201    1.5525177
N    -1.3848245    1.3848245    2.2284393
H    -1.9337201    1.9337201    1.5525177
```


Ir$_2$N model
D$_{2d}$-symmetrical

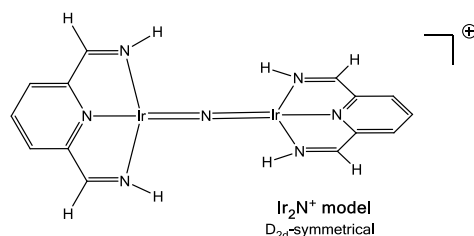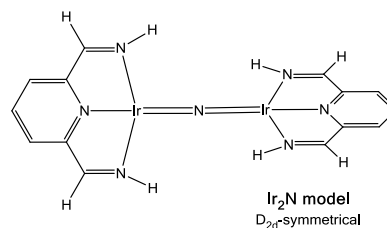**Table S12. DFT (BP86 functional) optimized geometry of the neutral model compound for Ir$_2$N (S=3/2, <S^2> = 3.76, D$_{2d}$ symmetry, xmol xyz format in Å). Electron configuration:**

α: .. 22(a$_1$)^1(3a$_2$)^1(4b$_1$)^1(21b$_2$)^1(21e)^1

β: .. 22(a$_1$)^1(3a$_2$)^1(3b$_1$)^1(21b$_2$)^1(20e)^1

37
Energy = -1133.716403252 Hartree quartet state

|			
H	-1.5458241	-1.5458241	-6.4272596
C	-0.8692331	-0.8692331	-5.8835590
C	0.8595527	0.8595527	-4.4644645
C	-0.8595527	-0.8595527	-4.4644645
C	-0.0000000	0.0000000	-6.5713164
C	0.8692331	0.8692331	-5.8835590
N	-0.0000000	0.0000000	-3.8075733
H	0.0000000	0.0000000	-7.6739735
H	1.5458241	1.5458241	-6.4272596
Ir	0.0000000	-0.0000000	-1.7883600
C	-1.6308999	-1.6308999	-3.5325940
H	-2.3765723	-2.3765723	-3.8544555
N	-1.4017432	-1.4017432	-2.2280845
H	-1.9537045	-1.9537045	-1.5604557
C	1.6308999	1.6308999	-3.5325940
H	2.3765723	2.3765723	-3.8544555
N	1.4017432	1.4017432	-2.2280845
H	1.9537045	1.9537045	-1.5604557
N	0.0000000	0.0000000	0.0000000
Ir	0.0000000	0.0000000	1.7883600
N	-0.0000000	-0.0000000	3.8075733
C	-0.0000000	-0.0000000	6.5713164
C	0.8595527	-0.8595527	4.4644645
C	-0.8595527	0.8595527	4.4644645
C	-0.8692331	0.8692331	5.8835590
C	0.8692331	-0.8692331	5.8835590
H	-1.5458241	1.5458241	6.4272596
H	1.5458241	-1.5458241	6.4272596
H	0.0000000	0.0000000	7.6739735
C	1.6308999	-1.6308999	3.5325940
H	2.3765723	-2.3765723	3.8544555
C	-1.6308999	1.6308999	3.5325940
H	-2.3765723	2.3765723	3.8544555
N	1.4017432	-1.4017432	2.2280845
H	1.9537045	-1.9537045	1.5604557
N	-1.4017432	1.4017432	2.2280845
H	-1.9537045	1.9537045	1.5604557

Ir$_2$N model
D$_{2d}$-symmetrical
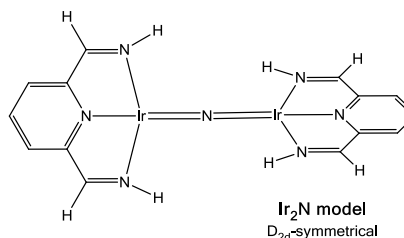
Table S13. DFT (BP86 functional) optimized geometry of the anionic model compound for Ir_2N^- in D_{2d} symmetry (xmol xyz format in Å).

```
37
Energy = -1133.820684559 Hartree
H    -1.5465735   -1.5465735   -6.4196086
C    -0.8703093   -0.8703093   -5.8699412
C     0.8714964    0.8714964   -4.4627162
C    -0.8714964   -0.8714964   -4.4627162
C    -0.0000000    0.0000000   -6.5656122
C     0.8703093    0.8703093   -5.8699412
N    -0.0000000    0.0000000   -3.7916399
H    -0.0000000    0.0000000   -7.6691736
H     1.5465735    1.5465735   -6.4196086
Ir   -0.0000000    0.0000000   -1.8129956
C    -1.6346282   -1.6346282   -3.5381662
H    -2.3850238   -2.3850238   -3.8364059
N    -1.3782008   -1.3782008   -2.2246022
H    -1.9257816   -1.9257816   -1.5460720
C     1.6346282    1.6346282   -3.5381662
H     2.3850238    2.3850238   -3.8364059
N     1.3782008    1.3782008   -2.2246022
H     1.9257816    1.9257816   -1.5460720
N    -0.0000000    0.0000000    0.0000000
Ir   -0.0000000   -0.0000000    1.8129956
N    -0.0000000   -0.0000000    3.7916399
C    -0.0000000   -0.0000000    6.5656122
C     0.8714964   -0.8714964    4.4627162
C    -0.8714964    0.8714964    4.4627162
C    -0.8703093    0.8703093    5.8699412
C     0.8703093   -0.8703093    5.8699412
H    -1.5465735    1.5465735    6.4196086
H     1.5465735   -1.5465735    6.4196086
H    -0.0000000   -0.0000000    7.6691736
C     1.6346282   -1.6346282    3.5381662
H     2.3850238   -2.3850238    3.8364059
C    -1.6346282    1.6346282    3.5381662
H    -2.3850238    2.3850238    3.8364059
N     1.3782008   -1.3782008    2.2246022
H     1.9257816   -1.9257816    1.5460720
N    -1.3782008    1.3782008    2.2246022
H    -1.9257816    1.9257816    1.5460720
```
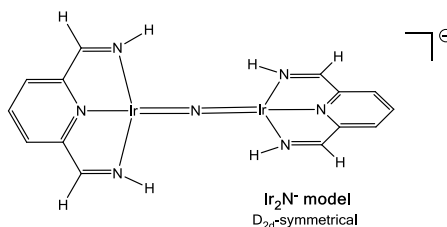
References

S1   M. A. Arthurs, J. Bickerton, S. R. Stobart, J. J. Wang, *Organometallics* 1998, **17**, 2743.

S2   J.-Y. Liu, Y. Zheng, N.-H. Hu, Y.-S. Li, *Chin. J. Chem.* 2006, **24**, 1447.

S3   I. Krossing, A. Reisinger, *Eur. J. Inorg. Chem.*, 2005, 1979.

S4   S. Nückel, P. Burger, *Organometallics* 2001, **20**, 4345.

S5   D. Sieh, M. Schlimm, L. Andernach, F. Angersbach, S. Nückel, J. Schöffel, N. Šušnjar, P. Burger, *Eur. J. Inorg. Chem.* 2012**,** 1444.

S6   D.F. Evans, *J. Chem. Soc.* 1959, 2003.

S7   E.M. Schubert, *J. Chem. Ed.* 1992, **69**, 62.

S8   G. P. Arrighini, M. Maestro, R. Moccia, *J. Chem. Phys.* 1968, **49**, 882.

S9   G.M. Sheldrick, in *SHELXS-97, SHELXL-97 programs for crystal structure solution and refinement.* (Universität Göttingen, Germany, 1993 and 1997).

S10   L.J. Farrugia, *J. Appl. Crystallogr.*, 1997, **30**, 568.

S11   D.R. Eaton, W.D. Phillips, D.J. Cadwell, *J. Am. Chem. Soc.,* 1963, **85**, 397; L.W. Pignolet, W.D. Horrocks, Jr. *J. Am. Chem. Soc.* 1969, **81**, 3976.

S12   O. Treutler, R. Ahlrichs *J. Chem. Phys.* 1995, **102**, 346; R. Ahlrichs, M. Bär, M. Häser, H. Horn, C. Kölmel, *Chem. Phys. Lett.* 1989, **162**, 165; TURBOMOLE V6.5 2013, a development of University of Karlsruhe and Forschungszentrum Karlsruhe GmbH, 1989-2007, since 2007; available from http://www.turbomole.com.

S13   A.D. Becke *Phys. Rev. A* 1988, **38**, 3098.

S14   J.P. Perdew, J.P. *Phys. Rev. B.*, 1986, **33**, 8822.

S16   D. Andrae, U. Haeussermann, M. Dolg, H. Stoll, H. Preuss, *Theor. Chim. Acta.* 1990, **77**, 1431.

S17   A.E. Reed, R.B. Weinstock, F. Weinhold *J. Chem. Phys.* 1985, **83**, 735 (charges and spin densities implemented in Turbomole).

S18   A.J.W. Thom, E.J. Sundstrom, M. Head-Gordon, *Phys. Chem. Chem. Phys*., 2009, **11**, 11297

S19   Multiwfn: http://multiwfn.codeplex.com/; T. Lu, F. Chen, J. Mol. Graph. Model., 2012, **38**, 314.

S20   Molden2AIM: http://people.smu.edu/wzou/program/

S21   http://www.chemcraftprog.com

S22   T. Soda, Y. Kitagawa, T. Onishi, Y. Takano, Y. Shigeta, H. Nagao, Y. Yoshioka, and K. Yamaguchi *Chem. Phys. Lett.*, 2000, **319**, 223.